Winter 2009

The generation of a diverse suite of Late Pleistocene and Holocene basaltic-andesite through dacite lavas from the northern Cascade arc at Mount Baker, Washington

Troy D. Baggerman
Western Washington University, troy22db@gmail.com

The generation of a diverse suite of Late Pleistocene and Holocene basaltic-andesite through dacite lavas from the northern Cascade arc at Mount Baker, Washington.

By
Troy D. Baggerman
February, 2009

Accepted In Partial Fulfillment
Of the Requirements for the Degree

Master of Science
Geology

Moheb A. Ghali, Dean of Graduate School

ADVISORY COMMITTEE

Chair, Dr. Susan DeBari

Dr. Scott Linneman

Dr. Pete Stelling

MASTER'S THESIS

In presenting this thesis in partial fulfillment of the requirements for a master's degree at Western Washington University, I agree that the Library shall make its copies freely available for inspection. I further agree that extensive copying of this thesis is allowable only for scholarly purposes. It is understood, however, that any copying or publication of this thesis for commercial purposes, or for financial gain, shall not be allowed without my written permission.

Signature _____

Date 2-27-09

MASTER'S THESIS

In presenting this thesis in partial fulfillment of the requirements for a master's degree at Western Washington University, I grant to Western Washington University the non-exclusive royalty-free right to archive, reproduce, distribute, and display the thesis in any and all forms, including electronic format, via any digital library mechanisms maintained by WWU.

I represent and warrant this is my original work, and does not infringe or violate any rights of others. I warrant that I have obtained written permissions from the owner of any third party copyrighted material included in these files.

I acknowledge that I retain ownership rights to the copyright of this work, including but not limited to the right to use all or part of this work in future works, such as articles or books.

Library users are granted permission for individual, research and non-commercial reproduction of this work for educational purposes only. Any further digital posting of this document requires specific permission from the author.

Any copying or publication of this thesis for commercial purposes, or for financial gain, is not allowed without my written permission.

Troy Baggerman
February 27, 2018

The generation of a diverse suite of Late Pleistocene and Holocene basaltic-andesite through dacite lavas from the northern Cascade arc at Mt. Baker, Washington.

A Thesis
Presented to
The Faculty of
Western Washington University

In Partial Fulfillment
Of the Requirements for the Degree
Master of Science

By
Troy D. Baggerman
February, 2009

ABSTRACT

This study highlights geochemical diversity in a spectrum of basaltic andesite through dacite lavas from Mount Baker, WA, and describes processes that are responsible for their generation. Petrographic observations, mineral chemistry, along with whole rock major oxide concentrations, and trace and REE data are provided for three Late Pleistocene and Holocene lava flows: the basaltic andesite of Sulphur Creek (SC) (52.5-55.8 wt.% SiO_2, Mg# 57-54), the andesite of Glacier Creek (GC) (58.3-58.7 wt.% SiO_2, Mg # 63-64), and the andesite and dacite of Boulder Glacier (BG) (60.2-64.2 wt.% SiO_2, Mg # 50-57). Major oxide concentrations for SC and BG display clear trends with increasing SiO_2. GC andesites are tightly clustered compositionally with elevated MgO and Ni compared to SC and BG for a given SiO_2. REE patterns are distinct for each unit but are not correlated with differentiation. The mafic lavas of SC have relatively elevated REE abundances with the lowest La/Yb (~4.5). The GC andesites have the lowest REE abundances and the largest La/Yb (~6.7). The BG lavas have intermediate REE abundances and La/Yb (~6.4). Phenocryst populations in all units display varying degrees of reaction textures and disequilibrium textures along with complicated zoning patterns indicative of magma mixing processes.

None of units can be related to each other through crystal fractionation processes, nor can crystal fractionation explain the compositional diversity within each unit as suggested by several major and trace element models including MELTS (Ghiorso, 1993) and REE Rayleigh fractionation. However, magma mixing between the mafic SC lavas with compositions similar to the dacites of BG in the proportions 70 % SC with 30% BG can account for the chemical trends displayed by the SC lavas. Given that the BG dacite mixing end-member erupted at 80 ka, and was mixed with the SC lavas at 9.8 ka, the process that produced this felsic end-member has been active or periodically active for at least 70 ka. The BG mixing end-member is comparable to silicic mixing end-members at other Cascade volcanoes where crustal melting processes have been called upon to explain their origin and the SC mixing end-member is presumably mantle derived.

GC andesites include a population of olivine that has been identified as xenocrystic based on size, composition and the observation of strong disequilibrium textures. The elevated MgO composition of the GC andesites is proposed as the result of the addition of ~4 wt% (by volume) of the xenocrystic GC olivine. The source of the xenocrystic olivine is unconstrained; however, it is most likely cumulate in origin or related to mafic plutonic roots. Compositions of GC andesites before the addition of 4% olivine lie on the straight line mixing trend formed by the SC basalts and BG dacites making them a possible product of magma mixing. All GC phenocrysts display varying degrees of reaction and disequilibrium textures along with complicated zoning patterns which are also supportive of magma mixing processes.

ACKNOWLEDGMENTS

This thesis is dedicated to my family.

First and foremost I would like to thank my entire family for their unconditional support and encouragement. Each member of my family supported me in their own special way, weather it be help in the lab, being my audience during practice talks, or intently listening to me babble on about magma, volcanic arcs and rare earth elements. I would like to thank Sue DeBari for being an excellent mentor and also for her constant enthusiasm and excitement about this project and science in general. Sue also deserves an extra special thanks for presenting my research at the AGU conference in San Francisco in December of 2007. Thanks to Pete Stelling and Scott Linneman for providing invaluable comments and thought provoking discussions. Scott and Pete have a genuine and contagious love for science which definitely has rubbed off on me. I would also like to acknowledge the WWU geology department. Every single faculty and staff member of the geology department has made my experience there one that has been extremely enjoyable and valuable. Every single one of my friends and peers also deserve a thank you for their encouragement and for constantly asking me the dreaded question; "when are you going to be done?"

I had many field and lab assistants throughout this project for whom I am greatly thankful for. These people include Kurt Parker, Brendon Hodge, Dylan McIntire, Melissa Park, Dave Tucker, Owen Callahan, my mom, my dad, my sister, and several of my Geology 211 students. A special thank you goes to Dave Tucker for donating three Sulphur Creek basalt samples from his personal collection for this study.

Research funding was provided by the Cascade Volcano Observatory through the Jack Kleinman Internship for Volcano Research, Sigma Xi, the Geology Department and the

Graduate School at Western Washington University. Funding for travel related expenses were provided by the National Science Foundation for travel to a MARGINS conference in Hawaii and by the Goldschmidt Foundation for travel to the 2008 annual Goldschmidt conference in Vancouver, B.C.

Geochemical analyses (XRF and ICP-MS) were performed at the GeoAnalytical lab at Washington State University by Diane Johnson Cornelius and Charles M. Knaack. Microprobe work was performed at the University of Washington under the supervision of Scott Kuehner.

TABLE OF CONTENTS

LIST OF TABLES

LIST OF FIGURES

INTRODUCTION

Calc-alkaline andesite lavas are a characteristic lava type associated with many continental arc volcanoes and are the most common lava type erupted in the North Cascade arc (Hildreth, 2007). Gill (1981) estimates that lavas with intermediate compositions (52-63 wt% SiO_2) are the most common lava type erupted at arcs worldwide. Andesitic lavas are not typically thought of as a primary lava type, therefore complex chemical and physical differentiation processes have been called upon to explain the development of these lavas as they migrate through Earth's crust. Fundamental processes of andesite generation are applied to arcs world wide and may include complex crystal fractionation processes (Grove and Baker, 1984), magma mixing processes (Eichelberger, 1975), assimilation of crustal material (Mason et al., 1996) and hybrid models with crystal fractionation coupled with magma recharge and mixing (Streck et al., 2002, Schaaf et al., 2005). In some cases, complex models are described in which each of the above processes works in conjunction to form andesite (Hildreth and Moorbath, 1988). Fortunately, each of the above processes often leaves behind distinct chemical and textural evidence in andesitic rocks and therefore provides the necessary means to distinguish between the various models of andesite generation.

The origin and evolution of intermediate lavas in the northern region of the Cascade arc, which includes Washington State and British Columbia, Canada, has thus far not been explored in any detail. The petrogenesis of lavas in the southern and middle region of the Cascade arc is better documented and provides a diverse range of models. Complex magma mixing processes between basaltic andesite and dacite to form intermediate lavas have been

proposed in the Southern Cascades at Lassen Peak (Clynne, 1999) and also further north at Mount Rainer (Venezky and Rutherford, 1997). At other volcanic centers such as Mount Shasta, crystal fractionation of a primitive high- magnesium andesite has been proposed as the main process for andesite generation (Grove et al., 2003), while other andesites have been considered primary mantle magmas (Grove et al., 2002). Other workers, however, have argued for magma mixing between dacitic and basaltic end-members combined with entrainment of an ultramafic component for the generation of Mount Shasta andesites (Streck et al., 2007). Medicine Lake Volcano has erupted an array of basalt through rhyolite, and the generation of those lavas is described to be a combination of fractionation, assimilation and magma mixing processes (Grove et al., 1981).

A common strategy for determining the origin and evolution of intermediate lavas is to identify the primary melts or end-member compositions and then to identify and quantify differentiation processes. For example, if one end-member is characterized as a product of crustal melting, then what is the protolith, and what is the degree of partial melting (e.g. Mount St. Helens, Smith and Leeman, 1987)? If mixing is thought to be a dominant process, what are the mixing end-members and what are the mixing proportions (e.g. Lassen Peak, Clynne 1999)? If pure crystal fractionation is dominant, mineral modes can be estimated and crystallization paths can be quantified (e.g. Mount Shasta, Grove et al., 2005).

Mount Baker has been historically active (Eichelberger et al., 1976) and is situated near several population centers (Figure 1), yet studies involving the origin and evolution of its lavas are scarce. This study reports distinguishing geochemical characteristics in the basaltic andesite through dacite lavas erupted from Mount Baker and describes processes that

may be responsible for the generation of these intermediate lava types. Presented within this thesis are petrographic observations, major oxide, trace, and REE concentrations from whole rock samples along with mineral chemistry for three Late Pleistocene and Holocene eruptive units from Mount Baker. The volcanic units in this study were previously mapped and characterized by Hildreth et al. (2003) and the basalts were also described by Green (1988). Units include the Basalt of Sulphur Creek (51.4-58.5 wt. % SiO_2, 3.9-5.6 % MgO), the Andesite of Glacier Creek (58.1-58.5 wt. % SiO_2, 4.5-4.9 % MgO), and the Andesite and Dacite of Boulder Glacier (56.6-64.4 wt. % SiO_2, 1.9-3.9 % MgO) (units, names and compositional ranges stated above are from Hildreth et al., 2003).

The primary goal of this study is to apply a petrogenetic model to a suite of intermediate lava types erupted at Mount Baker since the Late Pleistocene. The model addresses the petrologic relationship among flows and also considers with in flow chemical differentiation trends. Secondly, intensive parameters including temperature and oxygen fugacity (fO_2) conditions of the magmatic system are estimated.

McKeever (1977) collected a suite of samples from several lava flows on the southern flank of Mount Baker while noting stratigraphic relationships. McKeever analyzed each sample for major elements in an attempt to correlate geochemical signatures with stratigraphic units. He concluded that individual samples could be identified as belonging to one of two stratigraphic units that resulted from two eruptive phases. The younger phase (Koma Kulshan) is richer in SiO_2, Na_2O and K_2O and lower in FeO*, MgO and CaO than the older phase (Park Butte). In McKeever's study, identification of single flows based on major element composition was not possible. He concluded that the Mount Baker volcanics have a

complex development history and speculated on the possibility of a combination of crystal fractionation and magma mixing processes, but lacked sufficient evidence to quantify the degree of each process.

Swan (1980) attempted to resolve the petrogenetic history of the Mount Baker andesites. Magma mixing calculations and least squares fractionation calculations were inconclusive when applied to an extensive chemical data set. The lack of detailed lava stratigraphy and eruptive chronology of the Mount Baker volcanics at that time was a major limitation on the outcome of his study. Swan did however propose a complex hybrid model that included an intricate system of at least one magma chamber and several conduits in which magmas fractionate, mix and rise at different rates.

The detailed lava stratigraphy of Hildreth et al. (2003) provided a breakthrough for real understanding of the eruptive history at Mount Baker. They present a chronology of the main eruptive components that includes locations, descriptions, and ages of individual units of the Mount Baker volcanic field and their work is supplemented by a geologic map of all volcanic units (Figure 2). Their work also provides an extensive major element data set for lavas from the entire volcanic field along with petrographic observations of various reaction textures. However, Hildreth et al. (2003) include little interpretation of the petrologic data and observed textures. The work of Hildreth et al. (2003) provides a fundamental framework that was absent in previous petrologic studies, and their chronology and unit descriptions act as a foundation for this study.

GEOLOGY AND TECTONIC SETTING

Mount Baker is located in northern Washington State and is situated in the northern section of the Cascade volcanic arc about 50 km east of Bellingham Bay (Figure 1). Arc volcanism in the Northern Cascades is associated with the oblique subduction of the warm and young Juan de Fuca plate beneath the North American plate, where the trench lies ~350 km to the west of the volcanic front. The plates converge at a rate of 3-4 cm/yr (Heaton and Kanamori, 1984) with an estimated subduction angle of 20° in Washington and northern Oregon (McCrory et al., 2004). P-wave studies suggest that the crust beneath Mount Baker is 40-45 km thick (Mooney and Weaver, 1989, Ramachandran et al., 2006) with the subducting slab at a depth of 100-120 km (Bostock and VanDecar, 1995).

The Cascade arc is segmented due to structural changes in the subduction system and along arc magmatic trends (Hildreth, 2007). Guffanti and Weaver (1988) have identified five segments. Mount Baker is located in the northern segment, which is known as the Garibaldi Belt (Figure 1). The arc as a whole is characterized by a decrease in mafic magma production to the north, where primitive magmas become scarce in the Garibaldi belt (Hildreth, 2007). Arc parallel variations in magmatism have been credited to variables such as age of the subducting slab (Green and Harry, 1999), variations in slab- derived fluid fluxes, degrees of partial melting of different mantle sources, and variations in mantle H_2O (Green and Sinha, 2005).

Mount Baker is a dominantly andesitic stratovolcano that is currently the prominent feature of a multivent Quaternary volcanic field (Hildreth et al., 2003). Mount Baker is the tallest volcano in the Garibaldi belt at 3286 m. The volcano is blanketed with glaciers that

cover an estimated surface area of ~40 km^2 (Post et al., 1971). These glaciers are responsible for partial erosion of many of Mount Baker's volcanic units. The volcanic field is built on Mesozoic and Paleozoic rocks of oceanic affinity that were emplaced by strike slip faulting during the Paleogene (Tabor et el., 2003) and were metamorphosed to amphibolite facies (Miller et al., 2003). Volcanic products for the past 1.3 Ma have been linked to five main stages of volcanic activity that have been outlined by Hildreth et al. (2003): (1) pre Kulshan Caldera activity (1.3-1.15 Ma); (2) early post Kulshan Caldera activity (1.15-0.99 Ma); (3) widely scattered intracaldera and extracaldera activity, dominantly andesitic (0.9-0.5 Ma); (4) formation of Black Buttes stratovolcano and its satellites (0.5-0.2 Ma); and (5) formation of Mount Baker stratovolcano and its satellites (0.1 Ma to present).

This study focuses on three units from the late Pleistocene and Holocene that are used to investigate the generation of intermediate products during the formation of the Mount Baker stratocone and the associated satellite vents (Figure 2). The units are chosen to represent a range of ages and compositions erupted since the late Pleistocene. The Andesite of Glacier Creek and the Andesite and Dacite of Boulder Glacier are products of the late Pleistocene stratocone-forming lavas and the Basalt and Basaltic Andesite of Sulphur Creek is the result of a more recent Holocene flank eruption.

The basaltic andesite of Sulphur Creek is the product of a monogenic eruption on the southwest flank of the volcano, 7.8 km south of the main edifice in an area known as Schreibers Meadow (Figures 2 and 3). The eruption location is marked by a heavily vegetated ~100 m tall cinder cone with two small lakes in the crater marking two separate vent locations. Radiocarbon dates calibrated to calendar years suggest an age of 9.8 ka (Scott

et al., 2001) making it the youngest lava flow in the Mount Baker volcanic field. Carbon buried by scoria associated with the Schreibers Meadow cinder cone has been dated to 8750 ± 50 and 8830 ± 50 radiocarbon years bp (Scott et al., 2001). The flow is valley-confined and extends ~12 km to the SE of the vent. The most distal exposure is located on the east side of Baker Lake. Sub-aqueous lavas are also described near the west side of Baker Lake (Tucker and Scott, 2009). Exposures near the cinder cone are sparse due to a thick layer of Holocene debris flows (Hildreth et al. 2003), but when located are blocky spine shaped outcrops. Other exposures are located along road cuts or stream gorges and are generally massive to blocky and vesicular.

Major element analyses in this study are in the range of basaltic andesite (52.5-55.8 wt. % SiO_2 and 4.5-5.5 wt. % MgO, major element compositions from this study) with the more mafic compositions located in the most distal portion of the flow. At one location, 4 km down flow from the Schreibers Meadow cinder cone, Green (1988) noted basalt enclaves ranging in diameter from <1mm to 15 cm in the basaltic andesite. He used these enclaves to conclude that the basaltic andesite of Sulphur Creek is a result of mixing and quenching of basalt within a more differentiated basaltic andesite. The Sulphur Creek unit has the most Si-poor compositions in the suites of rocks collected for this study; however they are not the most Mg-rich lavas erupted from Mount Baker (Moore and DeBari, 2008).

The andesite of Glacier Creek is interpreted by Hildreth et al. (2003) to be a single canyon-confined flow with exposures in various locations within the Glacier Creek gorge which drains the Coleman Glacier on the northwest flank on the volcano (Figures 2 and 3). The exact origin of the flow is unknown. The most distal remnant of the flow is located ~8

km northwest of the summit of Mount Baker in the Glacier Creek gorge. Exposures within Glacier Creek gorge are up to 80 m thick and range from sub vertical, columnar jointed to massive or platy outcrops. Exposures at higher elevations confirmed to be the same lava flow through whole-rock chemistry can be found as sparse remnants on the western side of the Coleman glacier. Hildreth et al. (2003) also described a compositionally similar flow at the top of a locality known as the Roman Wall. The andesite of Glacier Creek is olivine bearing and has intermediate andesite compositions (58.3-58.7 wt. % SiO_2 and 4.6-4.9 wt. % MgO, major element compositions from this study). Hildreth et al. (2003) report one K-Ar date for the Glacier Creek unit of 14 ± 9 ka.

The andesite and dacite of Boulder Glacier is a series of stacked flows that caps the Boulder Ridge and occupy the upper valley of Boulder Creek adjacent to the terminus of the Boulder Glacier (Figures 2 and 3). Exposures consist of thick stacks (up to 200 m) of multiple columnar jointed to platy lava flows. Some locations expose basal sections of flow breccias. Thicknesses of single flows range from 5 m up to 50 m. Hildreth et al. (2003) estimate the entire Boulder Glacier unit is composed of at least 25 separate flows. It is the oldest unit recognized to erupt from the main edifice of Mount Baker with two K-Ar dates, each from a different flow. One flow is dated at 80 ± 14 ka and the other is dated at 90 ± 52 ka (Hildreth et al., 2003). The unit consists of two-pyroxene andesite to dacite with minor olivine bearing andesite (60.2-64.2 wt. % SiO_2 and 2.1-3.3 wt. % MgO, major element compositions from this study).

ANALYTICAL METHODS

Sample collection and Preparation

Sample locations of each flow (Figure 3) were selected in attempt to represent the entire spatial distribution of the three volcanic units as mapped by Hildreth et al. (2003). Some areas are not accessible and small gaps in sample distribution exist. In general, samples were collected from outcrops that are tabular to massive single or stacked flows with minor iron staining on joint surfaces. Samples with visual evidence of weathering textures were avoided in the field. Samples were crushed by hand and each piece selected for chemical analyses was closely examined for evidence of alteration and weathering. A minimum of 50 g of hand-selected crushed pieces were chipped by a Chipmunk Crusher equipped with tungsten carbide crushing plates and then prepped for XRF and ICP-MS analyses.

XRF

Seventeen samples were analyzed at the Washington State University (WSU) GeoAnalytical Laboratory for major element oxides and eighteen trace elements (Sc, V, Ni, Cr, Ba, Sr, Zr, Y, Rb, Nb, Ga, Cu, Zn, Pb, La, Ce, Th, Nd), using a ThermoARL Advant'XP+ sequential wavelength dispersive X-ray fluorescence spectrometer. Analytical methods, accuracy and precision are described by Johnson et al. (1999). Rock powders were prepared at Western Washington University (WWU) by grinding fresh rock chips in a tungsten carbide shatterbox for 4 minutes. The glass beads were prepared by fusing a 2:1 ratio of dry flux to dry rock powder in a pre-heated furnace at 1000° C for 10 minutes. Beads were then

reground in the tungsten carbide shatterbox, and re-fused as above to ensure complete homogeneity. A more detailed outline of sample preparation can be found in Appendix 1.

ICP-MS

Thirty two samples were analyzed at the WSU GeoAnalytical Laboratory for 14 rare earth elements (REE) and 13 additional trace elements (Ba, Th, Nb, Y, Hf, Ta, U, Pb, Rb, Cs, Sr, Sc, Zr) using an Agilent 4500+ Inductively Coupled Plasma Mass Spectrometer (ICP-MS). Samples were prepared at WWU according to the following protocol. Crushed rock material was ground to a fine powder in an alumina-ceramic shatterbox for five minutes. Glass beads were prepared by fusing a 1:1 ratio of dry flux to dry rock powder in a pre-heated furnace at 1000° C for 10 minutes. Beads were then reground to a fine powder in the alumina ceramic shatterbox to ensure homogeneity. A detailed description of sample preparation can be found in Appendix 1. Analytical techniques, accuracy and precision for the ICP-MS analyses, are available from the WSU GeoAnalytical Laboratory at (http://www.sees.wsu.edu/Geolab/note/icpms.html).

Electron Microprobe

Compositions of olivine, pyroxene, plagioclase, and Fe-Ti oxide minerals were determined by electron microprobe analyses of nine polished thin sections (3 thin sections for each unit). Thin sections used for microprobe analyses were chosen to represent all minerals and the range of textures observed in each unit. Analyzed minerals were selected in an attempt to collect data from the entire size and textural range observed in each thin section.

The analyses were performed in the Electron Microprobe Laboratory at the University of Washington, using a JEOL Superprobe 733 electron microprobe equipped with 4 wavelength dispersive spectrometers (WDS) and an energy dispersive spectrometer (EDS). Calibration was performed using a standardized set of natural and synthetic minerals. An accelerating voltage of 15 kV was used for all minerals. A 3μ beam diameter with a beam current of 10nA was used for feldspar analysis while a beam diameter of <1μ and a beam current of 15nA was used for analyses of olivine, pyroxene and oxide minerals. Peak counting times range from 20-40 seconds and are dependent on how long it took to achieve a 0.4% statistical error. Analytical error is < 3% for major elements and < 8% for minor elements. ZAF corrections were applied to the data based on the methods of Armstrong (1988), and Fe-Ti oxides were further corrected using the methods of Evans et al. (2006).

PETROGRAPHY AND MINERAL CHEMISTRY

Introduction

In general, mineral chemistry coupled with textural relationships are complex and highly variable in all units. For example, it is not uncommon to see highly corroded phenocrysts with strong chemical disequilibrium textures situated adjacent to a phenocryst of the same variety in semi pristine condition. Petrographic characteristics of each unit are summarized in Table 1. Compositions of each phenocryst phase tend to have compositional similarity between units and wide compositional ranges within units (Figures 4A, 4B, 4C and Tables 2-5).

Sulphur Creek Basaltic Andesite

The Sulphur Creek unit is porphyritic to strongly porphyritic with 20-50% phenocrysts and microphenocrysts in a hypocrystalline to cryptocrystalline groundmass. Plagioclase constitutes 65-80% of the phenocryst and microphenocryst population and occurs as 0.5-3.5 mm sub- to euhedral columnar crystals. Equant to elongate orthopyroxene phenocrysts and microphenocrysts account for 5-20% of the phenocryst population and are 0.5-3.0 mm in length. Clinopyroxene accounts for 5-15% of the phenocryst population and are also 0.5-3.0 mm in length. Clinopyroxene phenocrysts occasionally show ophitic textures with intergrowths of plagioclase grains. The Sulphur Creek unit is characteristically rich in olivine phenocrysts and microphenocrysts compared to the other units at 5-15% of the phenocryst population. Olivine crystals are typically 0.5-2.5 mm in length and are sub- to euhedral hopper-shaped crystals. The groundmass is composed of 70-90% pilotaxitic

plagioclase, 2-10% olivine and 2-10% orthopyroxene with 1-5% glass. An assortment of oxide minerals make up 1-2% of the Sulphur Creek unit and occur as groundmass phases or as inclusions in phenocrysts.

Olivine phenocrysts are typically isolated and often reveal normal and complicated zoning patterns. Two grains with multiple point analyses (SC-7TB Oa and SC-6TB Oa) show oscillatory zoning patterns with compositional reversals where Fo compositions increase from Fo_{80} and Fo_{84} in the cores to Fo_{84} and Fo_{86}, respectively, in the middle section of the transect and then decrease to Fo_{77} and Fo_{78} at the rim, respectively (Table 4). Nearly half of the olivine crystal population displays varying degrees of chemical disequilibrium textures that are shown as corroded and embayed grain boundaries (Figure 5). Less commonly, disequilibrium textures include grains that are mantled with orthopyroxene and plagioclase microphenocrysts. Nearly all olivine crystals have inclusions of Fe-Ti oxide minerals while only some have Cr spinel inclusions. Olivine core compositions are in the range of Fo_{86-64} and rim compositions are in the range of Fo_{77-65} where compositions decrease by Fo_{1-14} from core compositions to rim in normally zoned grains. Sulphur Creek olivine phenocrysts can be distinguished from those of Glacier Creek and Boulder Glacier by characteristically high CaO concentrations with an average value of 0.21 wt. % CaO. An olivine groundmass grain in sample SC-6TB has a composition of Fo_{60}, which is lower then the compositional range of olivine phenocrysts.

Clinopyroxene and orthopyroxene phenocrysts display similar textures. Nearly all pyroxene phenocrysts contain inclusions of Fe- Ti oxides while 50% display disequilibrium textures such as corroded and embayed rims (Figure 5). In contrast to olivine and

plagioclase, pyroxene compositions in the Sulphur Creek unit are homogenous. Orthopyroxene compositions are $Wo_{3-4}En_{65-70}Fs_{26-31}$ with Mg#'s (Mg# =100 x (Mg / Mg + Fe*)) of 67-73. Clinopyroxene compositions are $Wo_{39-41}En_{42-43}Fs_{15-17}$ with Mg#'s of 70-75. Two clinopyroxene grains with core and rim analyses showed an average decrease of in Mg# of 3 between the core and rim.

The majority of plagioclase phenocrysts and microphenocrysts, 90%, display moderate to weak patchy concentric normal zoning patterns, yet oscillatory and reversed chemical zoning patterns were observed in some phenocrysts with multiple point analysis transects. Microphenocrysts (0.5-1.0 mm) are mostly inclusion free, while the larger crystals (> 1 mm) contain inclusions of Fe-Ti oxides. About 70% of the plagioclase phenocryst population displays reaction textures such as sieved rims and/or cores, and embayed and corroded rims (Figure 5). Microphenocrysts display similar textures but with less frequency. Phenocrysts compositions are in the range of An_{47-70} with An_{51-70} cores and An_{47-62} rims. Normally zoned plagioclase phenocrysts decrease by an average of An_6 from core to rim. Plagioclase microlites in the groundmass range in composition from An_{45-57} and are comparable to compositions of phenocryst rims. Overall, plagioclase compositions and textures are highly variable and complex.

Oxide minerals in the Sulphur Creek unit are represented by Cr-spinel and ulvospinel. Both types of oxide minerals are < 0.5 mm in diameter. Chromium spinel minerals occur as a groundmass phase while ulvospinel occur as a ground mass phase and as inclusions in all phenocryst varieties. Ulvospinel has compositions in the range of 69.0-79.3 wt. % FeO* and 18.8-20.1 wt. % TiO_2.

Glacier Creek Andesite

The Glacier Creek unit is strongly porphyritic with 47-61% phenocrysts and microphenocrysts in a holocrystalline to cryptocrystalline groundmass. Plagioclase dominates the phenocryst and microphenocryst population at 70-73% of all phenocrysts and occurs as sub- euhedral, equant to elongate crystals. The Glacier Creek unit is distinctive in that plagioclase phenocrysts tend to have a bimodal size distribution. Approximately 25% of crystals are 1.2-4.2 mm in diameter while the remaining population is 0.1-0.8 mm in diameter. Olivine, the next most abundant phenocrysts phase accounts for 11-12% of the phenocrysts population as sub- to euhedral, granular or hopper shaped crystals that are in the size range of 0.5-3.0 mm. Orthopyroxene accounts for 7-10% of the phenocryst population and occurs as 0.1-2.0 mm sub-euhedral, rounded prismatic to elongate crystals. Clinopyroxene constitutes 7-8% of the phenocrysts population and shares the same textural attributes as the orthopyroxene phenocrysts. The groundmass includes pilotaxitic and sometimes trachytic plagioclase laths with minor (<1%) orthopyroxene and glass. Fe-Ti oxides account for 1-2% of the Glacier Creek unit and occur as a groundmass phase, a phenocryst phase or as inclusions in phenocrysts. Occasional apatite is observed in the groundmass, and accounts for < 0.5% of the crystal population in the Glacier Creek rocks.

Olivine exists as a sparsely distributed phenocryst phase in the Glacier Creek unit. Phenocrysts often contain inclusions of Fe-Ti oxides and commonly contain wormy fracture patterns that are filled with iddingsite. Nearly all olivine phenocrysts display weak to strong chemical disequilibrium textures that are dominated by rounded and embayed grain boundaries (Figure 5). Also, phenocrysts are often surrounded by microphenocrysts of

plagioclase and orthopyroxene. The majority of grains analyzed display normal chemical zoning patterns, however, some phenocrysts with reverse zoning patterns are observed. Olivine compositions fall in the range of Fo_{86-68} with core compositions of Fo_{86-68} and rim compositions of Fo_{79-68}. Normally zoned olivine phenocryst compositions decrease by an average of Fo_5 from the core to the rim. Glacier Creek olivine phenocrysts have a bimodal size distribution. The larger (> 1.0 mm) olivine phenocryst population represents 50% of the olivine phenocrysts and tends have more primitive core compositions (3 at Mg# ~86). The larger olivine population is also characterized as having pronounced disequilibrium textures compared to the small variety. The smaller olivine (< 1.0 mm) population represents the other half of the olivine population and tends to have more evolved core compositions where the majority of compositions are below Mg# 78 but are within the range of Mg# 68-82. The olivine phenocrysts in the Glacier Creek unit can be distinguished from olivine phenocrysts in the other units by elevated concentrations of NiO with an average of 0.26 wt. %, compared to 0.12 and 0.10 wt. % in the Sulphur Creek and Boulder glacier units, respectively.

Orthopyroxene and clinopyroxene phenocrysts share similar textures. Nearly all pyroxene phenocrysts have inclusions of Fe-Ti oxides and display weak to moderate disequilibrium textures such as rounded and embayed grain boundaries (Figure 5). Orthopyroxene phenocrysts are sometimes ophitic with plagioclase microphenocrysts. Orthopyroxene in the Glacier Creek Andesite has compositions of $Wo_{3-4}En_{56-71}Fs_{26-40}$ with Mg#'s of 64-77. Groundmass orthopyroxene is within the compositional range of the orthopyroxene phenocryst compositions. Clinopyroxene compositions are in the range of $Wo_{40-43}En_{41-43}Fs_{15-19}$ with Mg#'s of 68-74 with one groundmass grain at Mg# 71.

Plagioclase phenocrysts are dominated by disequilibrium textures such as embayed or resorbed rims and sieve textures. While these textures are less pronounced in smaller grains, they are more pervasive in larger grains. Sieve patterns are particularly complex with some grains containing sieved and corroded cores and intact rims, while others have sieved outer rims with pristine cores (Figure 5). Nearly all plagioclase phenocrysts display simple patchy normal concentric zoning patterns while some samples (GC-6TB Pb and GC-12TB Pa) show complex oscillatory or reverse zoning patterns. Plagioclase phenocryst compositions are in the range of An_{45-75} with core compositions of An_{45-75} and rim compositions of An_{45-61}. Normally zoned plagioclase phenocrysts decrease by an average of An_9 from core to rim. Plagioclase groundmass compositions are slightly more sodic than phenocryst compositions and are in the range of An_{43-51}.

Fe-Ti oxide minerals in the Glacier Creek lavas exists as isolated grains of ulvospinel and ilmenite, as coexisting pairs, or as inclusions of either mineral in all phenocryst phases. Ulvospinel has compositions of 73.1-83.4 wt. % FeO* and 4.7-16.4 wt. % TiO_2. Ilmenite compositions have compositions of 43.5-53.3 wt. % FeO and 36.9-49.3 TiO_2.

Boulder Glacier Andesite and Dacite

The Boulder Glacier lavas are strongly porphyritic with 50-60% phenocrysts. Plagioclase is the dominant phenocryst and microphenocryst phase at 65-90% of the phenocryst population and is characterized by 0.2-3.5 mm, sub- to euhedral, equant to elongate crystals. Orthopyroxene is the second most abundant phenocryst phase at 7-30% and occurs as 0.1-2.0 mm equant, prismatic and elongate, sub- to euhedral crystals.

Clinopyroxene accounts for 1-10% of the phenocryst population and is 0.1-1.5 mm. Clinopyroxene occurs as prismatic and, to a lesser degree, elongate, sub- to euhedral crystals. Olivine is observed as a minor phase (<1%) in six of the eleven Boulder Glacier samples. When present, it is characterized by 0.5-1.5 mm hopper or granular shaped phenocrysts. Apatite microphenocrysts were observed in some samples in trace amounts (<1%). The groundmass is composed of 95% intragranular pilotaxitic plagioclase with ~5% orthopyroxene. Fe-Ti oxide minerals occur as a groundmass and minor phenocryst phase and account for 2% of the crystals in the Boulder Glacier lavas.

Olivine was analyzed in only one sample (BG-3TB) in the Boulder Glacier lavas. The olivine phenocryst has a core composition of Fo_{74} and a rim composition of Fo_{72}. Compared to smaller grains, larger grains display strong reaction textures (Figure 5). Olivine phenocrysts are often mantled by plagioclase and orthopyroxene, contain inclusions of Fe-Ti oxide minerals and have a wormy fractured texture with iddingsite occupying the fractures.

Orthopyroxene has compositions of $Wo_3En_{60-63}Fs_{33-37}$ with Mg#'s of 62-66. Clinopyroxene has compositions of $Wo_{42-43}En_{40-41}Fs_{33-37}$, with Mg#'s of 70-73. Most pyroxene phenocrysts contain inclusions of Fe-Ti oxide minerals and plagioclase, while elongate crystals are sometimes ophitic with plagioclase. Forty percent of the pyroxene phenocrysts display moderate disequilibrium textures such as embayed rims and rounded corners (Figure 5).

Textures in plagioclase phenocrysts are dominated by chemical disequilibrium textures such as sieve textures and/or embayed rims (Figure 5). Sieve patterns are often observed in or near the core of crystals and are bounded by intact rims. In rare cases,

plagioclase grains are skeletal and have been replaced with plagioclase microphenocrysts, opaque minerals and minor pyroxene. Most phenocrysts have normal chemical zoning patterns however one phenocryst in sample BG-7TB displays oscillatory zoning patterns. Inclusions of Fe-Ti oxide minerals occur in most crystals, but are more abundant in phenocrysts greater than 1 mm. Plagioclase phenocrysts compositions have a range of An_{32-62}. Core compositions are in the range of An_{52-62} while rim compositions have a range of An_{42-52}. Normally zoned plagioclase phenocrysts decrease by an average of An_9 from core to rim. One plagioclase grain in sample BG-10TB considered to be part of the groundmass has a composition of An_{32} which is significantly more sodic than any phenocrysts.

Ulvospinel and ilmenite occur in the Boulder Glacier lavas as coexisting pairs or as isolated crystals in the groundmass or as inclusions in plagioclase, pyroxene and olivine phenocrysts. Ulvospinel grains have compositions of 75.2-78.0 wt. % FeO* and 12.2-14.1 wt. % TiO_2. Ilmenite has compositions of 45.1-49.8 wt. % FeO and 43.0-46.8 wt. %.

Crystal Clots

Cumulophyric crystal clots are a common feature noted in the units studied in this paper and are a topic of discussion of several other authors who studied the petrography of the Mount Baker lavas (Coombs, 1939; Stavert 1971; McKeever, 1977; Swan, 1980; Green, 1988 and Hildreth et al. 2003). The clots can be large enough to see in hand sample and are a distinct feature when viewed in thin section. Cumulophyric crystal clots and glomerocrysts seem to be common in Cascade lavas and have been noted by several authors at other locations such as Glacier Peak (Taylor, 2001). However, there is little interpretation on the

origin of this distinct texture.

Two types of crystal clots with distinct phase components and textural characteristics are identified in this paper. The type of clots commonly found in the Sulphur Creek lavas are characterized by clusters of plagioclase + orthopyroxene + clinopyroxene ± olivine that are <1mm-15mm in diameter. The Andesite of Glacier Creek lacks the type found in the Sulphur Creek unit, however, crystal clots with cores of Fe-Ti oxides and rims of granular orthopyroxene + plagioclase microphenocrysts are found in about half of the samples. The Boulder Glacier lavas contain two populations of crystal clots. One population is similar to, but less abundant than the plagioclase + orthopyroxene + clinopyroxene ± olivine cumulophyric crystal clots observed in the Sulphur Creek lavas. The second population is observed in nearly every thin section and is similar to the variety noted in the Glacier Creek lavas, but is more abundant and is characteristically oval shaped.

MAJOR AND TRACE ELEMENT WHOLE ROCK CHEMISTRY

Introduction

Whole rock major, minor and trace elements analyzed in this study are presented in Table 6 and in SiO_2 variation diagrams in Figures 6A and 7. The units in this study are all medium K and calk-alkaline (Figure 6). Major element compositions range from basaltic andesite to dacite and have distinct silica ranges for each individual unit (Figures 6A and 7). Trace element concentrations are enriched in large ion lithophile (LILE) compared to primitive mantle compositions of Sun and McDonough (1989) such as Rb, Ba, Th, and K, coupled with a pronounced Nb-Ta trough (Figure 8). Some LILE correlate with SiO_2 between units while others do not (Figures 8 and 9). Between units, REE concentrations do not correlate with a typical fractionation trend of increasing REE concentrations with SiO_2 (Figure 10).

The following sections describe the whole rock chemistry for each individual unit in detail and discuss distinct characteristics of each unit relative to the others.

Sulphur Creek Basaltic Andesite

The Sulphur Creek unit is the most mafic in the suites of samples analyzed and has the lowest SiO_2 values in the range of 52.5-55.8 wt. %. All samples are classified as medium-K basaltic andesites based on the criteria of Gill (1981) (Figure 6a). Concentrations of TiO_2, FeO*, MgO, Na_2O, Al_2O_3 and CaO decrease with increasing SiO_2 and form near linear trends (Figure 7). K_2O concentrations vs. SiO_2 also form a sub-linear trend, and increase with increasing SiO_2. Mg#'s are tightly clustered in the range of 57-58. Although

increase with increasing SiO_2. Mg#'s are tightly clustered in the range of 57-58. Although the Sulphur Creek unit has the lowest SiO_2 concentrations, it has intermediate Mg#'s compared to the andesite of Glacier Creek and the andesite and dacite of Boulder Glacier (Figure 7).

The primitive mantle normalized multi-element spider diagram (Figure 8) shows that the samples of Sulphur Creek are distinguished from the samples of Boulder Glacier and Glacier Creek by relative depletion in some large ion lithophile elements (LILE) such as Rb, Ba and K and enrichment in most high field strength elements (HFSE) such as P, Sm, Eu, Tb, Yb and Ti (Figure 8). Other distinct trace element characteristics of the Sulphur Creek unit include enrichment in Sc, V, Cr, Y and Tm for a given SiO_2 concentration relative to the other units (Figure 9, Sc, V and Tm are not shown). Trace elements and REE's correlate fairly well with SiO_2 and generally form sub linear trends with increasing or decreasing concentrations depending on the element (Figures 8, 9 and 10).

REE patterns for the Sulphur Creek unit are distinguished from the other units by their higher concentrations of the middle REE's (Eu-Ho, 11-33 x chondrites) and heavy REE's (Er, Yb, and Lu, 7-11 x chondrites) (Sun and McDonough, 1989) (Figure 10). The Sulphur Creek unit is unlike the other units in that it has the flattest REE slopes, with an average $(La/Yb)_N$ of 4.7 where Glacier Creek and Boulder Glacier units average 6.7 and 6.3 respectively. Within-flow variations are characterized by slightly increasing LREE concentrations with increasing SiO_2 and decreasing HREE concentrations with increasing SiO_2 (Figure 10). Eu anomalies in the Sulphur Creek unit are either very weakly negative or non existent.

Whole rock chemistry, including both trace element and major element concentrations reveal a compositional gap between two chemically distinct groups within the Sulphur Creek unit (Figures 6A, 6B, 7, 8, 9 and 10). The groups can be divided into a mafic group and a more felsic group based on the following criteria. The mafic group has SiO_2 concentrations in the range of 52.5-53.5 wt. % and ~5.5 wt. % MgO. The felsic group has SiO_2 concentrations in the range of 55.2-55.8 wt. % and MgO concentrations in the range of 4.5-4.9 wt. %. Trace element concentrations also distinguish the two groups. The mafic group has lower abundances of LILE such as Rb, Ba, Th, K and higher abundances in less compatible elements such as Ti and Tb compared to the more felsic group (Figure 8). These two subgroups are separated spatially, with the more mafic samples located on the most distal portions of the lava flow on the east side of Baker Lake (Figure 2). The more felsic samples occupy the rest of the flow and samples with compositions in between the sub groups have not been observed. The same chemical grouping and spatial relationship can be observed in whole rock data and sample locations presented by Hildreth et al. (2003). The petrologic relationship between these two groups will be discussed in a later section of this paper.

Glacier Creek Andesite

The Glacier Creek unit is classified as medium K andesites (58.3-58.7 wt. % SiO_2) based on the criteria of Gill (1981). Compositions of all major elements are tightly clustered on SiO_2 variation diagrams with elevated MgO (4.6-4.9 wt. % MgO) concentrations for a given SiO_2 concentration, relative to the Sulphur Creek and Boulder Glacier units (Figure 7).

Mg#'s in the Glacier Creek andesite samples have the highest values of the three units, but with intermediate SiO_2 compositions relative to the other units. Like major element concentrations, Mg#'s also have a small range of values and tightly cluster between Mg# 63-64 (Figure 7).

The mantle normalized multi-element spider diagram (Figure 8) shows characteristic depletion in most HFSE (Zr, Hf, Tb, Ho, Yb and Lu). Other notable trace element features include elevated abundances of Ni (67-82 ppm), Cr (89-100 ppm) and Sr (841-866 ppm) and depleted concentrations of Y (18 ppm) relative to the Sulphur Creek and Boulder Glacier units for a given concentration of SiO_2 (Figures 8 and 9). Like major element concentrations, a defining characteristic of the Glacier Creek samples is a small range of concentrations for most trace elements, excluding Ni, Cu and Ga.

REE concentrations form concave up patterns on the chondrite-normalized diagram for HREE's at 10-30 times chondrite values of Sun and McDonough (1989), with concave down patterns for LREE's at 40-60 times chondrite values (Figure 10). REE abundances lack correlation with SiO_2 (Figure 10). REE patterns lack Eu anomalies and can be distinguished from the Sulphur Creek and Boulder Glacier units by having the lowest overall REE abundances and the steepest slopes with an average chondrite normalized La/Yb of 6.7.

Boulder Glacier Andesite and Dacite

The Boulder Glacier unit is the most Si-rich unit considered in this study and samples are classified as medium-K and to a lesser degree, high-K andesites and dacites (Figures 6A and 6B). SiO_2 concentrations are in the range of 60.2-64.2 wt. %. The remaining major

element concentrations, excluding Al_2O_3, form clear trends with increasing SiO_2 that are continuous with trends formed by the Sulphur Creek unit (Figures 7). Mg#'s for the Boulder Glacier unit are relatively low with a range of Mg# 50-57 (Figure 7).

The mantle normalized multi-element spider diagram (Figure 8) shows that the Boulder Glacier unit has higher abundances in several LILE (Rb, Ba, Th, K, La, Ce) and lower abundances in some HFSE (P and Ti) relative to the Sulphur Creek and Glacier Creek units (Figure 8). The Boulder Glacier unit has distinct compositions of some trace elements such as lower abundances of Ni and Cr and higher abundances of Rb and Ba relative to the Sulphur Creek and Glacier Creek units (Figures 8 and 9). Most trace elements correlate fairly well with SiO_2 concentrations; however, there are some exceptions such as Ga, Tm and Pb (Table 6).

The Boulder Glacier unit displays the widest range of REE concentrations among the three units in this study (Figure 10). REE patterns are distinguished from other units by having high abundances of LREE, with La concentrations of 75-105 times chondrite values of Sun and McDonough (1989). LREE concentrations form concave down patterns while HREE patterns are concave up with intermediate abundances relative to HREE abundances of the other units. The Boulder Glacier unit is also characterized by having the most pronounced negative Eu anomaly among the three units, with values of Eu at 19-24 times chondrite values of Sun and McDonough (1989). Within flow REE concentrations lack any systematic variation with SiO_2 (Figure 10), however there is a weak correlation in some element abundances such as increasing Sm, Eu, and Y with increasing SiO_2 (Figures 9 and 10).

DISCUSSION

Intensive parameters

The Fe-Ti oxide geothermometer of Andersen and Lindsley (1985) was used to constrain liquidus temperatures and assess fO_2 conditions for the Mount Baker magmatic system. Coexisting ulvospinel and ferian ilmenite were found in both the Glacier Creek lavas and the Boulder Glacier lavas; however, coexisting Fe-Ti oxide pairs were not observed in the lavas of Sulphur Creek. Prior to calculating temperatures and fO_2 conditions, Fe-Ti oxide pairs were tested for equilibrium following the methods of Bacon and Hirschmann (1988), and only oxide pairs determined to be in or near equilibrium were used for the calculations. ILMAT (Lepage, 2003), a worksheet for ilmenite-magnetite geothermometry and barometry was used to carry out the equilibrium calculations. Results presented here are from calculations based on the methods of (Andersen and Lindsley, 1985 and Anderson et al., 1993). ILMAT also calculates the concentrations of Fe^{3+} prior to equilibrium calculations. Coexisting oxide pair chemistry along with the calculated liquidus temperatures and fO_2 conditions are displayed in Table 7. Calculated fO_2 conditions are oxidizing at values slightly above or below the nickel-nickel-oxide buffer (Table 7 and Figure 11) with a range of -13.9 to -14.8 log units from the quartz-fayalite-magnetite buffer for the Glacier Creek unit and a range of -11.2 to -12.2 for the Boulder Glacier unit. Calculated liquidus temperatures for the Glacier Creek unit are in the range of 745-827°C while temperatures for the Boulder Glacier unit are calculated in the range of 882-924°C (Table 7 and Figure 11). Errors using Fe-Ti oxide pairs for fO_2 calculations are ± 0.1 log units and errors for temperature calculations are ± 10°C (Anderson et al., 1993).

Estimation of liquidus temperatures for coexisting pyroxene pairs is also possible based on the methods described by Andersen and Lindsley (1985) and is applied using the QUILF software package of Anderson et al. (1993). A total of six temperatures are presented with two for each unit discussed in this paper. Equilibrium condition of the pyroxene pairs was taken into consideration during the selection of pyroxene analyses and was based on the difference in Mg# (ΔMg#), between each component of the coexisting pairs. Pyroxene pairs generally have a ΔMg# <3; however, due to limited pyroxene data for sample BG-3TB a ΔMg# of 5 was used, which may represent disequilibrium conditions.

Since pressure condition estimates in the Mount Baker magmatic system are unavailable, values reported here are calculated at an estimated pressure of 3 kbar. The effect of deviating ± 1.5 kbar from the estimated 3 kbar was tested and found to produce < ± 6°C difference in the calculated temperatures. The Sulphur Creek basaltic andesites yield the widest range of pyroxene temperatures including the hottest temperature, which is expected for this relatively mafic unit, at values of 999°C for SC-6TB and 1027°C for SC-3TB (Table 7). The intermediate andesites of Glacier Creek yielded a tight range of intermediate values at 1013°C for sample GC-6TB and 1015°C for sample GC-12TB (Table 7). The more silicic lavas of Boulder Glacier yielded relatively low temperatures at 994°C for sample BG-3TB and 983°C for sample BG-7TB (Table 7). Errors for all temperatures calculated form pyroxene pairs are estimated to be ± 10°C.

Sisson and Grove (1993) observe the liquidus temperature of both oxide minerals and pyroxene in several melting experiments. Pyroxene liquidus temperature discussed by Sisson and Grove (1993) are around 1050°C in hydrous high alumina basalts. Magnetite generally

has a liquidus temperature below 1000°C but not lower then 960°C. Also noted by Sisson and Grove (1993) is the effect that H_2O contents can have on the crystallization temperature of oxide minerals where dryer melts can crystallize oxide minerals up to 275° below the oxide liquidus of the melt.

Both oxide mineral and pyroxene liquidus temperatures (Table 7) in the units studied here are slightly lower compared to experimentally determined temperatures. One explanation for lower temperatures may be the influence or lack of magmatic water in the Mount Baker system. Sisson and Grove (1993) indicate that magmatic water plays an important role and dryer conditions may lower the liquidus temperature of certain phases. Another possibility for the relatively low temperatures is that the Fe-Ti oxide minerals and pyroxenes have experienced post crystallization re-equilibration.

Petrologic Relationships

Introduction

In order to provide a complete picture of intermediate lava generation associated with the units discussed, a two tiered approach is applied. Discussed first are petrologic relationships *between* the units to determine whether or not they could be genetically related. The second approach highlights and discusses the differentiation processes responsible for chemical variations *within* each specific unit. This more focused approach allows for analysis of the origin of each unit and provides insight into the development of each unit's characteristic chemical features.

Petrologic Relationships Between Units

Major and trace element variations between the Sulphur Creek, Glacier Creek and Boulder Glacier units cannot be related by pure crystal fractionation processes based on the following data: 1) The presence of two chemically distinct andesite types, 2) Failed major and trace element fractionation modeling, 3) Mineral textures and chemical relationships that are inconsistent with fractionation processes. The following is a discussion of the above data in detail.

Samples with intermediate compositions (57-63 wt. % SiO_2) can be separated into two andesite types. Type 1 includes the Andesite of Glacier Creek, which is characterized by elevated MgO concentrations (4.6-4.9 wt. %), very low variability in major and trace element concentrations, and depletion in nearly all REE concentrations with elevated La/Yb. Type 2 includes the andesite and dacite of Boulder Glacier, which is characterized by comparatively low MgO concentrations (2.1-3.3 wt. %), sub-linear trends on element variation diagrams that appear continuous with the lavas of Sulphur Creek, and relatively enriched REE concentrations. These two separate andesite types cannot be produced by closed system crystal fractionation from the same mafic parent.

The existence of multiple types of andesite at other Cascade volcanoes has been attributed to an assortment of open system possibilities that include mixtures of crustal melts and various mafic to intermediate magmas (Clynne, 1999, Bullen et al., 1990). More complicated processes have been proposed that include the deep crustal hot zone model proposed by Annen et al. (2006) or the deep crustal melting assimilation storage and homogenization (MASH) model presented by Hildreth and Moorbath (1988). Hildreth

(2007) also discusses the MASH model in the context of the Cascades. Other authors have described lavas that have been modified by assimilation of crustal material (Mason et al., 1996) or assimilation mafic-ultramafic crystal debris (Streck et al. 2007, Arculus, 1983).

Alternatively, the Glacier Creek and Boulder Glacier units may be the fractionated products of two unique parental magmas. If so, a suitable parental magma for the relatively high-magnesium Glacier Creek andesite must also be inherently enriched in MgO, Ni and Cr compared to the parent magma for the andesites of the Boulder Glacier unit. The description of a compositionally heterogeneous mantle that is presumed to be the source of various types of parental magmas is a common theme in the Cascade arc (Green and Harry, 1999, Bacon et al. 1997, Leeman et al., 2005, Green and Sinha, 2005). Glacier Peak, Mount Baker's neighboring volcano to the south was found to have at least three chemically distinct parental magmas (Taylor, 2001). The variety of mantle sources at Mount Baker has yet to be constrained and the existence of multiple basalt types remains a possibility based on the existence of two genetically different andesites.

MELTS, a crystal fractionation model was applied to this suite of rocks utilizing whole rock major element compositions. MELTS (Ghiorso et al., 1993) is a thermodynamic model that considers fO_2, H_2O and pressure conditions of a fractionating system while estimating the compositions of coexisting melts and solid phases for realistic geologic systems. Appendix 3 includes a full description of the application of the MELTS model. In summary, fractionation of the most mafic Sulphur Creek sample according to major elements (bsc 442 from Hildreth et al., 2003) consistently produced intermediate compositions that are not in the range of observed Glacier Creek and Boulder Glacier andesite compositions. The

MELTS results produced compositions that have higher concentrations of Na_2O, P_2O and MnO and lower concentrations of MgO and CaO compared to compositions observed in other Mount Baker andesites (Figure A1 and Table A2).

A crucial test for fractionation processes in a suite of rocks should include application of the Rayleigh fractionation model. The Rayleigh equation is effective in predicting trace element behavior in a magmatic system based on the modal mineralogy and associated crystal/liquid partition coefficients (Kd's) (Arth, 1976).

As shown in Figure 12, the Rayleigh fractionation equation was used to model progressive crystal fractionation of the most mafic sample according to REE's in the Sulphur Creek suite (Qbsc-4). Starting compositions are different in REE models compared to major element models because REE data is not available for sample bsc-442. The modeled REE concentrations are compared to observed REE concentrations of the intermediate lavas of Glacier Creek and Boulder Glacier to test if either of these suites can be produced by this particular crystal fractionation model. A fractionating assemblage of Plg + Opx + Olv + minor Fe-Ti Oxides ± Cpx minerals (mineral mode is dependent on sample used) along with published Kd's (Table A1) consistently produces increasing REE concentrations with increasing values of *F* (% crystallization) while REE pattern slopes ($[La/Yb]_N$) remain nearly constant (Figure 12A). Conversely, observed REE abundances decrease between the Sulphur Creek basaltic andesites and the more silicic andesites of Glacier Creek and Boulder Glacier (Figure 10 and 12A). This observed relationship of decreasing REE with increasing SiO_2 precludes a simple fractionation model involving only pyroxene, olivine, and plagioclase.

Decreasing REE concentrations with degree of differentiation have been attributed to

the fractionation of mineral phases that have high REE Kd values. An example is apatite, which has proportionally high Kd values for the mid to heavy REE's in andesite compositions (Kd=10-100, Table A1, Fujimaki, 1986). Garnet also has high Kd values for the mid to heavy REE's for basalt and andesite compositions (Kd=1-60, Table A1). Hornblende has moderately high Kd values for the mid REE's in basalt and andesite compositions (Kd=1-2, Table A1) and is often considered a cryptic fractionating phase (Davidson et al., 2007). In minor amounts (<1-5% mineral mode %), these minerals can have a dramatic effect on REE depletion during fractionation and certain combinations can produce depleted REE patterns in evolved compositions.

Hornblende was not observed in any samples in this suite of rocks, but has been observed in pre-late Pleistocene units associated with the Mount Baker volcanic field by Hildreth et al. (2003). Modal hornblende proportions are not available in the above reference, but its presence in older Mount Baker effusives may suggest a cryptic amphibole component in differentiation (Davidson et al., 2007). Apatite was also observed in trace amounts (< 0.5%) in some Glacier Creek and Boulder Glacier samples. Garnet has not been observed in any Mount Baker eruptive units and therefore has been ruled out as a possible fractionating phase.

An alternative REE Rayleigh fractionation model considering the effects of hornblende and apatite is shown in Figure 12B. Starting compositions are taken from sample Qbsc-4. Fractionating proportions are similar to observed proportion, but have been slightly adjusted to add hornblende as a major fractionating phase. Fractionating proportions are 50% plagioclase + 30% hornblende + 10% olivine + 9.5% orthopyroxene + 0.5% apatite.

Several published sets of kd's for hornblende (Fujamaki 1984, Sisson 1994) were applied to the model and kd's used in the model in Figure 12B are those of Fujamaki (1984). This particular model shows that even with excessive amounts of hornblende and apatite as a fractionating phase, the depleted REE concentrations of the Glacier Creek and Boulder Glacier units can not be reproduced. Even with the addition of hornblende and apatite, modeled REE concentrations increase with differentiation.

In summary, pure crystal fractionation does not seem to be a reasonable way to produce either of the intermediate andesite suites (Glacier Creek or Boulder Glacier) from the basaltic andesites of Sulphur Creek.

Disequilibrium mineral textures are a common characteristic of each unit in this study. Textures observed include phenocrysts with a bimodal size and composition distribution with reaction textures and complex zoning patterns (Figure 5 and Table 1). These reaction textures contradict a crystal fractionation model where crystallizing phases are in chemical equilibrium with the host liquid. A common explanation of similar textures has been attributed to magma mixing processes (Eichelberger, 1975).

Sulphur Creek Basaltic Andesite

Previously, the Sulphur Creek basaltic andesite has been described as the result of a magma mixing process between basalt and basaltic andesite (Green, 1988). This conclusion was drawn from chemical and textural relationships manifested in basaltic inclusions that are sparsely distributed throughout the basaltic andesite. Interpretations of geochemical data presented within this study support an alternative mixing model for the Sulphur Creek unit

that calls upon a felsic end-member component similar to the dacite of Boulder Glacier.

Within-flow chemical variations in the Sulphur Creek unit have led to the characterization of two chemically distinct sub-groups (Figure 13A). As discussed above, Raleigh fractionation of observed modes of plagioclase + clinopyroxene + orthopyroxene + olivine from compositions in the mafic group predicts increasing abundances in all REE (Figure 12A). The model is inconsistent with the actual lower mid-heavy REE abundances in the more felsic group (Figure 13A), and suggests that the two Sulphur Creek units are not related by pure crystal fractionation. Furthermore, the well defined compositional gap between the two subgroups seems to contradict a continuous crystal fractionation processes.

As discussed above, cryptic hornblende fractionation has been considered an important role in arc volcanoes. An alternative REE model attempting to relate the two Sulphur Creek subgroups through crystal fractionation that includes hornblende as a fractionating phase is presented in Figure 13B. The model uses compositions from Qbsc-4 as starting concentrations and hypothetical fractionating modes adjusted from original proportions to include hornblende are 50% plagioclase + 20% hornblende + 14% olivine + 8% orthopyroxene + 8% clinopyroxene. Several published sets of kd's for hornblende (Fujamaki, 1984 and Sisson, 1994) were applied to the model and kd's used in the model in Figure 12B are those of Sisson (1994) (Table A1). The model shows that even when hornblende is included as a fractionating phase the observed composition of the felsic subgroup can not be reproduced.

Alternative hypotheses include magma mixing processes. As discussed previously, the three units studied here show bimodal phenocryst populations with disequilibrium and reaction textures coexisting with phenocrysts without these textures (see Sulphur Creek petrography and mineral chemistry). At other arc volcanoes, these types of textures are often associated with magma mixing models (Madeleine et al., 2006, Venezky and Rutherford, 1997). Conversely, disequilibrium textures have been described as the result of rapid ascent of magma (Annen, 2006). However, plagioclase and olivine phenocrysts in the Sulphur Creek unit have a wide range of compositions that largely overlap with mineral compositions from the Boulder Glacier and Glacier Creek units (Figure 4). If magma mixing processes are responsible for the disequilibrium textures in these units, the overlapping mineral compositions may be a result of varying degrees of mixing between compositions that span the range between two compositionally distinct end-members.

Magma mixing calculations show that certain compositions from the Boulder Glacier unit can be combined with compositions from the mafic group of Sulphur Creek to produce compositions that are comparable to those in the Sulphur Creek felsic group (Figure 14). Mixing proportions are dependent upon samples used in the calculations. Hybrid mixtures that are consistent with felsic Sulphur Creek compositions range from 60%-70% Boulder Glacier dacites with 30%-40% Sulphur Creek mafic group compositions. Figure 14 shows the results of a representative mixing calculation for a hybrid mixture that is produced by combining 70% BG-3TB with 30% Qbsc-4 and compared to sample SC-7TB.

Hybrid compositions produced by the above mixing calculations generally matches Sulphur Creek felsic group compositions well for most major, trace and rare earth elements;

however there are some inconsistencies. Most notable is the elevated MgO, Ni and Cr in actual Sulphur Creek felsic group compositions relative to modeled hybrid mixtures. Elevated MgO, Ni and Cr are also observed in other Mount Baker volcanics and may be linked to the addition of small amounts of olivine (see Glacier Creek andesite discussion). Also, the magma mixing calculations break down when andesitic samples, rather than dacitic samples, from the Boulder Glacier unit are used as the felsic end-member. This relationship may indicate that the more dacitic compositions from the Boulder Glacier unit more closely represent the original felsic end-member compositions.

The origin of the end-members used in the above mixing model are not constrained in this paper, however the model does strongly suggest that the mafic Sulphur Creek and Boulder Glacier compositions may be similar to original mixing end-member compositions. Mixing models at other arc volcanoes provide several hypotheses for the origin of mixing end-members. In the Cascades, felsic end-members are often described as partial melts of a crustal protolith while mafic end-members are often described as mantle-derived basalts (Conrey et al. 2001; Streck et al. 2007; Smith and Leeman, 1987; Venezky and Rutherford, 1997).

The Mount Baker mixing model suggests that the 9.8 ka Sulphur Creek unit is mixed with dacitic compositions similar to the Boulder Glacier unit which is dated at 80-90 ka. The significant age gap implies that the process responsible for generating the Boulder Glacier felsic end-member is long lived and has been active or recurring up until the eruption of the Sulphur Creek lava at 9.8 ka. Further geochemical investigations concerning other eruptive units at Mount Baker with eruptive ages between the late Pleistocene and Holocene may aid

in constraining production intervals and time spans of Boulder Glacier like felsic end-members.

Glacier Creek Andesite

The Glacier Creek andesite has chemical attributes such as high Mg#'s (63-64), high Ni (67-82 ppm) and Cr (89-100) abundances, elevated La/Yb (~6.7), and depleted REE's compared to average continental arc andesite. Andesites with these characteristics are sometimes classified has high magnesium andesites or primitive andesites (Grove et al. 2002; Streck et al, 2007; Kelemen, 1994), but the Glacier Creek andesites fall short of the criteria in MgO, Ni and Cr concentrations to be classified as such. However, crystal fractionation of a high magnesium andesite is an accepted hypothesis for the generation of andesites with elevated MgO, Ni and Cr, and depleted REE concentrations (Grove et al. 2005). Alternative models for the generation of andesites similar to the Glacier Creek andesite describe the addition of ultramafic or mafic crystalline material to andesites which in turn, causes elevated MgO, Ni and Cr concentrations in the whole rock (Streck, 2007: Arculus et al. 1983).

A model that describes the Glacier Creek andesite as a product of crystal fractionation requires a parent composition that is inherently REE depleted and rich in MgO, Ni and Cr or similar to the high magnesium andesites described by Kelemen (1994) and discussed in context with Mount Shasta, CA, by Grove et al. (2002). As of yet, no volcanic unit at Mount Baker has been classified as a high magnesium andesite which makes this model difficult to consider; nevertheless, the possibility remains that a suitable parent magma is present

beneath Mount Baker.

When considering the possibility of a model that includes the addition of mafic/ultramafic crystalline material to explain the chemical characteristics of the Glacier Creek andesite, we must first determine if a foreign mafic or ultramafic component exists in those rocks. At other volcanic centers, the foreign component has been identified as ultramafic xenocrysts composed of olivine ± orthopyroxene (e.g. Mount Shasta, Streck et al. 2007). Minerals that make up those xenocrysts have strong reaction textures due to disequilibrium conditions when incorporated into new magmas. A characteristic feature of the Glacier Creek andesite is that it contains a population of olivine phenocrysts that have particularly strong disequilibrium textures and are relatively large (> 1mm) when compared to the remainder of olivine in Glacier Creek rocks. Olivine with disequilibrium textures indicate they may be xenocrystic in origin and are a potential candidate for an added mafic component to Glacier Creek andesites. In order to characterize the potentially xenocrystic olivine, a detailed chemical and petrographic examination of Glacier Creek olivine is outlined below.

Microprobe data suggests that the two Glacier Creek olivine size populations also correspond with a notable compositional trend. Core compositions from larger phenocrysts (>1 mm) are more mafic (3 cores at Mg# 86) relative to the smaller olivine phenocryst core compositions where the majority are below Mg# 78, but are within range of Mg# 68-82 . The microprobe data are limited and in order to confirm the composition and size relationship, data are supplemented with additional Scanning Electron Microscope (SEM) and energy dispersive spectrometer (EDS) analyses. SEM data described here are qualitative

and cannot be compared directly to microprobe data. Figure 15 shows approximate Mg#'s calculated for olivine core compositions compared to olivine size from SEM analyses. Olivine >1mm tend to have higher core Mg#'s relative to cores in olivine <1mm. Figure 15 also shows that there is some overlap between the two olivine populations. Microprobe and SEM data along with textural observations confirm that olivine in the Glacier Creek andesite comprise two populations that are distinct in size, core composition and texture. Figure 16 graphically summarizes the relationship between size, compositions and texture of the two olivine populations. Under the postulation that the large mafic olivine (Mg# ≥82) with strong disequilibrium textures are a xenocrystic component in the Glacier Creek lava, an olivine addition model is proposed.

A caution to the olivine addition model is that it is only valid under the hypothesis that there is in fact a xenocrystic olivine component in the Glacier Creek andesite. The strong reaction textures and bi-model size distribution that are used as lines of evidence to support the existence of xenocrystic olivine could be explained by an alternate hypothesis. The strong reaction textures observed in those olivine phenocrysts could be the result of a sudden pressure change caused by a rapid accent of magma (e.g., Annen, 2006).

The olivine addition model is considered a preliminary investigation. A logical next step would require a more robust petrographic and chemical evaluation of olivine and possibly other potentially added phases in the Glacier Creek andesite aimed at further characterizing xenocrystic components which would aid in discriminating between the above alternate hypothesis and the olivine addition hypothesis.

Glacier Creek Andesite Olivine Addition Model

In considering an olivine addition model in the Glacier Creek andesites, potential sources for the added olivine are outlined, followed by a discussion on quantifying the amount of added olivine.

At Mount Baker, an interesting possibility for the source of an added ultramafic component in the local geology is the Paleozoic Twin Sisters dunite. The dunite is exposed on the surface 13 km SW of the summit of Mount Baker and only 5 km from the flanks of Mount Baker to the nearest border of the dunite body. The Twin Sisters dunite ranges from harzburgite to pure olivine and is chromite bearing (Tabor et al., 2003). MgO compositions of olivine in the Twin Sisters Dunite are more primitive (48-55 wt. % MgO, Onyeagocha, 1978) than all olivine observed in the Glacier Creek unit (33-46 wt. % MgO). The dunite body is bound by SW dipping high angle thrust faults and is interpreted project away from Mount Baker at depth, where it pinches out about 2 km below the surface (Tabor et al., 2003). The dunite is not expected to underlie Mount Baker, and compositions are not comparable to Glacier Creek olivine making it an unlikely source, however, components similar to the Twin Sisters dunite could potentially lie deeper in the crust.

A variety of other sources for added mafic/ultramafic crystalline material at other volcanoes has been proposed. Sources include ophiolite bodies underlying volcanic centers (Streck et al. 2007; Arculus et al. 1983) and mafic plutonic roots (Dungan and Davidson, 2004). In these models, magma bodies are thought to interact with these potential sources where crystalline material may be incorporated into a magma body. An alternative potential source could simply be mafic cumulates from a previously fractionating magma body.

At Mount Baker, an ophiolite body has never been recognized which makes an ophiolite an unlikely candidate for a potential source. Cumulate bodies or mafic plutonic roots however, may be a more reasonable source. When considering a cumulate body or mafic plutonic roots, it is hard to imagine a pure olivine source. Mafic or ultramafic crystalline material derived from either of these sources could potentially include small percentages of other minerals phases that are added to the liquid as well.

The olivine/liquid equilibrium relationship described by Roeder and Emslie is used to quantify the amount of olivine addition and evaluate olivine/liquid equilibrium conditions in the Glacier Creek andesite. The relationship is described as;

$$Kd = (Fe/Mg)_{Olv}/(Fe^{2+}/Mg)_{Liq} = 0.3 \text{ where } Fe^{2+} \text{ is calculated as } 0.85\ FeO^*$$

The relationship is used to calculate Mg#'s of hypothetical liquids ($Mg\#_{Liq}$) that are in equilibrium with known olivine compositions from microprobe analyses (Figure 17 and Table 8).

Figure 17 shows that liquid compositions calculated based on olivine compositions ($Mg\#_{Liq}$) for most core compositions have lower Mg#'s ($Mg\#_{Liq}$ 38-57) than whole rock Mg#'s ($Mg\#_{WR}$ 38-57) indicating equilibrium with a more felsic liquid than whole rock compositions. The potentially xenocrystc olivine population (3 cores at $Mg\#_{Liq}$ ~64) appear to be in or slightly above equilibrium with whole rock compositions, however, in this olivine addition model, whole rock compositions can not represent an equilibrium state due to the influence of the xenocrystic olivine. Therefore, xenocrystic olivine must be removed to restore whole rock compositions to an equilibrium state.

In essence an olivine subtraction calculation is used to restore equilibrium conditions between whole rock compositions and the more felsic non-xenocrystic olivine population by subtracting potentially xenocrystic olivine from whole rock compositions. In the following calculations, equilibrium conditions are satisfied when whole rock compositions (liquid plus crystal), minus xenocrystic olivine, are comparable to non-xenocrystic olivine cores. The amount of subtracted olivine when equilibrium conditions are achieved is equal to the amount of olivine that has been added to the Glacier Creek andesite. If the model is valid, then the amount of olivine subtracted from whole rock compositions should be comparable to the observed mode of the xenocrystic olivine population in whole rock samples.

Figure 18 shows the results of the olivine subtraction calculation. Compositions and calculations used in the model are presented Table 9. The composition of the subtracted olivine is within the range of olivine classified as being xenocrystic. $Mg\#_{WR}$ values range from 63-64 (calculated with $Fe^{2+} = 0.85\ Fe^*$) prior to olivine subtraction while core compositions of non-xenocrystic olivine predict a range of $Mg\#_{Liq}$ 38-57. Subtraction of 4.0 wt. % olivine from whole-rock compositions results in new Mg#'s that are in equilibrium with core compositions from the non-xenocrystic olivine population.

In general, the subtraction model satisfies the parameter to be considered valid. New whole rock compositions are more felsic than observed whole rock compositions with significantly lower Mg#'s (Figure 18 and Table 9). Proportions of the xenocrystic olivine variety are estimated from petrographic observation (based on 1000 point counts) to be 2.5-3.7% by volume of a given Glacier Creek sample which is slightly lower, yet comparable to the olivine subtraction calculation.

The model is sensitive to many parameters and the small discrepancy (1% by volume) could be a result of several possibilities: 1) errors in the quantified estimates of the amount of xenocrystic olivine in the Glacier Creek samples; 2) added olivine may have been absorbed in to the host liquid post addition, making the observed amount lower then the actual added amount; 3) subtracted olivine compositions are not representative of the added olivine component; 4) inaccurate Fe concentrations and ultimately Mg#'s due to assumed oxygen fugacity conditions that are misrepresentative of the magmatic system; 5) the added mafic/ultramafic material is not pure olivine and may contain other minerals.

If the olivine addition model is considered valid, then compositions of Glacier Creek andesites after olivine subtraction should be more representative of liquid composition prior to olivine addition. The calculated initial MgO, FeO and SiO2 compositions of the Glacier Creek liquid (prior to olivine addition) can be compared to compositions of the Sulphur Creek and Boulder Glacier units in Figure 19. The above comparison shows that Glacier Creek liquid MgO compositions plot slightly below the straight line trends produced by the other units with 4.0% subtraction of olivine. Concentrations of FeO* in liquid compositions prior to olivine addition are slightly more mafic and are in range with a straight line trend consistent with FeO* compositions in the other units. Other major element compositions (TiO_2, K_2O, Na_2O, P_2O_5 and MnO, Table 9) are not shown in Figure 18, but are relatively unaffected by olivine addition and are close to straight line trends between the Boulder Glacier and Sulphur Creek units. CaO compositions however, have slightly elevated compositions compared to straight line trends.

Discussed earlier, the straight line trends produced by the Sulphur Creek and Boulder Glacier unit may be the result of magma mixing processes. The Glacier Creek compositions prior to olivine addition plot on or near the same mixing trend. Glacier Creek samples also share physical characteristics indicative of magma mixing processes such as resorbed and embayed rims and reverse chemical zoning patters in all phenocryst phases (Figure 5). It is not surprising that these textures are observed in the added olivine component due to disequilibrium conditions during addition, but these textures in the native olivine population may suggest disequilibrium conditions sometime prior to olivine addition. Figure 20 shows a compositional profile from SEM data of an olivine grain from the small less Mg-rich population with a reverse chemical zoning pattern that switches to normal zoning near the rim. Glacier Creek phenocryst textures, coupled with presumed compositions prior to olivine addition that are part of a mixing trend, make magma mixing processes a possible primary mechanism for the generation of Glacier Creek compositions. Therefore, I propose a model where the Glacier Creek andesites are formed by a two step process; the generation of intermediate compositions by magma mixing of mafic and felsic end-members followed by the addition of a foreign olivine component.

One outstanding problem in the magma mixing and olivine addition model is that the origin of the REE-depleted nature of the Glacier Creek compositions is not explained. This problem may be addressed by considering possible mixing end-members. One end-member could simply be similar to either the felsic or mafic mixing end-member described in the discussion concerning the Sulphur Creek unit. The other end-member, mafic or felsic, must be inherently depleted in REE to account for Glacier Creek REE abundances. At Mount

Baker, the lack of REE data for its eruptive units make identification of a REE depleted end-member difficult. At other arc volcanoes REE-depleted primary melts are characterized as primitive magnesium andesites. These andesites are described by Kelemen (1994) and discussed in context with Mount Shasta (Grove et al., 2002), and may provide one possibility for a mafic REE depleted mixing end-member. Also possible is a REE depleted felsic end-member that was generated by partial melting of a protolith that includes some combination off REE compatible phases such as garnet, hornblende and/or apatite.

Boulder Glacier Andesite and Dacite

Models describing the generation of intermediate to felsic volcanic rocks in the Cascade arc that are comparable to the andesites and dacites of Boulder Glacier can be placed into two different categories. At Mount St. Helens some researchers have interpreted dacites as the result of partial melting of a lower crustal basaltic amphibolite source (Smith and Leeman, 1987). Similar interpretations have been made at Mount Jefferson where two types of crustal melting to form intermediate to felsic rocks have been identified; melting of a basaltic amphibolite to form rhyodacite, and melting of a MORB-like granulite to form Sr-rich andesite (Conrey et al., 2001). Also at Mount Rainer, crustal melting processes are speculated upon for the formation of a felsic end-member, but the melting source is not identified (Venesky and Rutherford, 1997). In contrast to crustal melting models, Hildreth (2007) proposes that the majority of dacites in the Cascade arc are slightly evolved products of an andesitic liquid. Bacon and Druitt (1988) also favor a crystal fractionation model for generation of rhyodacites at Crater Lake Caldera. A model that is less common describes

Mount St. Helens dacites not as partial melts of lower crust, but as partial melts of the subducting slab (Defant and Drummond, 1993).

To test a fractionation model, REE modeling is utilized with the Rayleigh fractionation equation. Both the Sulphur Creek and Glacier Creek compositions are tested as starting compositions. As shown in Figure 12A and B, Rayleigh fractionation models using the Sulphur Creek basaltic andesite as a starting composition predict REE concentrations in fractionated products that are too high to be compared to the Boulder Glacier andesite and dacite. An alternative Rayleigh fractionation model using the Glacier Creek andesite sample as a starting composition is shown in Figure 21. In this model, fractionation of 70% plagioclase + 18% orthopyroxene + 10% olivine + 2% magnetite + 0.1% apatite predict compositions that are comparable in the light to mid REE (La-Sm) abundances to observed Boulder Glacier samples after high amounts of fractionation (~70-80%). However, modeled concentrations for the HREE and Eu are too low at the same amount of fractionation compared to observed Boulder Glacier compositions. Suspiciously high amounts of fraction and inconsistent REE concentrations seem to disqualify this REE crystal fractionation model.

Fractional crystallization of the Glacier Creek unit was also tested using whole rock major element compositions with the MELTS model (Ghiorso et al., 1993). Fractionation of sample GC-6TB at the NNO buffer and pressures ranging from 1-3 kbar consistently produced liquid compositions with lower concentrations of MgO and Al_2O_3 and higher concentrations of TiO_2 and K_2O compared to observed Boulder Glacier compositions.

On the basis of major element and REE modeling, it is unlikely that the Boulder Glacier andesites and dacites are fractionated products of either the Sulphur Creek basaltic

andesite or the Glacier Creek andesite. Fractional crystallization from other parent compositions should not be ruled out, but are not considered in this study due to the lack of published trace element data for other Mount Baker eruptive units.

In discussion of crustal melting models, an important first order consideration is the mechanism that induces melting of a crustal component. A common theme in the Mount Jefferson (Conrey et al., 2001) and the Mount St. Helens (Smith and Leeman, 1987) crustal melting models is the underplating of mafic mantle-derived magmas, which provides a heat source for the melting of lower crustal compositions. Annen et al. (2006) propose a similar model in which they describe a "deep crustal hot zone" in which silicic and intermediate melts are generated when hot, mantle-derived basalt are emplaced into the lower crust in a series of sills and dikes. Partial melting of the lower crust and partial crystallization of the basalt sills together produce intermediate to felsic residual melts.

The biggest influence on the composition of intermediate to felsic magmas generated by a crustal melting model is the compositions of the protolith. REE concentrations are particularly useful for identifying certain mineral phases that may have been present in the protolith. For example, a certain variety of rhyolite at the Lassen Volcanic Center has characteristically depleted MREE concentrations which are attributed to the influence of residual amphibole in the melting source (Borg and Clynne, 1998). Similarly, depleted HREE abundances and relatively high La/Yb can be linked to the presence of residual garnet in a deeper melting source. The Boulder Glacier unit has both MREE and HREE abundances that are lower than the basaltic andesites in this study which may suggest an influence from a combination of garnet and amphibole in their melting source.

Crustal compositions beneath Mount Baker are not well constrained, but a review of regional and local crustal structure and geology is outlined below. Miller et al. (2003) describe the North Cascades crystalline core as generally composed of amphibolite facies metamorphic rocks that have been successively intruded by arc plutons. At Mount Baker, adjacent and potentially underlying basement rocks consist of multiple accreted terranes (Tabor et al., 2003). The most common unit around Mount Baker is the Nooksack formation which is composed of Jurrassic age shales, meta-sediments and some greenstone. Other units include the Paleozoic Yellow Aster complex which is composed of meta-quartz diorite, meta-hornblendite and meta-trondhjemite; and the Chilliwack formation which is composed of meta-sediments and meta-volcanics (Tabor et al., 2003). This brief discussion highlights the complex and heterogeneous geology that lies beneath Mount Baker and it is uncertain how these units project at depth. It is presumed that melting of a crust hosting a variety of lithologies can potentially produce variable compositions of crustal melts.

The Boulder Glacier lavas are variable in both composition and age. Hildreth et al. (2003) describe the Boulder Glacier unit as a series of several flows and they provide two separate K-Ar dates separated by ~10 ± 52 ka (see unit description). The difference in composition and age in the Boulder Glacier unit may have originated by varying degrees of partial melting or melting of slightly different crustal sources over a time period of at least 10 ka, and most likely longer. Alternatively, variable compositions may be the result of small amounts of differentiation within the Boulder Glacier unit over the same time frame.

A common theme in crustal melting models is the recognition of crustal melts as felsic end-members in mixing models that produce andesitic compositions. At Mount St.

Helens, dacitic mixing end-members presumed to be derived by crustal melting mix with basaltic compositions to form andesites (Smith and Leeman, 1993; Gardner et al., 1995). The dacitic end member described at Mount St. Helens is similar to the Boulder Glacier unit in that they both have slightly variable major and trace element compositions. At Mount St. Helens these variations are speculated to be a result of small amounts of fractionation subsequent to mixing events (Smith and Leeman, 1993). A comparable model is applied to Mount Jefferson where intermediate rocks are produced by mixing processes and the felsic end-member is produced by crustal melting (Conrey et al., 2001). In this model small variations from linear mixing trends at Mount Jefferson have been speculated to be the result of small amounts of fractionation accompanying or preceding mixing events.

Similar to the above models, the Boulder Glacier unit is considered to be a felsic end member for the formation of the basaltic andesite of Sulphur Creek. From this model, two important observations concerning the Boulder Glacier unit are noted as follows. 1) The Boulder Glacier unit is dated 80-90 ka and the Sulphur Creek basaltic andesite is dated at 9.8 ka (Hildreth et al., 2003). The co-existence of the young Sulphur Creek unit and the older Boulder Glacier unit on the same mixing trend suggest processes responsible for the formation of the felsic end-member are long lived and at least active or periodically active for ~70-80 ka. 2) Mixing calculations (see Sulphur Creek discussion and Figure 14) work best when the most felsic samples from the Boulder Glacier unit are used. This may indicate that the more felsic samples more closely represent the original felsic end-member compositions and that the more intermediate Boulder Glacier compositions may be reflecting varying degrees of crustal melting or melting of a heterogeneous source.

SUMMARY AND CONCLUSIONS

The late Pleistocene Glacier Creek andesite, the Boulder Glacier andesite and dacite, and the Holocene Sulphur Creek basaltic andesite contain chemical and textural characteristics that are distinctive to each unit. The distinct features of each unit are described as a result of a diverse range of differentiation processes at work to form intermediate magma compositions at Mount Baker. Each differentiation process identified and the units involved are described below.

Magma mixing processes are manifested in the Sulphur Creek basaltic andesites. Pervasive disequilibrium textures coupled with chemical data indicate that the bimodal compositions in the Sulphur Creek unit are the result of varying degrees of mixing with a dacitic end-member that is similar to the dacitic compositions of the Boulder Glacier unit. All Sulphur Creek samples display textural evidence indicating that they have been mixed to some degree; however the samples in the more felsic group require mixing proportions of a maximum of 70% mafic Sulphur Creek magma and a minimum of 30% Boulder Glacier dacite.

The generation of the Glacier Creek andesite is described as a two step process. First, disequilibrium textures in all phenocryst types coupled with presumed original liquid compositions are generated through magma mixing processes. Mixing end-members are not identified, but one must have inherently low REE abundances and the other may be similar to either mixing end-member in the Sulphur Creek and Boulder Glacier mixing model. Second, addition of ~4 wt% xenocrystic olivine from an unconstrained mafic/ultramafic source modified those intermediate magma compositions. Olivine addition is manifested by

elevated MgO, Ni, and Cr abundances and strong disequilibrium textures in the olivine bearing Glacier Creek andesite. The source for the xenocrystic olivine is unconstrained, but the most likly possibilities include olivine rich cumulates left behind from a previously fractionating magma body or crystalline material from mafic plutonic roots.

The andesites and dacites of Boulder Glacier cannot be related to the Sulphur Creek or Glacier Creek units through crystal fractionation, and are more likely derived by partial melting of a crustal protolith. A melting protolith is not constrained, but a suitable protolith may be amphibolite with residual amphibole and garnet and possibly apatite to produce depleted REE concentrations observed in Boulder Glacier samples. Variations in the protolith composition and small influences from magma mixing processes are reflected in the variable whole rock compositions of Boulder Glacier. Processes responsible for the generation of the Boulder Glacier unit are long lived and active for up to 70-80 ka. If consistent with the majority of crustal melting models in the literature, it is likely that melting occurs in lower crustal levels where mantle-derived basalts provide a heat flux that induces melting. In this model, the influx of basalt and partial melting may occur consistently or periodically, over long time periods of at least 70-80 ka.

When combined, the story of each unit in this study provides a possible petrogenetic model for the generation of intermediate lavas at Mount Baker (Figure 22). Magma mixing seems to be a principal process that influences the chemical signatures and textural characteristics of intermediate compositions studied here and may also be a significant process for intermediate lavas generated in the last 100 ka at Mount Baker. In the mixing model there must be at least three compositionally distinct end-members; 1) a mafic end-

member that is similar but more primitive than the Sulphur Creek basaltic andesite, 2) a felsic end-member that is similar to the more dacitic compositions of the Boulder Glacier dacite and andesite, 3) a third end-member that is not well constrained, but may have similar major element compositions to either of the first two mixing end-members, but must have inherently depleted REE concentrations in order to produce Glacier Creek type REE concentrations. Mafic end-members are presumably mantle-derived, while felsic end-members are likely generated by partial melting of a crustal protolith. The crustal protolith is not well constrained, but amphibolite is considered as a first order possibility. Addition of xenocrystic mafic crystal debris may have a significant effect on intermediate magma compositions post mixing events. Intermediate compositions may deviate slightly from the main mixing trend due to small amounts of differentiation, but the prevailing geochemical signature is controlled by mixing processes.

Exceptions to the model may occur where parental basalts or crustal melts migrate relatively unmodified into shallower crustal levels where they erupt with near parental compositions. It is not uncommon in the Cascades for basalts with near primary compositions to have migrated through the crustal column relatively unmodified (Bacon et al., 1997).

An important factor that can not be disregarded in the above model is the previously recognized heterogeneous mantle in the Cascade arc, which is responsible for producing several varieties of basaltic primary magmas (Leeman et al, 1990). The characterization of these basalt types is beyond the scope of this paper, however, when they are characterized at Mount Baker they will have significant implications for the above model. More than one

type of mantle-derived basalt would produce varying types of mafic inputs into the model described above which could be used to further characterize intermediate lavas at Mount Baker. Conversely, observation of only one type of mantle-derived basalt would indicate that all intermediate lavas on Mount Baker share a common mafic end-member.

REFERENCES

Andersen, D. J., and Lindsley, D. H., 1985, New (and final!) models for the Ti-magnetite/ilmenite geothermometer and oxygen barometer: Eos, Transactions, American Geophysical Union, v. 66, no. 18, p. 416.

Andersen, D. J., Lindsley, D. H., and Davidson, P. M., 1993, QUILF; a Pascal program to assess equilibrium among Fe-Mg-Mn-Ti oxides, pyroxenes, olivine, and quartz: Computers & Geosciences, v. 19, no. 9, p. 1333-1350.

Annen, C., Blundy, J. D., and Sparks, R. S. J., 2006, The genesis of intermediate and silicic magmas in deep crustal hot zones: Journal of Petrology, v. 47, no. 3, p. 505-539.

Arculus, R. J., Johnson, R. W., Chappell, B. W., McKee, C. O., and Sakai, H., 1983, Ophiolite-contaminated andesites, trachybasalts, and cognate inclusions of Mount Lamington, Papua New Guinea; anhydrite-amphibole-bearing lavas and the 1951 cumulodome: Journal of Volcanology and Geothermal Research, v. 18, no. 1-4, p. 215-247.

Armstrong, J., 1988, Bence-Albee after 20 years: review of the accuracy of a-factor correction procedures for oxide and silicate minerals, in Microbeam Analysis-1988, p. 469-76

Arth, J. G., 1976, Behavior of trace elements during magmatic processes; a summary of theoretical models and their applications: Journal of Research of the U. S. Geological Survey, v. 4, no. 1, p. 41-47.

Bacon, C. R., Bruggman, P. E., Christiansen, R. L., Clynne, M. A., Donnelly-Nolan, J. M., and Hildreth, W., 1997, Primitive magmas at five Cascade volcanic fields; melts from hot, heterogeneous sub-arc mantle: The Canadian Mineralogist, v. 35, no. 2, p. 397-423.

Bacon, C. R., and Druitt, T. H., 1988, Compositional evolution of the zoned calcalkaline magma chamber of Mount Mazama, Crater Lake, Oregon: Contributions to Mineralogy and Petrology, v. 98, no. 2, p. 224-256.

Bacon, C. R., and Hirschmann, M. M., 1988, Mg/Mn partitioning as a test for equilibrium between coexisting Fe-Ti oxides: American Mineralogist, v. 73, no. 1-2, p. 57-61.

Borg, L. E., and Clynne, M. A., 1998, The petrogenesis of felsic calc-alkaline magmas from the southernmost Cascades, California; origin by partial melting of basaltic lower crust: Journal of Petrology, v. 39, no. 6, p. 1197-1222.

Bostock, M. G., and VanDecar, J. C., 1995, Upper mantle structure of the northern Cascadia subduction zone: Canadian Journal of Earth Sciences = Journal Canadien des Sciences de la Terre, v. 32, no. 1, p. 1-12.

Bullen, T. D., Clynne, M. A., and Muffler, L. J. P., 1990, Trace element and isotopic constraints on magmatic evolution at Lassen volcanic center: Journal of Geophysical Research, v. 95, no. B12, p. 19,671-19,691.

Clynne, M. A., 1999, A complex magma mixing origin for rocks erupted in 1915, Lassen Peak, California: Journal of Petrology, v. 40, no. 1, p. 105-132.

Conrey, R. M., Hooper, P. R., Larson, P. B., Chesley, J., and Ruiz, J., 2001, Trace element and isotopic evidence for two types of crustal melting beneath a High Cascade volcanic center, Mt. Jefferson, Oregon: Contributions to Mineralogy and Petrology, v. 141, no. 6, p. 710-732.

Coombs, H. A., 1939, Mount Baker, a Cascade volcano: Geological Society of America Bulletin, v. 50, no. 10, p. 1493-1509.

Davidson, J., Turner, S., Handley, H., Macpherson, C., and Dosseto, A., 2007, Amphibole "sponge" in arc crust?: Geology, v. 35, no. 9, p. 787-790.

Defant, M. J., and Drummond, M. S., 1993, Mount St. Helens; potential example of the partial melting of the subducted lithosphere in a volcanic arc: Geology, v. 21, no. 6, p. 547-550.

Dungan, M. A., and Davidson, J., 2004, Partial assimilative recycling of the mafic plutonic roots of arc volcanoes; an example from the Chilean Andes: Geology, v. 32, no. 9, p. 773-776.

Eichelberger, J. C., 1975, Origin of andesite and dacite; evidence of mixing at Glass Mountain in California and at other Circum-Pacific volcanoes: Geological Society of America Bulletin, v. 86, no. 10, p. 1381-1391.

Eichelberger, J. C., Heiken, F., Widdicombe, R., Wright, D., Keady, C. J., and Cobb, D. D., 1976, New fumarolic activity on Mount Baker; observations during April through July, 1975: Journal of Volcanology and Geothermal Research, v. 1, no. 1, p. 35-53.

Eugster, H. P., and Wones, D. R., 1962, Stability relations of the ferruginous biotite, annite: Journal of Petrology, v. 3, no. 1, p. 82-125.

Evans, B. W., Scaillet, B., and Kuehner, S. M., 2006, Experimental determination of coexisting iron-titanium oxides in the systems FeTiAlO, FeTiAlMgO, FeTiAlMnO, and FeTiAlMgMnO at 800 and 900 degrees C, 1-4 kbar, and relatively high oxygen fugacity: Contributions to Mineralogy and Petrology, v. 152, no. 2, p. 149-167.

Fujimaki, H., 1986, Partition coefficients of Hf, Zr, and REE between zircon, apatite, and liquid: Contributions to Mineralogy and Petrology, v. 94, no. 1, p. 42-45.

Fujimaki, H., Tatsumoto, M., and Aoki, K.-i., 1984, Partition coefficients of Hf, Zr, and REE between phenocrysts and groundmasses: Journal of Geophysical Research, v. 89, Suppl., no. B, p. 662-672.

Gardner, J. E., Carey, S., Rutherford, M. J., and Sigurdsson, H., 1995, Petrologic diversity in Mount St. Helens dacites during the last 4,000 years; implications for magma mixing: Contributions to Mineralogy and Petrology, v. 119, no. 2-3, p. 224-238.

Ghiorso, M. S., Sack, R. O., and Anonymous, 1993, MELTS; software for the thermodynamic analysis of phase equilibria in magmatic systems: Abstracts with Programs - Geological Society of America, v. 25, no. 6, p. 96.

Gill, J. B., 1981, Orogenic andesites and plate tectonics, Minerals and rocks: Berlin ; New York, Springer-Verlag, xiv, 385 p. p.

Green, N. L., 1988, Basalt-basaltic andesite mixing at Mount Baker Volcano, Washington; Estimation of mixing conditions: Journal of Volcanology and Geothermal Research, v. 34, no. 3-4, p. 251-265.

Green, N. L., and Harry, D. L., 1999, On the relationship between subducted slab age and arc basalt petrogenesis, Cascadia subduction system, North America: Earth and Planetary Science Letters, v. 171, no. 3, p. 367-381.

Green, N. L., and Sinha, A. K., 2005, Consequences of varied slab age and thermal structure on enrichment processes in the sub-arc mantle of the northern Cascadia subduction system: Journal of Volcanology and Geothermal Research, v. 140, no. 1-3, p. 107-132.

Grove, T. L., and Baker, M. B., 1984, Phase equilibrium controls on the tholeiitic versus calc-alkaline differentiation trends: Journal of Geophysical Research, v. 89, no. B5, p. 3253-3274.

Grove, T. L., Baker, M. B., Price, R. C., Parman, S. W., Elkins-Tanton, L. T., Chatterjee, N., and Muentener, O., 2005, Magnesian andesite and dacite lavas from Mt. Shasta, Northern California; products of fractional crystallization of H_2O-rich mantle melts: Contributions to Mineralogy and Petrology, v. 148, no. 5, p. 542-565.

Grove, T. L., Elkins-Tanton, L. T., Parman, S. W., Chatterjee, N., Muentener, O., and Gaetani, G. A., 2003, Fractional crystallization and mantle-melting controls on calc-alkaline differentiation trends: Contributions to Mineralogy and Petrology, v. 145, no. 5, p. 515-533.

Grove, T. L., Gerlach, D. C., and Sando, T. W., 1981, The role of combined assimilation, fractionation, and mixing in the production of calc-alkaline series magmas: Eos, Transactions, American Geophysical Union, v. 62, no. 45, p. 1086.

Grove, T. L., Parman, S. W., Bowring, S. A., Price, R. C., and Baker, M. B., 2002, The role of an H_2O-rich fluid component in the generation of primitive basaltic andesites and andesites from the Mt. Shasta region, N California: Contributions to Mineralogy and Petrology, v. 142, no. 4, p. 375-396.

Guffanti, M., and Weaver, C. S., 1988, Distribution of late Cenozoic volcanic vents in the Cascade Range; volcanic arc segmentation and regional tectonic considerations: Journal of Geophysical Research, v. 93, no. B6, p. 6513-6529.

Heaton, T. H., and Kanamori, H., 1984, Seismic potential associated with subduction in the northwestern United States: Bulletin of the Seismological Society of America, v. 74, no. 3, p. 933-941.

Hildreth, W., 2007, Quaternary magmatism in the Cascades; geologic perspectives: USGS Professional Paper, no. P 1744, p. 125.

Hildreth, W., Fierstein, J., and Lanphere, M. A., 2003, Eruptive history and geochronology of the Mount Baker volcanic field, Washington: Geological Society of America Bulletin, v. 115, no. 6, p. 729-764.

Hildreth, W., and Moorbath, S., 1988, Crustal contributions to arc magmatism in the Andes of central Chile: Contributions to Mineralogy and Petrology, v. 98, no. 4, p. 455-489.

Irvine, T. N., and Baragar, W. R. A., 1971, A guide to the chemical classification of the common volcanic rocks: Canadian Journal of Earth Sciences = Journal Canadien des Sciences de la Terre, v. 8, no. 5, p. 523-548.

Irving, A. J., Frey, F. A., Drake, M. J., and Holloway, J. R., 1978, Distribution of trace elements between garnet megacrysts and host volcanic liquids of kimberlitic to rhyolitic composition: Geochimica et Cosmochimica Acta, v. 42, no. 6A, p. 771-788.

Johnson, D. M., Hooper, P. R., and Conrey, R. M., 1999, XRF analysis of rocks and minerals for major and trace elements on a single low dilution Li-tetraborate fused bead: Advances in X-Ray Analysis, v. 41, p. 843-867.

Kelemen, P. B., 1994, Origin of high Mg# andesite and the continental crust: Mineralogical Magazine, v. 58A, no. A-K, p. 464-465.

Leeman, W. P., Lewis, J. F., Evarts, R. C., Conrey, R. M., and Streck, M. J., 2005, Petrologic constraints on the thermal structure of the Cascades Arc: Journal of Volcanology and Geothermal Research, v. 140, no. 1-3, p. 67-105.

Leeman, W. P., Smith, D. R., Hildreth, W., Palacz, Z. A., Rogers, N. W., and Muffler, L. J. P., 1990, Compositional diversity of late Cenozoic basalts in a transect across the southern Washington Cascades; implications for subduction zone magmatism: Journal of Geophysical Research, v. 95, no. B12, p. 19,561-19,582.

Lepage, L., 2003, ILMAT: an Excel worksheet for ilmenite-magnetite geothermometry and geobarometry: Computers and Geosciences, v. 29, p. 673-678

Madeleine, C. S. H., Blundy, J. D., and Sparks, R. S. J., 2006, Magma evolution and open-system processes at Shiveluch Volcano; insights from phenocryst zoning: Journal of Petrology, v. 47, no. 12, p. 2303-2334.

Martin, H., 1987, Petrogenesis of Archaean trondhjemites, tonalites and granodiorites from eastern Finland; major and trace element geochemistry: Journal of Petrology, v. 28, no. 5, p. 921-953.

Mason, P. R. D., Downes, H., Thirlwall, M. F., Seghedi, I., Szakacs, A., Lowry, D., and Mattey, D., 1996, Crustal assimilation as a major petrogenetic process in the East Carpathian Neogene and Quaternary continental margin arc, Romania: Journal of Petrology, v. 37, no. 4, p. 927-959.

McCrory, P. A., Blair, J. L., Oppenheimer, D. H., and Walter, S. R., 1994, Depth to the Juan de Fuca slab beneath the Cascadia subduction margin - a 3-D model for sorting earthquakes, Series 91, U.S. Geological Survey Data, CD-Rom.

McKeever, D., 1977, Volcanology and geochemistry of the south flank of Mount Baker, Cascade Range, Washington: Western Washington University, M.S. Thesis, 126 p.

Miller, R. B., Matzel, J. P., Paterson, S. R., and Stowell, H., 2003, Cretaceous to Paleogene Cascades Arc; structure, metamorphism, and timescales of magmatism, burial, and exhumation of a crustal section: GSA Field Guide, v. 4, p. 107-135.

Mooney, W. D., and Weaver, C. S., 1989, Regional crustal structure and tectonics of the Pacific coastal states; California, Oregon, and Washington: Memoir - Geological Society of America, v. 172, p. 129-161.

Moore, N.E. and DeBari, S.M., 2008, Origin and geochemical evolution of mafic magmas from the Cascade arc, Mount Baker, Washington: probes into mantle processes, 18th Annual Goldschmidt Conference Abstracts, v. 72, no. 12, p. A647.

Onyeagocha, A. C., 1978, Twin Sisters Dunite; petrology and mineral chemistry: Geological Society of America Bulletin, v. 89, no. 10, p. 1459-1474.

Post, A., Richardson, D., Tangborn, W. V., and Rosselot, F. L., 1971, Inventory of glaciers in the North Cascades, Washington: USGS Professional Paper 705a, p. 26.

Ramachandran, K., Hyndman, R. D., and Brocher, T. M., 2006, Regional P wave velocity structure of the northern Cascadia subduction zone: Journal of Geophysical Research, v. 111, p. 15.

Roeder, P. L., and Emslie, R. F., 1970, Olivine-liquid equilibrium: Contributions to Mineralogy and Petrology, v. 29, no. 4, p. 275-289.

Schaaf, P., Stimac, J., Siebe, C., and Macias, J. L., 2005, Geochemical evidence for mantle origin and crustal processes in volcanic rocks from Popocatepetl and surrounding monogenetic volcanoes, central Mexico: Journal of Petrology, v. 46, no. 6, p. 1243-1282.

Schock, H. H., 1979, Distribution of rare-earth and other trace elements in magnetites: Chemical Geology, v. 26, no. 1-2, p. 119-133.

Scott, K. M., Macias, J. L., Naranjo, J. A., Rodriguez, S., and McGeehin, J. P., 2001, Catastrophic debris flows transformed from landslides in volcanic terrains; mobility, hazard assessment, and mitigation strategies: USGS Professional Paper 1630, p. 59.

Sisson, T. W., and Grove, T. L., 1993, Experimental investigations of the role of H_2O in calc-alkaline differentiation and subduction zone magmatism: Contributions to Mineralogy and Petrology, v. 113, no. 2, p. 143-166.

Sisson, T. W., 1994, Hornblende-melt trace-element partitioning measured by ion microprobe: Chemical Geology, v. 117, no. 1-4, p. 331-344.

Smith, D. R., and Leeman, W. P., 1987, Petrogenesis of Mount St. Helens dacitic magmas: Journal of Geophysical Research, v. 92, no. B10, p. 10,313-10,334.

Stavert, L. W., 1971, A geochemical reconnaissance investigation of Mount Baker andesites: Western Washington University, M.S. Thesis, 60 p.

Streck, M. J., Dungan, M. A., Malavassi, E., Reagan, M. K., and Bussy, F., 2002, The role of basalt replenishment in the generation of basaltic andesites of the ongoing activity at Arenal Volcano, Costa Rica; evidence from clinopyroxene and spinel: Bulletin of Volcanology, v. 64, no. 5, p. 316-327.

Streck, M. J., Leeman, W. P., and Chesley, J., 2007, High-magnesium andesite from Mount Shasta; a product of magma mixing and contamination, not a primitive mantle melt: Geology, v. 35, no. 4, p. 351-354.

Sun, S. S., and McDonough, W. F., 1989, Chemical and isotopic systematics of oceanic basalts; implications for mantle composition and processes: Geological Society Special Publications, v. 42, p. 313-345.

Swan, V. L., 1980, The petrogenesis of the Mount Baker volcanics, Washington: Washington State University, Ph.D.

Tabor, R. W., Haugerud, R. A., Hildreth, W., and Brown, E. H., 2003, Geologic map of the Mount Baker 30- by 60-minute quadrangle, Washington: Publications of the U. S. Geological Survey, scale 1:100,000.

Taylor, D. D., 2001, Petrology and geochemistry of mafic lavas near Glacier Peak, North Cascades, Washington: Western Washington University, M.S. Thesis, 86 p.

Tucker, D. S., Scott, K. M., and Lewis, D. R., 2007b, Field guide to Mount Baker volcanic deposits in the Baker River valley; nineteenth century lahars, tephras, debris avalanches, and early Holocene sub-aqueous lava: GSA Field Guide, v. 9, p. 83-98.

Venezky, D. Y., and Rutherford, M. J., 1997, Pre-eruption conditions and timing of dacite-andesite magma mixing in the 2.2 ka eruption at Mount Rainier: Journal of Geophysical Research, v. 102, no. B9, p. 20,069-20,086.

Table 1. Summary of petrographic observations

Unit	Phenocryst %	Phenocryst Modes	Size Range	% with Reaction Textures	Types of Zoning Patterns	Other
Sulphur Creek Basaltic Andesite	20-50%	Olivine: 5-15%	0.5-2.5 mm	50%	normal, reverse, oscillatory	Sometimes mantled by plag + opx
		Plagioclase: 65-80%	0.5-3.5 mm	70%	normal, reverse, oscillatory	
		Clinopyroxene: 5-15%	0.5-3.0 mm	50%	reverse	Ophitic texture with plagioclase overgrowths
		Orthopyroxene: 5-20%	0.5-2.5 mm	50%	na	
		Fe-Ti Oxide: 1-2%	< 1.0 mm			
		Trace Cr Spinel				
Glacier Creek Andesite	47-61%	Olivine: 11-12%	1.0-3.0 mm	90%	normal, rare reverse	Elevated NiO, often mantled by plag +opx, bimodal size distribution
		Plagioclase: 70-73%	0.1-0.8 mm, 1.2-4.2mm	65%	normal, reverse, oscillatory	Bimodal size distribution, complicated sieve textures
		Clinopyroxene: 7-8%	0.1-2.0 mm	80%	na	
		Orthopyroxene: 7-10%	0.1-2.0 mm	80%	normal	Ophitic texture with plagioclase overgrowths
		Fe-Ti Oxide: 1-2%	< 1.0 mm			
		Trace Apatite				
Boulder Glacier Andesite and Dacite	50-60%	Olivine:< 1% in 6 samples	0.5-1.5 mm	50%	normal,	mantled by plag +opx
		Plagioclase: 65-90%	0.2-3.5 mm	75%	normal, oscillatory	
		Clinopyroxene: 1-10%	0.1-1.5 mm	40%	na	Ophitic texture with plagioclase overgrowths
		Orthopyroxene: 70-30%	0.1-2.0 mm	40%	na	Ophitic texture with plagioclase overgrowths
		Fe-Ti Oxide: 2%	< 1.0 mm			
		Trace Apatite				

Table 1. Petrographic summary of the basaltic andesite of Sulphur Creek, the andesite of Glacier Creek and the andesite and dacite of Boulder Glacier. Percentage values for the Sulphur Creek basalt and Boulder Glacier andesite and dacite are visual estimates while values for the Glacier Creek andesite are based on 1000 point counts. Phenocryst mode totals are based on the total phenocryst population.

Table 2. Plagioclase compositions

Label	SiO_2	Al_2O_3	FeO*	MgO	CaO	Na_2O	K_2O	SrO	Total	An
Sulphur Creek										
SC-3TB PAc	54.79	27.40	0.52	0.06	10.82	2.55	0.29	0.12	96.55	70.13
SC-3TB PBc	55.14	27.90	0.58	0.03	10.68	5.07	0.29	0.09	99.77	53.79
SC-3TB PBr	55.87	26.45	0.59	0.05	9.28	5.80	0.42	0.12	98.58	46.93
SC-3TB PCc	55.53	27.47	0.54	0.11	9.97	5.47	0.32	0.14	99.56	50.18
SC-3TB PD clot	52.12	29.25	0.59	0.04	12.49	4.19	0.16	0.13	98.96	62.23
SC-3TB Pgm	54.78	27.09	0.87	0.10	9.93	5.06	0.38	0.14	98.36	52.03
SC-3TB Pgm2	53.45	28.15	1.01	0.09	11.53	4.80	0.31	0.00	99.33	57.03
SC-6TB PAc	51.31	30.48	0.45	0.10	13.73	3.76	0.14	0.14	100.10	66.86
SC-6TB PAr	53.25	27.84	0.57	0.08	10.76	5.22	0.26	0.15	98.13	53.25
SC-6TB PBc	52.80	29.58	0.56	0.06	12.68	4.22	0.19	0.13	100.23	62.41
SC-6TB PBr	51.96	29.39	0.53	0.08	12.55	4.25	0.18	0.12	99.05	62.00
SC-6TB PCc	53.70	28.24	0.57	0.06	11.61	4.69	0.25	0.13	99.25	57.77
SC-6TB PCr	55.18	27.67	0.59	0.09	10.72	5.22	0.26	0.14	99.86	53.16
SC-6TB Pgm	56.32	26.59	0.94	0.09	9.68	5.90	0.47	0.12	100.10	47.55
SC-6TB Pgm2	55.66	26.87	0.80	0.10	9.79	5.61	0.41	0.02	99.27	49.09
SC-7TB PAc	55.16	27.49	0.61	0.08	10.41	5.31	0.28	0.15	99.49	52.00
SC-7TB PAm1	53.41	27.38	0.63	0.08	10.62	5.46	0.26	0.14	97.97	51.80
SC-7TB PAm2	52.66	29.34	0.57	0.07	12.46	4.45	0.19	0.15	99.87	60.74
SC-7TB PAr	53.54	27.84	0.56	0.08	10.64	5.22	0.25	0.15	98.29	52.97
SC-7TB PBc	55.67	27.53	0.56	0.04	10.14	5.43	0.34	0.18	99.90	50.79
SC-7TB PBr	51.79	28.45	0.73	0.10	11.81	4.51	0.24	0.17	97.81	59.13
SC-7TB PCc	53.57	28.64	0.55	0.07	11.71	4.62	0.25	0.12	99.53	58.34
SC-7TB PCr	53.51	27.98	0.60	0.11	11.20	5.06	0.26	0.14	98.86	55.02
Glacier Creek										
GC-3TB PAc	51.77	29.57	0.56	0.05	12.88	4.18	0.19	0.17	99.39	63.00
GC-3TB PAr	57.04	25.95	0.61	0.07	8.91	6.01	0.50	0.23	99.31	45.03
GC-3TB PBc	56.80	26.15	0.60	0.04	9.25	6.07	0.46	0.19	99.57	45.71
GC-6TB PAc	54.42	27.02	0.61	0.07	11.15	5.38	0.34	0.14	99.13	53.39
GC-6TB PAr	55.10	27.11	0.64	0.10	10.43	5.26	0.35	0.17	99.16	52.28
GC-6TB PBc	48.65	31.55	0.53	0.04	15.20	2.84	0.10	0.13	99.03	74.76
GC-6TB PBm	57.53	26.45	0.52	0.06	9.16	6.22	0.45	0.16	100.55	44.87
GC-6TB PBr	52.79	28.81	0.76	0.08	12.25	4.34	0.24	0.21	99.47	60.93
GC-6TB PCc	54.80	27.83	0.67	0.07	10.90	5.05	0.34	0.20	99.86	54.40
GC-6TB PCr	54.54	28.23	0.66	0.09	11.44	5.14	0.29	0.18	100.56	55.16
GC-6TB Pgm	60.76	23.49	0.77	0.00	7.46	5.41	1.71	0.15	99.76	43.25
GC-6TB Pgm2	55.56	26.52	0.89	0.05	10.06	5.21	0.50	0.16	98.94	51.62
GC-12TB PAc	55.54	27.29	0.52	0.05	10.36	5.37	0.35	0.12	99.62	51.60
GC-12TB PAm	50.55	30.34	0.61	0.05	13.62	3.43	0.17	0.19	98.96	68.69
GC-12TB PAr	55.21	27.28	0.59	0.09	10.23	5.47	0.37	0.15	99.39	50.82
GC-12TB PBc	57.51	25.98	0.63	0.07	8.94	6.05	0.45	0.17	99.80	44.95
GC-12TB PBr	54.51	26.88	0.64	0.09	10.07	5.44	0.32	0.00	97.94	50.57
GC-12TB PCc	55.93	25.93	0.52	0.09	9.28	5.86	0.40	0.18	98.19	46.67
GC-12TB Pgm	55.96	26.56	1.13	0.03	9.40	5.86	0.35	0.21	99.50	46.99
GC-12TB Pgm2	56.91	25.68	0.94	0.02	8.86	5.99	0.44	0.16	99.00	44.98

Individual mineral grains analyzed in each sample are assigned a letter followed by an additional letter indicating a location of the analyses (c- core, r- rim, m- middle, gm- groundmass). For example: GC-3TB PBc would be a core analyses in plagioclase B from sample GC-3TB. An indicates the Anorthite content of each analysis. Analytical error is <3% for major elements and <8% for minor elements.

Table 2. Plagioclase compositions cont.

Label	SiO_2	Al_2O_3	FeO*	MgO	CaO	Na_2O	K_2O	SrO	Total	An
Boulder Glacier										
BG-3TB PAc	54.12	28.11	0.64	0.10	11.32	4.66	0.25	0.21	99.41	57.31
BG-3TB PBc	51.72	30.00	0.46	0.05	13.17	3.77	0.16	0.14	99.48	65.88
BG-3TB PCc	55.91	26.54	0.37	0.03	9.67	5.82	0.36	0.07	98.77	47.87
BG-7TB PAc	52.91	29.54	0.51	0.01	12.37	4.47	0.22	0.12	100.15	60.46
BG-7TB PAm	60.67	23.80	0.70	0.08	6.87	6.92	0.71	0.18	99.93	35.43
BG-7TB PAr	54.64	27.15	0.96	0.34	10.58	5.18	0.32	0.12	99.30	53.02
BG-7TB PBc	55.58	28.02	0.30	0.03	10.59	5.41	0.26	0.19	100.39	51.96
BG-7TB PBr	57.58	23.97	0.58	0.06	8.95	6.80	0.55	0.12	98.60	42.11
BG-7TB PCc	55.83	26.16	0.89	0.16	9.93	4.67	0.63	0.13	98.40	54.02
BG-10TB PAc	52.57	29.30	0.51	0.03	12.37	4.26	0.20	0.15	99.41	61.61
BG-10TB PAr	54.88	27.79	0.58	0.10	10.74	5.34	0.27	0.14	99.84	52.64
BG-10TB PBc	55.83	27.50	0.58	0.10	10.41	5.36	0.37	0.17	100.32	51.77
BG-10TB Pgm	64.54	19.59	1.37	0.08	4.60	5.44	2.56	0.08	98.27	31.85

Table 3. Pyroxene compositions

Clinopyroxene

Label	SiO_2	Al_2O_3	TiO_2	FeO*	MnO	MgO	CaO	Na_2O	Cr_2O_3	Total	Mg #	Wo	En	Fs
Sulphur Creek														
SC-3TB CpxAc	51.40	2.14	0.80	9.92	0.27	14.66	19.79	0.33	0.02	99.33	72.48	41.29	42.56	16.16
SC-3TB CpxBc	51.74	1.93	0.71	10.73	0.34	14.37	19.77	0.36	0.00	99.94	70.48	41.07	41.53	17.40
SC-3TB CpxBr	52.25	2.01	0.81	9.12	0.30	15.13	19.35	0.42	0.02	99.41	74.73	40.72	44.30	14.98
SC-3TB Cpxclot	52.43	2.12	0.87	9.74	0.31	15.14	18.61	0.41	0.02	99.64	73.48	39.36	44.56	16.08
SC-6TB CpxAc	52.64	1.60	0.59	10.20	0.29	14.21	19.55	0.31	0.00	99.39	71.29	41.35	41.81	16.84
SC-6TB CpxAr	50.94	2.01	0.80	9.65	0.25	14.77	19.48	0.42	0.00	98.31	73.18	40.96	43.21	15.84
Glacier Creek														
GC-3TB CpxAc	53.30	1.14	0.34	10.80	0.40	14.04	19.49	0.35	0.01	99.88	69.86	41.07	41.16	17.76
GC-6TB CpxAc	52.29	2.39	0.47	8.93	0.25	14.46	20.16	0.37	0.39	99.71	74.27	42.67	42.58	14.75
GC-6TB CpxBc	51.97	1.66	0.59	10.47	0.30	14.30	19.52	0.40	0.02	99.23	70.89	41.02	41.81	17.17
GC-12TB CpxAc	52.47	2.12	0.74	9.57	0.24	14.61	19.82	0.34	0.04	99.95	73.13	41.62	42.69	15.69
GC-12TB CpxBc	50.96	1.69	0.69	11.45	0.33	13.90	18.95	0.41	0.00	98.40	68.39	40.12	40.95	18.92
GC-12TB Cpxgm	50.44	1.06	0.84	10.91	0.36	14.67	19.02	0.49	0.00	97.79	70.56	39.67	42.57	17.76
Boulder Glacier														
BG-3TB CpxAc	54.04	0.84	0.30	9.92	0.46	13.92	20.55	0.37	0.00	100.40	71.44	43.12	40.64	16.25
BG-3TB CpxBc	53.05	1.23	0.43	10.05	0.34	13.98	20.76	0.36	0.00	100.21	71.26	43.20	40.48	16.32
BG-7TB CpxBc	50.70	1.64	0.57	10.43	0.33	13.86	19.63	0.38	0.00	97.54	70.32	41.72	40.98	17.30
BG-7TB CpxCc	52.76	1.27	0.45	9.29	0.43	14.29	20.81	0.37	0.00	99.68	73.28	43.40	41.47	15.13
BG-10TB CpxAc	52.54	1.69	0.59	10.56	0.42	13.83	20.26	0.37	0.00	100.26	70.01	42.43	40.30	17.26

Orthopyroxene

Label	SiO_2	Al_2O_3	TiO_2	FeO*	MnO	MgO	CaO	Na_2O	Cr_2O_3	Total	Mg #	Wo	En	Fs
Sulphur Creek														
SC-3TB OpxAc	52.19	0.94	0.41	19.52	0.62	22.63	1.69	0.05	0.01	98.06	67.39	3.49	65.04	31.47
SC-3TB Opxclot	54.00	0.93	0.36	16.80	0.47	25.25	1.70	0.06	0.00	99.56	72.82	3.40	70.35	26.26
SC-6TB OpxAc	52.72	0.82	0.35	19.98	0.49	22.70	1.69	0.04	0.00	98.79	66.95	3.46	64.63	31.91
Glacier Creek														
GC-6TB OpxAc	52.95	0.89	0.40	20.58	0.47	22.23	1.78	0.05	0.00	99.34	65.82	3.65	63.42	32.94
GC-6TB OpxBc	53.78	0.88	0.40	19.48	0.46	22.87	1.77	0.05	0.01	99.69	67.67	3.62	65.21	31.16
GC-6TB Olv inc	54.54	0.98	0.38	17.43	0.41	25.11	1.37	0.06	0.01	100.29	71.97	2.74	70.00	27.26
GC-6TB Cpx inc	52.74	0.53	0.43	24.12	0.57	18.81	1.93	0.06	0.02	99.21	58.16	4.11	55.77	40.12
GC-12TB OpxAc	53.74	0.98	0.32	16.42	0.42	25.17	1.48	0.01	0.00	98.53	73.21	3.01	71.01	25.99
GC-12TB OpxAr	52.86	0.57	0.50	20.62	0.56	20.93	1.71	0.03	0.00	97.78	64.41	3.63	62.06	34.30
GC-12TB OpxBr	53.85	1.96	0.54	17.88	0.38	23.36	1.44	0.04	0.04	99.50	69.96	3.01	67.85	29.14
GC-12TB Opxgm	53.19	0.92	0.49	20.53	0.54	21.88	1.90	0.02	0.04	99.52	65.52	3.94	62.93	33.13
GC-12TB Opxclot	53.68	1.90	0.33	17.37	0.34	24.53	1.59	0.05	0.08	99.87	71.57	3.23	69.25	27.51
Boulder Glacier														
BG-3TB OpxAc	51.97	0.70	0.28	22.68	0.64	20.82	1.60	0.02	0.02	98.72	62.07	3.31	60.01	36.68
BG-3TB OpxBc	53.39	0.48	0.12	20.88	0.67	22.47	1.26	0.02	0.01	99.32	65.73	2.58	64.04	33.38
BG-7TB OpxAc	52.08	0.91	0.28	20.87	0.77	20.88	1.27	0.02	0.00	97.08	64.07	2.71	62.33	34.95
BG-7TB OpxBc	52.51	0.94	0.31	20.86	0.77	20.95	1.35	0.08	0.00	97.78	64.16	2.88	62.31	34.81
BG-7TB OpxCc	53.50	0.64	0.33	21.43	0.79	21.89	1.38	0.03	0.01	99.99	64.55	2.84	62.72	34.45

Clot- phenocrysts in crystal clot, inc- mineral analyzed was an inclusion in another mineral, gm- groundmass, c- core, r- rim, Wo- wollastonite content, En- enstatite content, Fs- ferrosilite content.
Analytical error is <3% for major elements and <8% for minor elements.

Table 4. Olivine compositions

Label	SiO_2	FeO*	MnO	NiO	MgO	CaO	Total	Fo
Sulphur Creek								
SC-3TB OAc	40.12	13.80	0.22	0.20	45.09	0.18	99.62	85.35
SC-3TB OAr	36.64	30.58	0.46	0.05	31.13	0.27	99.13	64.48
SC-3TB OBc	36.81	30.43	0.53	0.04	31.06	0.27	99.15	64.54
SC-3TB OBr	36.06	30.77	0.56	0.04	30.93	0.29	98.66	64.19
SC-3TB OCc	37.05	27.10	0.41	0.01	33.16	0.28	98.02	68.57
SC-6TB OAc	39.67	15.08	0.27	0.18	43.97	0.14	99.30	83.87
SC-6TB OAm	40.42	12.93	0.25	0.24	45.56	0.18	99.58	86.27
SC-6TB OAr	38.30	20.04	0.27	0.16	39.86	0.15	98.79	78.00
SC-6TB OBc	40.21	13.04	0.18	0.21	45.91	0.17	99.71	86.26
SC-6TB OBr	37.49	26.93	0.47	0.09	33.99	0.23	99.20	69.23
SC-6TB OCgm	36.33	33.36	0.53	0.01	28.13	0.27	98.63	60.05
SC-7TB OAc	39.23	18.57	0.32	0.10	41.64	0.18	100.04	79.99
SC-7TB OAm	39.57	15.15	0.23	0.20	44.51	0.21	99.87	83.97
SC-7TB OAr	38.28	20.80	0.31	0.15	39.51	0.17	99.23	77.20
SC-7TB OBc	38.92	17.63	0.36	0.17	41.80	0.17	99.05	80.87
SC-7TB OBr	37.90	24.67	0.43	0.07	36.13	0.16	99.36	72.31
Glacier Creek								
GC-3TB OAc	39.94	13.49	0.22	0.36	45.47	0.13	99.61	85.73
GC-3TB OAr	38.15	21.19	0.37	0.27	39.03	0.14	99.16	76.66
GC-6TB OAc	37.70	26.12	0.45	0.23	35.38	0.10	99.98	70.72
GC-6TB OAr	37.81	26.63	0.40	0.19	34.64	0.13	99.81	69.87
GC-6TB OBc	39.77	13.71	0.19	0.35	45.43	0.10	99.55	85.52
GC-6TB OBr	37.59	25.70	0.43	0.13	35.40	0.15	99.39	71.06
GC-6TB OCc	40.00	13.45	0.20	0.32	45.54	0.10	99.61	85.79
GC-6TB OCr	38.79	19.37	0.25	0.22	40.32	0.12	99.07	78.77
GC-12TB Oclot	37.55	25.27	0.34	0.19	35.83	0.15	99.34	71.65
GC-12TB OAc	38.70	21.57	0.34	0.16	38.76	0.13	99.67	76.21
GC-12TB OAr	37.68	25.02	0.41	0.24	35.85	0.15	99.35	71.87
GC-12TB OBc	37.17	28.33	0.47	0.21	33.04	0.14	99.37	67.52
GC-12TB OBr	37.25	27.78	0.49	0.22	33.39	0.07	99.20	68.18
GC-12TB OCc	38.84	20.45	0.24	0.31	39.62	0.16	99.62	77.55
GC-12TB OCr	38.83	21.16	0.30	0.31	39.47	0.13	100.20	76.88
GC-12TB ODc	39.22	16.90	0.27	0.36	42.62	0.10	99.45	81.81
GC-12TB ODr	38.54	20.76	0.28	0.32	39.08	0.11	99.09	77.04
Boulder Glacier								
BG-3TB OAc	38.03	23.36	0.51	0.11	37.69	0.09	99.79	74.20
BG-3TB OAm	38.11	24.85	0.51	0.09	36.35	0.08	100.01	72.28

Clot- phenocrysts in crystal clot, inc- mineral analyzed was an inclusion in another mineral, gm- groundmass, c-core, r- rim, Fo- forsterite content. Analytical error is <3% for major elements and <8% for minor elements.

Table 5. Fe-Ti oxide compositions

Ferrian Ilmenite

Label	SiO_2	TiO_2	Al_2O_3	Cr_2O_3	FeO*	MgO	MnO	Total
Glacier Creek								
GC-3TB IA	0.06	49.33	0.09	0.14	43.47	3.60	0.53	97.22
GC-3TB IB	0.16	40.69	0.10	0.01	50.53	0.40	0.85	92.74
GC-3TB IC	0.02	44.47	0.22	0.08	50.58	1.30	0.38	97.04
GC-6TB IA	0.04	45.56	0.07	0.08	47.57	1.14	0.84	95.31
GC-6TB IB	0.85	45.31	0.07	0.03	45.97	1.25	0.70	94.18
GC-6TB ID	0.11	45.86	0.05	0.05	46.85	1.22	0.81	94.95
GC-12TB IA	0.11	36.93	0.20	0.17	53.25	1.67	0.69	93.03
GC-12TB IB	0.08	44.93	0.08	0.04	46.04	1.98	0.79	93.94
GC-12TB IC	0.07	44.52	0.05	0.11	47.44	1.37	0.83	94.39
Boulder Glacier								
BG-3TB IA	0.03	43.59	0.20	0.00	48.68	2.23	0.53	95.26
BG-3TB IB	0.02	44.08	0.22	0.00	49.80	2.49	0.50	97.12
BG-7TB IA	0.11	46.19	0.12	0.01	47.17	2.54	0.74	96.88
BG-7TB IB	0.09	45.87	0.13	0.03	46.58	2.74	0.62	96.06
BG-10TB IB	0.26	46.77	0.18	0.02	45.11	2.21	0.66	95.21
BG-10TB IC	0.75	43.06	0.36	0.00	48.93	1.72	0.68	95.50

Ulvospinel

Label	SiO_2	TiO_2	Al_2O_3	Cr_2O_3	FeO*	MgO	MnO	Total
Sulphur Creek								
SC-6TB MA	0.09	18.84	2.60	0.69	69.08	3.24	0.53	95.07
SC-6TB MC	0.54	20.05	1.20	0.07	70.26	1.36	0.61	94.10
SC-3TB MA	0.08	19.37	2.70	0.26	69.00	3.87	0.45	95.72
Glacier Creek								
GC-3TB MA	0.06	16.38	1.88	0.29	73.83	2.16	0.38	94.98
GC-3TB MB	0.09	7.69	0.61	0.19	82.62	0.14	0.28	91.62
GC-3TB MC	0.08	9.51	2.09	0.54	79.88	0.56	0.38	93.06
GC-6TB MA	0.14	8.22	0.97	0.28	81.41	0.42	0.40	91.85
GC-6TB MB	0.41	5.95	0.72	0.21	81.80	0.31	0.24	89.64
GC-12TB MB	0.19	4.68	0.68	0.19	83.39	0.55	0.27	89.95
GC-12TB MC	0.11	7.06	0.85	0.29	81.30	0.45	0.25	90.31
Boulder Glacier								
BG-3TB MA	0.08	14.07	1.89	0.07	77.31	1.59	0.45	95.46
BG-3TB MB	0.12	12.24	1.61	0.09	77.98	1.58	0.48	94.10
BG-7TB MA	0.08	13.49	1.70	0.01	76.65	1.34	0.45	93.71
BG-7TB MB	0.09	14.42	1.63	0.05	76.87	1.54	0.58	95.19
BG-7TB MC	0.24	13.55	1.67	0.06	75.84	1.19	0.55	93.10
BG-7TB MD	0.17	13.48	1.64	0.04	75.18	1.25	0.64	92.40

Chromium Spinel

Label	SiO_2	TiO_2	Al_2O_3	Cr_2O_3	FeO*	MgO	MnO	Total
Sulphur Creek								
SC-7TB MA	0.10	16.78	2.84	4.14	67.57	3.05	0.49	94.97
SC-7TB MB	0.05	8.64	7.28	21.58	51.96	5.63	0.44	95.58
SC-7TB MC	0.27	16.59	2.35	3.02	69.12	2.00	0.49	93.84
SC-7TB MD	0.02	8.32	7.61	21.67	52.94	5.08	0.42	96.06

Analytical error is <3% for major elements and <8% for minor elements.

Table 6. Whole-Rock Data

Unit	Sulphur Creek	Sulphur Creek	Sulphur Creek	Sulphur Creek	Sulphur Creek	Sulphur Creek	Sulphur Creek
Sample	SC-1TB	SC-2TB	SC-3TB	SC-4TB	SC-5TB	SC-6TB	SC-7TB
UTM E	594686	590005	589369	592347	592713	591279	593098
UTM N	5391874	5392629	5392029	5392169	5392079	5392878	5392047
Major Elements (wt%)							
SiO_2			55.78			55.66	55.70
TiO_2			1.27			1.32	1.34
Al_2O_3			17.15			17.25	17.11
FeO*			7.35			7.44	7.51
MnO			0.14			0.14	0.15
MgO			4.70			4.86	4.92
CaO			7.29			7.33	7.36
Na_2O			4.21			4.25	4.30
K_2O			1.38			1.36	1.37
P_2O_5			0.36			0.38	0.39
Total			99.64			99.98	100.14
Mg#			57			58	58
XRF analyzed minor elements (ppm)							
Ni	40.8	41.0	38.7	41.3	42.9	43.0	43.1
Cr	96.5	98.6	94.4	99.0	101.5	105.5	104.2
Sc	25.5	24.2	24.7	24.6	24.7	24.3	24.2
V	179.3	178.7	180.6	180.7	180.8	181.1	183.8
Rb	21.9	22.5	22.1	21.7	22.3	21.7	22.0
Sr	546.0	556.9	558.1	543.8	548.1	567.8	538.8
Zr	203.7	184.3	182.4	200.9	188.9	192.2	190.3
Ba	401.4	405.5	399.0	396.0	391.9	395.4	390.2
Ga	20.1	20.6	19.3	20.5	20.2	19.2	18.1
Nb	8.3	7.8	7.7	8.1	7.8	7.9	7.7
Y	29.9	27.2	27.5	29.4	27.8	28.9	28.1
Cu	36.1	36.5	36.7	32.0	33.7	37.6	36.1
Zn	85.5	83.6	82.0	80.7	85.2	84.7	112.3
ICP-MS analyzed trace elements (ppm)							
La	18.64	17.75	17.68	18.52	17.49	18.25	17.73
Ce	42.73	40.15	39.60	42.38	40.14	40.50	40.20
Pr	5.64	5.30	5.24	5.55	5.29	5.44	5.36
Nd	23.98	22.30	22.12	23.63	22.47	22.76	22.60
Sm	5.62	5.14	5.10	5.50	5.27	5.30	5.35
Eu	1.69	1.57	1.56	1.73	1.63	1.65	1.62
Gd	5.54	5.07	5.11	5.50	5.30	5.31	5.24
Tb	0.92	0.85	0.86	0.92	0.88	0.89	0.89
Dy	5.69	5.19	5.28	5.72	5.35	5.31	5.38
Ho	1.15	1.07	1.08	1.15	1.10	1.12	1.10
Er	3.24	2.95	2.94	3.18	2.98	3.00	3.06
Yb	2.89	2.66	2.67	2.90	2.73	2.73	2.75
Lu	0.47	0.43	0.43	0.46	0.43	0.43	0.44
Th	3.08	3.07	3.16	3.03	3.07	3.16	3.03
Hf	4.77	4.39	4.36	4.73	4.49	4.48	4.40
Ta	0.55	0.53	0.52	0.54	0.52	0.53	0.51
U	1.19	1.21	1.25	1.19	1.21	1.24	1.20
Pb	5.23	5.05	5.41	5.12	4.95	5.08	5.10
Cs	0.60	0.65	0.65	0.63	0.63	0.60	0.63
Tm	0.46	0.43	0.42	0.47	0.44	0.44	0.44

Analysis performed at the Washington State University Geoanylitical Laboratory. Sample locations are reported in Universal Transverse Mercator coordinate system (UTM) NAD83. Accuracy and precision estimates for major element analyses and XRF analyzed minor elements are available in Johnson et al., (1999). Mg# = $Mg/(Fe^{2+} + Mg) \times 100$ with Fe^{2+} calculated as 0.85 FeO*.

Table 6. Whole-Rock Data cont.

Unit	Sulphur Creek	Sulphur Creek	Sulphur Creek	Sulphur Creek	Sulphur Creek	Glacier Creek	Glacier Creek
Sample	SC-8TB	SC-9TB	QBSC-2	QBSC-3	QBSC-4	GC-1TB	GC-2TB
UTM E	587374	594969	594951	595757	597244	580726	580785
UTM N	5394632	5390321	5390306	5389932	5391290	5408823	5408697
Major Elements (wt%)							
SiO_2	55.21	55.77	53.47	52.60	52.52		
TiO_2	1.38	1.26	1.63	1.65	1.67		
Al_2O_3	17.43	17.37	19.11	19.04	18.57		
FeO*	7.66	7.10	8.68	8.79	8.84		
MnO	0.15	0.14	0.16	0.16	0.17		
MgO	4.93	4.48	5.48	5.48	5.54		
CaO	7.52	7.23	8.37	8.45	8.54		
Na_2O	4.38	4.32	4.52	4.47	4.38		
K_2O	1.29	1.40	0.91	0.85	0.78		
P_2O_5	0.40	0.37	0.44	0.44	0.44		
Total	100.35	99.44	102.77	101.94	101.45		
Mg#	57	57	57	57	57		
XRF analyzed minor elements (ppm)							
Ni	41.2	45.6	45.0	43.8	43.3	75.1	77.2
Cr	100.3	107.4	105.1	106.8	100.3	90.6	92.8
Sc	24.0	25.0	25.5	26.1	26.9	18.5	18.9
V	179.4	181.1	203.6	208.1	207.6	133.9	136.9
Rb	23.3	19.5	9.7	8.4	7.7	22.2	22.4
Sr	560.2	543.0	543.3	537.9	549.9	872.7	866.5
Zr	188.6	194.9	189.5	190.8	194.0	136.6	135.8
Ba	410.3	375.5	278.4	272.5	279.1	420.2	417.7
Ga	19.5	19.1	18.9	17.6	19.7	20.9	20.8
Nb	7.9	7.8	7.0	7.0	7.2	5.0	5.0
Y	27.7	29.1	30.4	31.0	31.1	17.5	17.8
Cu	34.5	34.2	34.1	41.2	42.6	35.3	35.2
Zn	90.0	83.0	85.8	87.0	87.2	67.4	66.8
ICP-MS analyzed trace elements (ppm)							
La	18.15	17.70	16.06	16.08	16.20	15.57	15.36
Ce	41.46	40.73	38.25	38.71	38.85	33.95	33.92
Pr	5.43	5.46	5.28	5.30	5.36	4.45	4.40
Nd	22.78	23.26	22.99	23.18	23.22	18.27	18.32
Sm	5.26	5.52	5.63	5.71	5.74	3.93	3.91
Eu	1.60	1.76	1.88	1.89	1.93	1.21	1.20
Gd	5.21	5.37	5.75	5.85	5.91	3.72	3.64
Tb	0.87	0.93	0.96	0.98	1.00	0.57	0.57
Dy	5.34	5.57	5.86	6.02	6.07	3.37	3.38
Ho	1.11	1.15	1.21	1.22	1.23	0.68	0.66
Er	2.93	3.14	3.25	3.34	3.41	1.84	1.83
Yb	2.73	2.91	2.96	3.04	3.02	1.68	1.66
Lu	0.44	0.46	0.47	0.47	0.48	0.27	0.26
Th	3.18	2.70	1.38	1.26	1.25	3.02	3.03
Hf	4.47	4.54	4.23	4.29	4.30	3.64	3.60
Ta	0.52	0.53	0.47	0.48	0.49	0.34	0.33
U	1.25	1.04	0.57	0.53	0.52	1.10	1.09
Pb	6.17	4.74	3.69	3.32	2.80	5.81	5.85
Cs	0.66	0.50	0.19	0.21	0.20	0.52	0.52
Tm	0.44	0.46	0.47	0.48	0.49	0.27	0.26

Table 6. Whole-Rock Data cont.

Unit	Glacier Creek	Glacier Creek	Glacier Creek	Glacier Creek	Glacier Creek	Glacier Creek	Glacier Creek
Sample	GC-3TB	GC-4TB	GC-5TB	GC-6TB	GC-7TB	GC-9TB	GC-10TB
UTM E	583714	583795	583414	582497	583313	580807	580895
UTM N	5405079	5404948	5405559	5405689	5405241	5408568	5408558
Major Elements (wt%)							
SiO_2	58.70		58.74	58.34	58.51		
TiO_2	0.87		0.85	0.85	0.84		
Al_2O_3	17.24		17.56	17.25	17.27		
FeO*	5.69		5.93	5.61	5.74		
MnO	0.11		0.11	0.10	0.11		
MgO	4.68		4.89	4.56	4.88		
CaO	7.09		7.20	7.02	7.10		
Na_2O	3.85		3.80	3.86	3.79		
K_2O	1.58		1.53	1.58	1.52		
P_2O_5	0.25		0.24	0.24	0.24		
Total	100.04		100.86	99.42	100.00		
Mg#	63		63	63	64		
XRF analyzed minor elements (ppm)							
Ni	69.8	68.1	74.5	67.1	76.6	81.5	77.5
Cr	90.7	89.1	99.3	87.7	98.7	90.1	91.6
Sc	19.0	18.8	18.1	18.1	18.7	18.4	18.5
V	142.8	142.4	140.8	143.9	146.4	141.0	138.8
Rb	24.6	24.7	22.1	24.0	22.9	21.9	21.5
Sr	850.9	849.2	853.0	840.6	840.9	854.2	859.6
Zr	146.4	147.0	139.0	147.7	140.4	136.3	136.0
Ba	445.0	447.8	427.5	463.5	432.5	420.7	419.5
Ga	20.1	21.0	20.3	19.7	20.2	19.4	20.5
Nb	5.4	5.5	5.1	5.5	5.2	5.0	4.9
Y	18.8	18.9	17.9	18.7	17.9	17.5	17.3
Cu	32.9	25.6	21.7	33.3	44.4	42.8	39.3
Zn	70.7	72.3	70.0	67.7	73.7	68.0	69.5
ICP-MS analyzed trace elements (ppm)							
La	16.59	16.67	15.96	16.88	15.73	15.37	15.33
Ce	36.48	36.74	34.97	37.06	34.62	33.94	33.75
Pr	4.76	4.78	4.56	4.84	4.57	4.45	4.44
Nd	19.54	19.43	18.81	19.85	18.74	18.13	18.31
Sm	4.22	4.17	3.99	4.26	4.04	3.92	3.93
Eu	1.27	1.23	1.21	1.27	1.22	1.20	1.22
Gd	3.87	3.76	3.74	3.87	3.72	3.62	3.64
Tb	0.61	0.60	0.58	0.62	0.59	0.56	0.57
Dy	3.63	3.59	3.45	3.56	3.49	3.31	3.36
Ho	0.72	0.73	0.70	0.72	0.71	0.67	0.68
Er	1.93	1.97	1.91	2.00	1.97	1.84	1.84
Yb	1.75	1.75	1.72	1.78	1.71	1.63	1.65
Lu	0.29	0.28	0.27	0.29	0.27	0.27	0.26
Th	3.39	3.42	3.05	3.37	3.15	2.99	2.96
Hf	3.84	3.87	3.70	3.92	3.73	3.57	3.62
Ta	0.36	0.37	0.35	0.36	0.35	0.33	0.32
U	1.24	1.24	1.15	1.24	1.18	1.10	1.08
Pb	5.19	6.76	9.93	5.99	5.76	6.01	5.50
Cs	0.54	0.45	0.30	0.29	0.42	0.55	0.42
Tm	0.28	0.29	0.27	0.29	0.28	0.27	0.26

Table 6. Whole-Rock Data cont.

Unit	Glacier Creek	Glacier Creek	Boulder Glacier	Boulder Glacier	Boulder Glacier	Boulder Glacier
Sample	GC-11TB	GC-12TB	BG-1TB	BG-2TB	BG-3TB	BG-4TB
UTM E	581493	580988	589947	590068	590216	588467
UTM N	5407523	5408143	5402550	5402397	5402430	5403037
Major Elements (wt%)						
SiO_2		58.72		61.80	64.22	60.18
TiO_2		0.83		0.74	0.65	0.85
Al_2O_3		17.55		17.73	16.44	17.73
FeO*		5.56		5.09	4.27	5.08
MnO		0.10		0.10	0.09	0.09
MgO		4.75		2.68	2.07	3.26
CaO		7.15		5.30	4.42	6.10
Na_2O		3.77		4.50	4.33	3.88
K_2O		1.50		1.98	2.48	1.78
P_2O_5		0.24		0.23	0.19	0.24
Total		100.18		100.15	99.17	99.19
Mg#		64		52	50	57
XRF analyzed minor elements (ppm)						
Ni	74.6	82.5	14.5	17.1	12.4	29.3
Cr	91.0	100.1	13.0	13.4	11.3	29.7
Sc	18.5	18.9	13.0	12.7	10.9	16.3
V	138.4	146.2	113.2	113.7	88.1	129.0
Rb	22.4	21.5	42.0	34.1	50.0	30.0
Sr	869.6	865.5	495.5	545.8	467.9	785.3
Zr	139.2	137.0	181.7	159.6	201.0	159.7
Ba	425.0	421.2	607.0	592.1	660.5	559.3
Ga	19.4	20.8	17.9	19.1	18.4	18.7
Nb	5.0	5.0	7.8	7.8	8.5	6.0
Y	17.7	17.7	21.1	20.1	23.0	21.8
Cu	36.5	22.1	15.8	26.8	23.5	29.8
Zn	69.9	65.5	69.6	69.0	66.1	70.4
ICP-MS analyzed trace elements (ppm)						
La	15.61	15.78	18.19	17.76	21.02	21.04
Ce	34.37	34.68	38.37	37.44	43.01	45.18
Pr	4.48	4.55	4.77	4.64	5.32	5.93
Nd	18.46	18.70	18.90	18.31	20.64	23.83
Sm	3.94	4.00	4.19	4.00	4.44	5.07
Eu	1.20	1.21	1.14	1.14	1.09	1.38
Gd	3.68	3.61	3.98	3.77	4.12	4.57
Tb	0.57	0.57	0.65	0.62	0.68	0.69
Dy	3.37	3.43	3.96	3.86	4.17	4.11
Ho	0.69	0.69	0.81	0.78	0.87	0.84
Er	1.86	1.85	2.29	2.15	2.42	2.27
Yb	1.68	1.69	2.18	2.11	2.36	2.02
Lu	0.27	0.27	0.35	0.33	0.38	0.32
Th	3.03	3.00	5.40	3.88	6.36	4.02
Hf	3.66	3.67	4.83	4.14	5.26	4.09
Ta	0.34	0.33	0.58	0.53	0.65	0.42
U	1.12	1.10	2.12	1.60	2.53	1.47
Pb	6.45	5.63	7.12	6.06	8.40	4.84
Cs	0.55	0.30	1.09	0.46	1.36	0.36
Tm	0.27	0.27	0.35	0.32	0.36	0.32

Table 6. Whole-Rock Data cont.

Unit	Boulder Glacier	Boulder Glacier	Boulder Glacier	Boulder Glacier
Sample	BG-7TB	BG-8TB	BG-9TB	BG-10TB
UTM E	589206	590566	591208	591304
UTM N	5402906	5402230	5401810	5401590
Major Elements (wt%)				
SiO_2	63.63			61.66
TiO_2	0.65			0.75
Al_2O_3	16.26			17.65
FeO*	4.32			5.16
MnO	0.09			0.11
MgO	2.07			2.76
CaO	4.37			5.35
Na_2O	4.29			4.48
K_2O	2.47			1.96
P_2O_5	0.19			0.23
Total	98.34			100.11
Mg#	50			53
XRF analyzed minor elements (ppm)				
Ni	13.4	14.0	25.8	22.9
Cr	12.9	14.2	24.0	45.1
Sc	14.9	12.8	14.8	20.0
V	110.8	99.5	118.6	147.4
Rb	43.2	45.0	54.4	33.0
Sr	509.2	486.6	667.8	601.9
Zr	179.6	186.8	208.6	171.8
Ba	597.4	631.5	668.5	548.3
Ga	18.8	18.2	20.7	20.2
Nb	8.0	8.1	8.8	7.3
Y	22.9	21.9	28.8	25.0
Cu	23.5	21.4	32.0	31.1
Zn	68.0	67.8	127.7	73.2
ICP-MS analyzed trace elements (ppm)				
La	19.50	20.07	24.69	19.05
Ce	39.65	41.69	53.58	40.41
Pr	5.03	5.10	6.93	5.43
Nd	19.81	19.87	27.99	22.19
Sm	4.32	4.27	6.26	4.96
Eu	1.15	1.12	1.53	1.39
Gd	4.14	3.98	5.81	4.82
Tb	0.68	0.66	0.93	0.78
Dy	4.19	4.11	5.62	4.73
Ho	0.86	0.83	1.11	0.96
Er	2.43	2.29	3.16	2.65
Yb	2.28	2.27	2.98	2.44
Lu	0.37	0.37	0.48	0.39
Th	5.36	5.73	7.67	4.00
Hf	4.70	4.86	5.39	4.37
Ta	0.59	0.61	0.68	0.51
U	2.10	2.27	2.91	1.60
Pb	7.92	8.58	8.88	6.62
Cs	1.16	1.17	1.23	0.91
Tm	0.36	0.35	0.47	0.39

Table 7. Fe-Ti oxide and pyroxene thermometry and barometry

	Ulvospinel						*Ferrian Ilmenite*							*Results*	
Oxide Pair		TiO_2	Fe_2O_3	FeO	Al_2O_3	MnO	MgO	TiO_2	Fe_2O_3	FeO	Al_2O_3	MnO	MgO	Temp. °C	fO_2
	Glacier Creek						*Glacier Creek*								
1	GC-3TB MA	16.38	34.83	42.49	1.88	0.38	2.16	GC-3TB IA	49.33	6.64	37.50	0.09	0.53	3.60	827.25	-14.14
2	GC-6TB MA	8.22	49.36	37.00	0.97	0.40	0.42	GC-6TB IA	45.56	10.46	38.16	0.07	0.84	1.14	785.45	-13.88
3	GC-6TB MB	5.95	52.08	34.93	0.72	0.24	0.31	GC-6TB IB	45.31	7.93	38.84	0.07	0.70	1.25	744.75	-14.82
4	GC-12TB MB	4.68	55.71	33.26	0.68	0.27	0.55	GC-12TB IB	44.93	10.97	36.17	0.08	0.79	1.98	749.56	-14.15
	Boulder Glacier							*Boulder Glacier*								
5	BG-3TB MA	14.07	39.81	41.49	1.89	0.45	1.59	BG-3TB IA	43.59	15.49	34.74	0.20	0.53	2.23	923.59	-11.19
6	BG-3TB MB	12.24	42.82	39.45	1.61	0.48	1.58	BG-3TB IB	44.08	16.74	34.74	0.22	0.50	2.49	899.85	-11.41
7	BG-7TB MA	13.49	39.89	40.75	1.70	0.45	1.34	BG-7TB IA	46.19	11.98	36.39	0.12	0.74	2.54	881.53	-12.15
8	BG-7TB MB	14.42	39.17	41.62	1.63	0.58	1.54	BG-7TB IB	45.87	11.93	35.85	0.13	0.62	2.74	894.18	-11.96

		Cpx		*Opx*		
Pyroxene Pair	Sample	En	Wo	En	Wo	Temp. °C
	Sulphur Creek					
1	SC-3TB	44	41	70	3	1027
2	SC-6TB	42	41	65	3	999
	Glacier Creek					
1	GC-6TB	43	43	65	4	1013
2	GC-12TB	41	40	68	3	1015
	Boulder Glacier					
1	BG-3TB	40	43	64	3	994
2	BG-7TB	41	42	62	3	977

Temperature and fO_2 conditions were calculated according to the techniques of Anderson and Lindsley (1985) using the Quilf software package (Anderson et al., 1993) and the ILMAT spreadsheet of Lapage (2003). The fO_2 conditions indicate log units different when compared to the Q-F-M buffer.

Table 8. Glacier Creek olivine/liquid equilibrium calculations

Label	SiO_2	Fe	Mg	$(Fe/Mg)_{Olv}$ / $(Fe^{2+}/Mg)_{WR}$	Mg $\#_{Liq}$	Mg $\#_{WR}$
Whole Rock						
GC-3TB	58.70	0.07	0.12	.44-.45		63
GC-6TB	58.34	0.07	0.11	.23-.62		63
GC-12TB	58.72	0.07	0.12	.34-71		64
Olivine Core						
GC-3TB OAc *	39.94	0.19	1.13	0.29	64	
GC- 6TB OAc	37.70	0.36	0.88	0.70	42	
GC- 6TB OBc *	39.77	0.19	1.13	0.29	64	
GC- 6TB OCc *	40.00	0.19	1.13	0.28	64	
GC-12TB OAc	38.70	0.30	0.96	0.56	49	
GC-12TB OBc	37.17	0.39	0.82	0.86	38	
GC-12TB OCc	38.84	0.28	0.98	0.52	51	
GC-12TB Odc	39.22	0.24	1.06	0.40	57	
Olivine Rim						
GC- 3TB OAr	38.15	0.29	0.97	0.53	50	
GC- 6TB OAr	37.81	0.37	0.86	0.73	41	
GC- 6TB OBr *	37.59	0.36	0.88	0.69	42	
GC- 6TB OCr *	38.79	0.27	1.00	0.46	53	
GC-12TB OAr	37.68	0.35	0.89	0.70	43	
GC-12TB OBr	37.25	0.39	0.83	0.83	39	
GC-12TB OCr	38.83	0.29	0.98	0.54	50	
GC-12TB Odr	38.54	0.29	0.97	0.53	50	

Olivine liquid equilibrium calculations follow the methods of Roeder and Emslie (1970). The relationship is described as $Kd=.03=(Fe/Mg)_{Olv} / (Fe/Mg)_{Liq}$. The equation is rearranged to calculate Mg#'s of liquids that are in equilibrium with olivine compositions. The rearranged equation is as follows: $Mg\#_{Liq} = 100 / [((Fe/Mg)_{Olv} / 0.3) + 1]$. Samples labels with an asterisk correspond to olivine classified as the large mafic variety. Whole rock Mg#'s are calculated as $(100 \times (Mg/Mg + Fe^{2+}))$. Fe^{2+} is calculated as 0.85 Fe* for whole rock compositions.

Table 9. Glacier Creek olivine subtraction calculations

Label	SiO_2	TiO_2	Al_2O_3	FeO*	MgO	CaO	Na_2O	K_2O	Total	Mg #
Original Whole Rock Composition										
GC-3TB	58.70	0.87	17.24	5.69	4.68	7.09	3.85	1.58	100.06	63
GC-6TB	58.34	0.85	17.25	5.61	4.56	7.02	3.86	1.58	99.41	63
GC-12TB	58.72	0.83	17.55	5.66	4.75	7.15	3.77	1.50	100.27	64
Subtracted Olivine Composition										
	38.00			15.00	40.00	7.00				
New Whole Rock Compositions after subtraction of 4.1 wt% olivine										
GC-3TB	59.56	0.91	17.96	5.30	3.21	7.09	4.01	1.65	99.69	56
GC-6TB	59.19	0.89	17.97	5.22	3.08	7.02	4.02	1.65	99.03	55
GC-12TB	59.58	0.86	18.28	5.27	3.28	7.16	3.93	1.56	99.93	57

Glacier Creek whole rock compositions before and after 4.0 wt % mafic olivine subtraction.

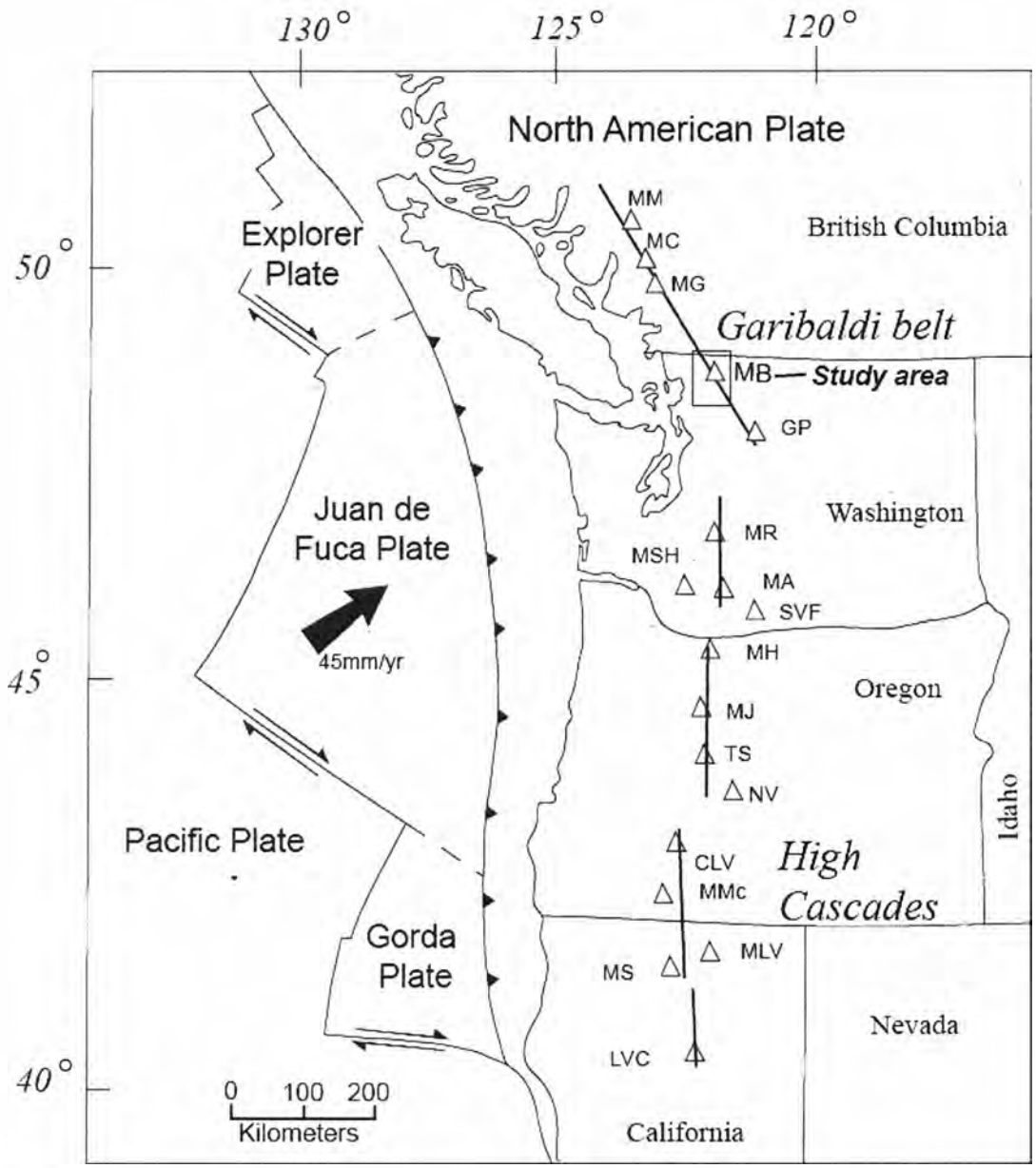

Figure 1.
Cascade magmatic arc. and tectonic setting. Black lines indicate the five segments of the Cascade arc after Guffanti and Weaver (1988) and Green and Harry (1999). The northernmost segment is the Garibaldi belt and Mount Baker is denoted as Study area. Locations of major volcanic centers throughout the Cascade arc are denoted by triangles with abbreviated labels; MM, Meager Mountain; MC, Mount Cayley; MG, Mount Garibaldi; MB, Mount Baker; GP, Glacier Peak; MR, Mount Rainier; MSH, Mount St. Helens; MA, Mount Adams; SVF, Simcoe Volcanic Field; MH, Mount Hood; MJ, Mount Jefferson; TS, Three Sisters; NV, Newberry Volcano; CLV, Crater Lake Volcano; MMc, Mount McLoughlin; MLV, Medicine Lake Volcano; MS, Mount Shasta; LVC, Lassen Volcanic Center.

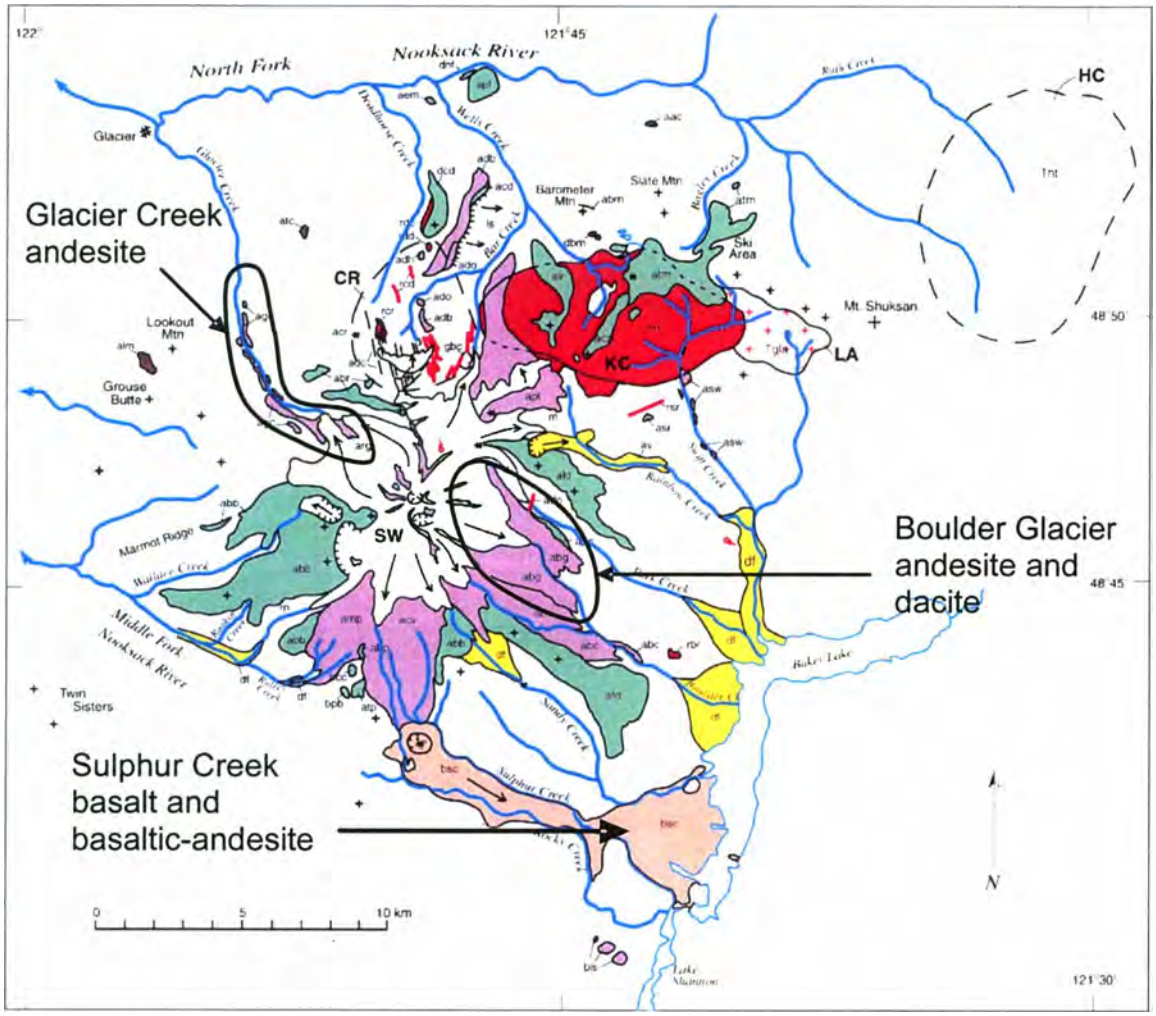

Figure 2.
Geologic map of Mount Baker and related volcanic units from Hildreth et al. (2003). Red units represent early Pleistocene rhyodacites, mainly the Kulshan caldera, green are mid Pleistocene units, purple are late Pleistocene units, orange are Holocene units, yellow are Holocene debris flows and white areas are glaciated.

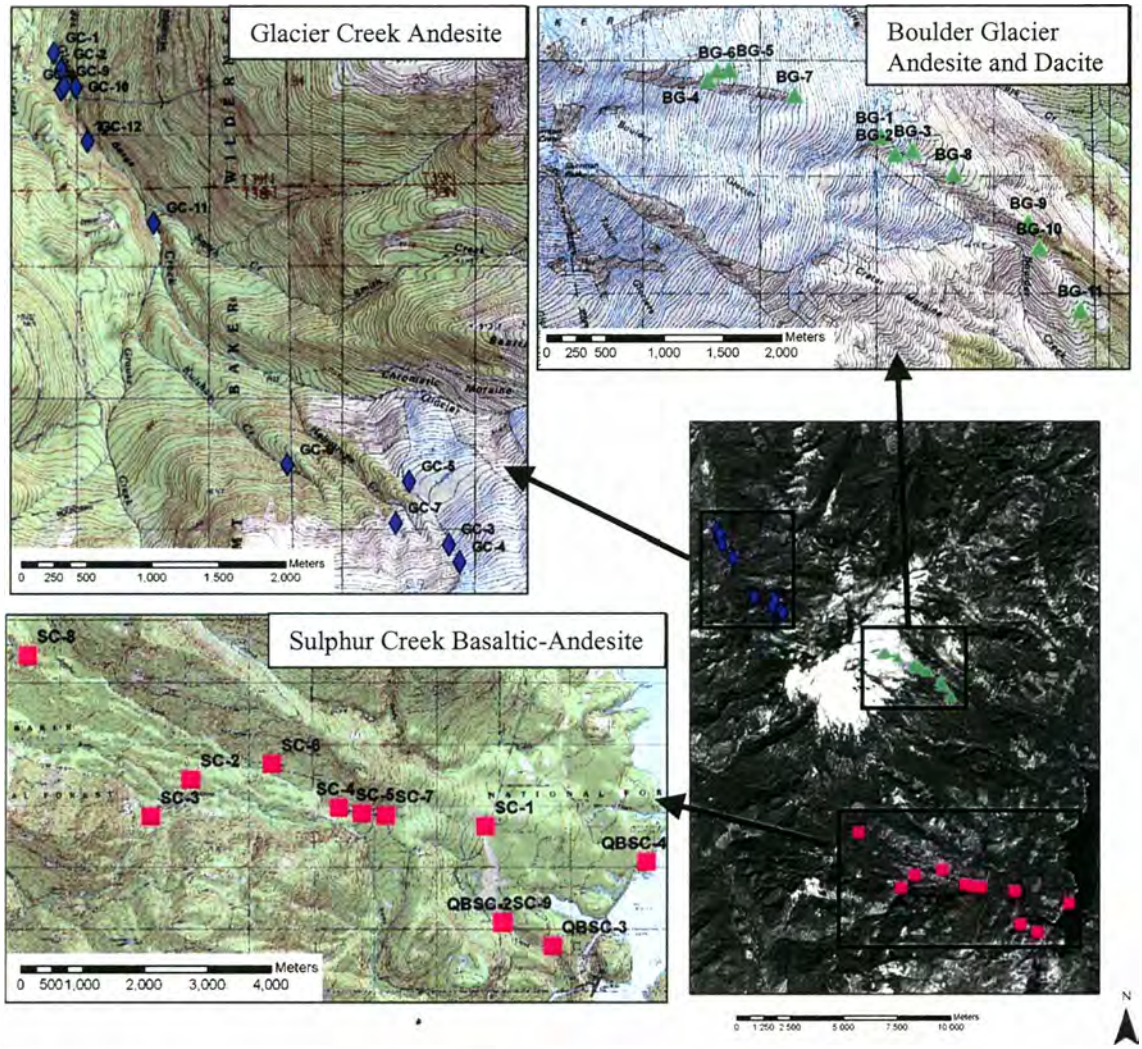

Figure 3.
Sample locations are plotted in Universal Transverse Mercator coordinate system (UTM) NAD83 on a composite 7.5 minute quadrangle topographic maps. Blue diamonds denote the Glacier Creek samples, green triangles denote the Boulder Glacier samples and pink squares denote the Sulphur Creek samples.

A. Plagioclase

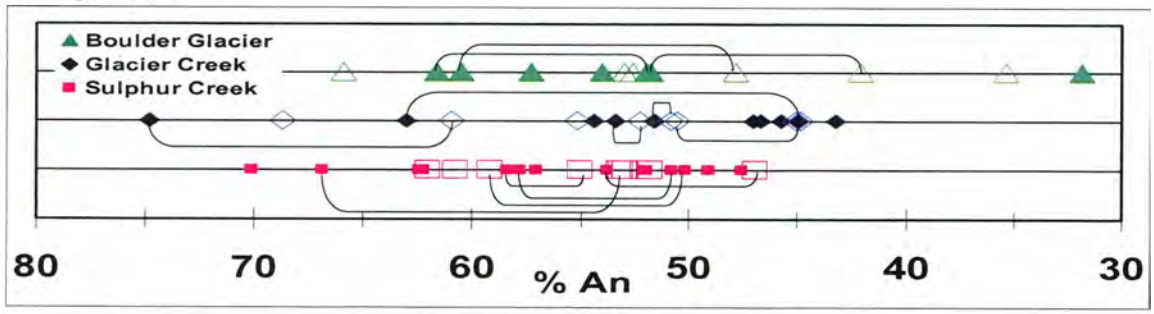

B. Olivine

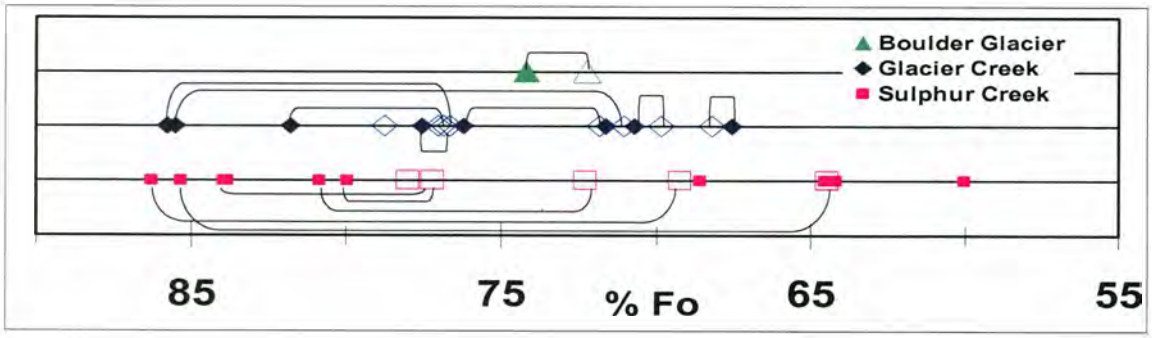

C. Pyroxene

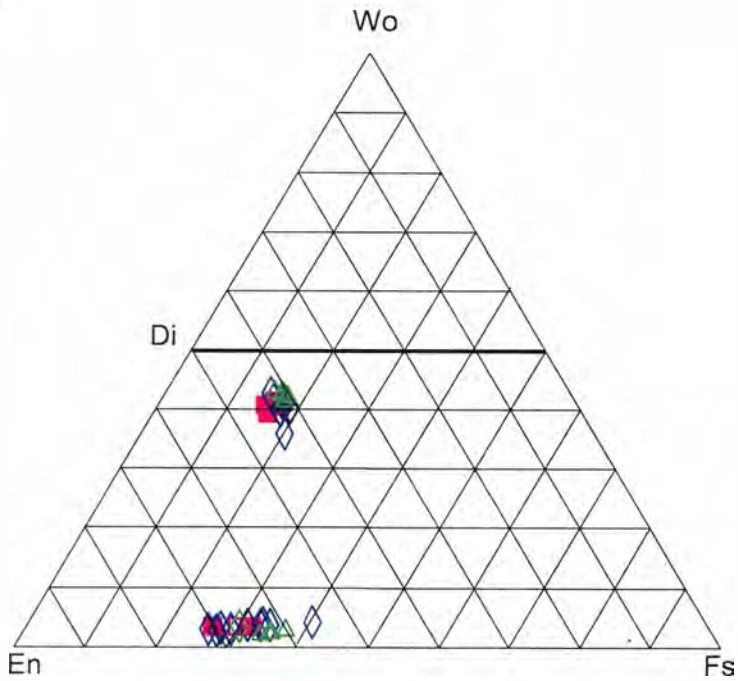

Figure 4.
Graphical representation of mineral compositions of (**A**) Plagioclase, An is anorthite (**B**) Olivine, Fo is forsterite. Brackets connect core and rim analyses from single phenocrysts. (**C**) Pyroxene, En is enstatite, Wo is wollastonite, Fs is ferrosilite. In figures 4A and 4B, solid shapes represent core compositions while open shapes represent rim compositions. Colors correspond to colors as in Figure 3.

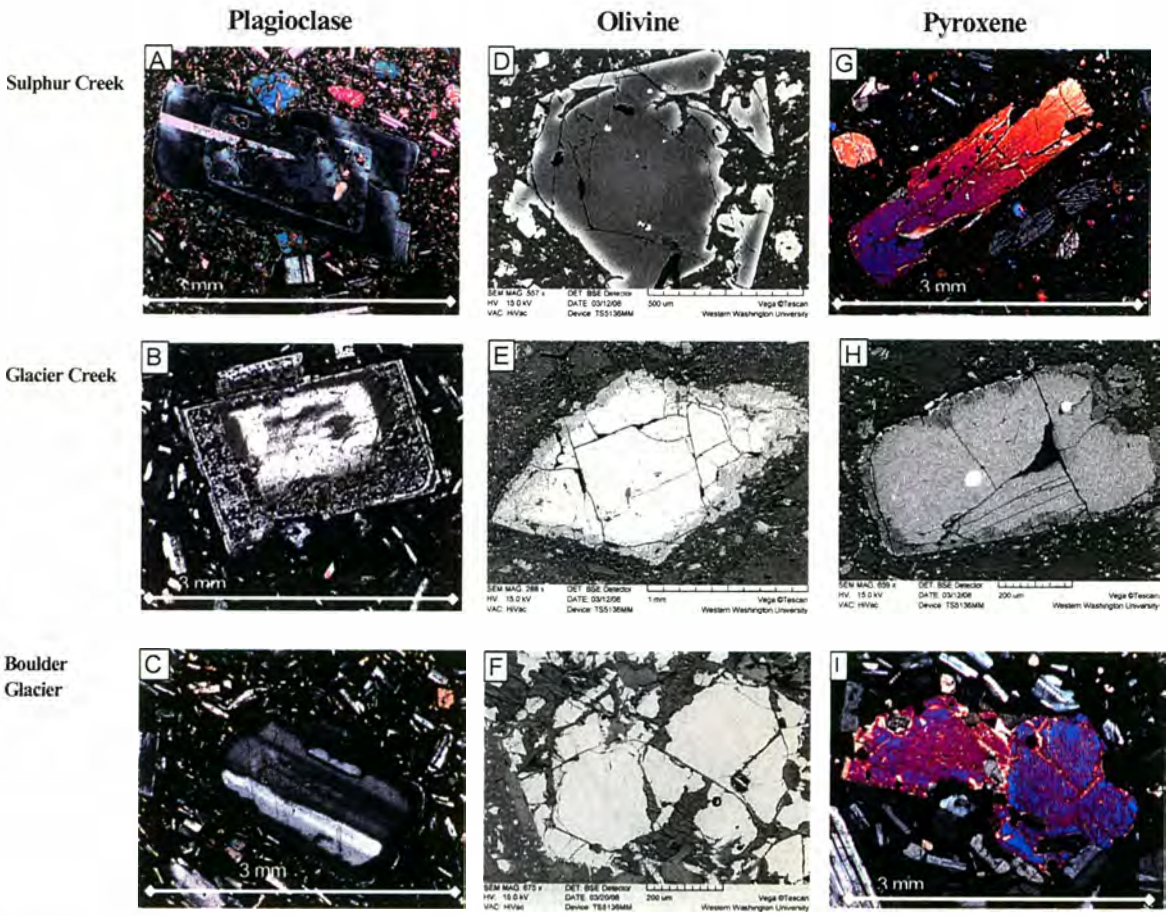

Figure 5.
Common reaction textures in plagioclase, olivine and pyroxene phenocrysts in each unit. Gray scale images are back scatter electron images and color images are photomicrographs in polarized light. **A**) Sulphur Creek plagioclase phenocryst with chemical zoning patterns and sieved core texture with a slightly embayed rim. **B**) Glacier Creek plagioclase phenocryst with a sieved rim. **C**) Boulder Glacier plagioclase phenocryst with a resorbed and sieved rim with inclusions of Fe-Ti oxide minerals in the core. **D**) Chemically zoned and resorbed olivine phenocryst with Fe-Ti oxide inclusions from Sulphur Creek. **E**) Chemically zoned and partially resorbed olivine phenocrysts from the lavas of Glacier Creek. **F**) Resorbed olivine phenocrysts in the lavas of Boulder Glacier. **G**) Sulphur Creek clinopyroxene phenocryst with a resorbed rim and inclusions of Fe-Ti oxides. **H**) Glacier Creek orthopyroxene phenocrysts with a reaction rim. **I**) Resorbed Boulder Glacier clinopyroxene phenocryst.

6A)

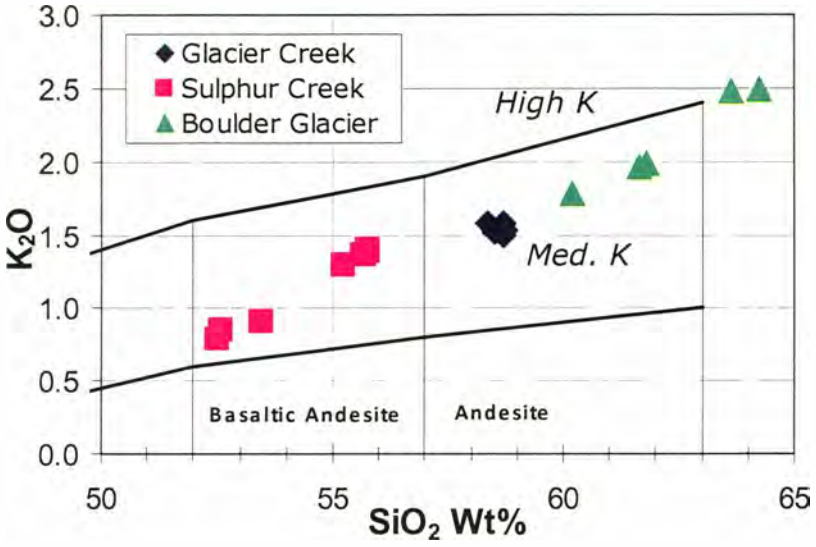

6B)

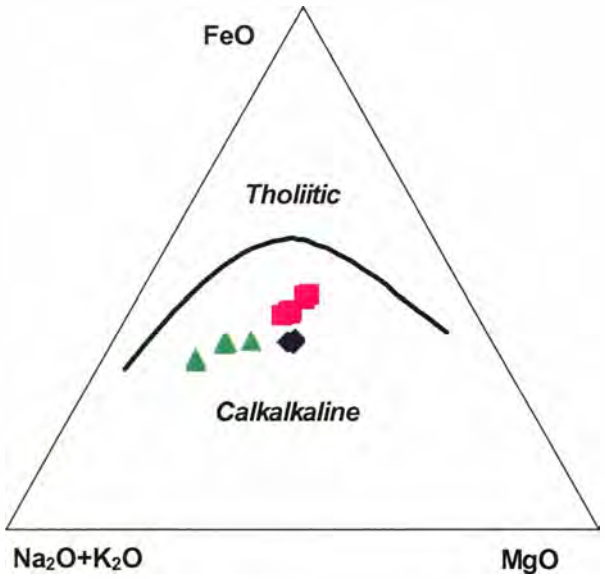

Figure 6.
A) K_2O vs. SiO_2 classification diagram after Gill (1981). **B)** AFM classification diagram after Irvine and Baragar (1971).

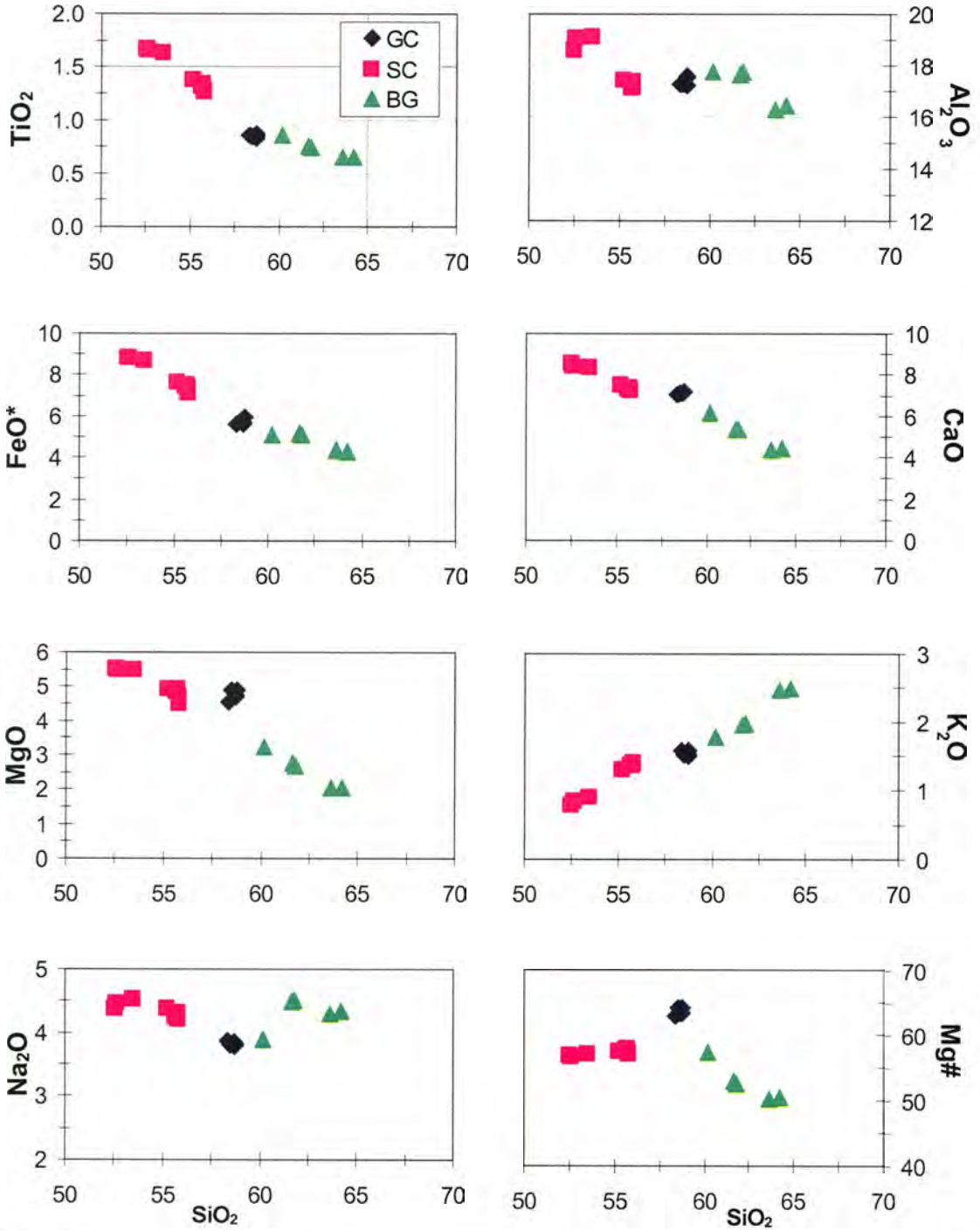

Figure 7.
Whole-rock major element compositions for the Sulphur Creek (SC), Glacier Creek (GC) and Boulder Glacier (BG) units. All major elements are plotted against SiO_2 on the x-axis. Mg# = Mg / (Mg + Fe^{2+}) with Fe^{2+} calculated as 0.85 FeO*. Major Element XRF precision and accuracy estimates are available in Johnson et al., (1999)

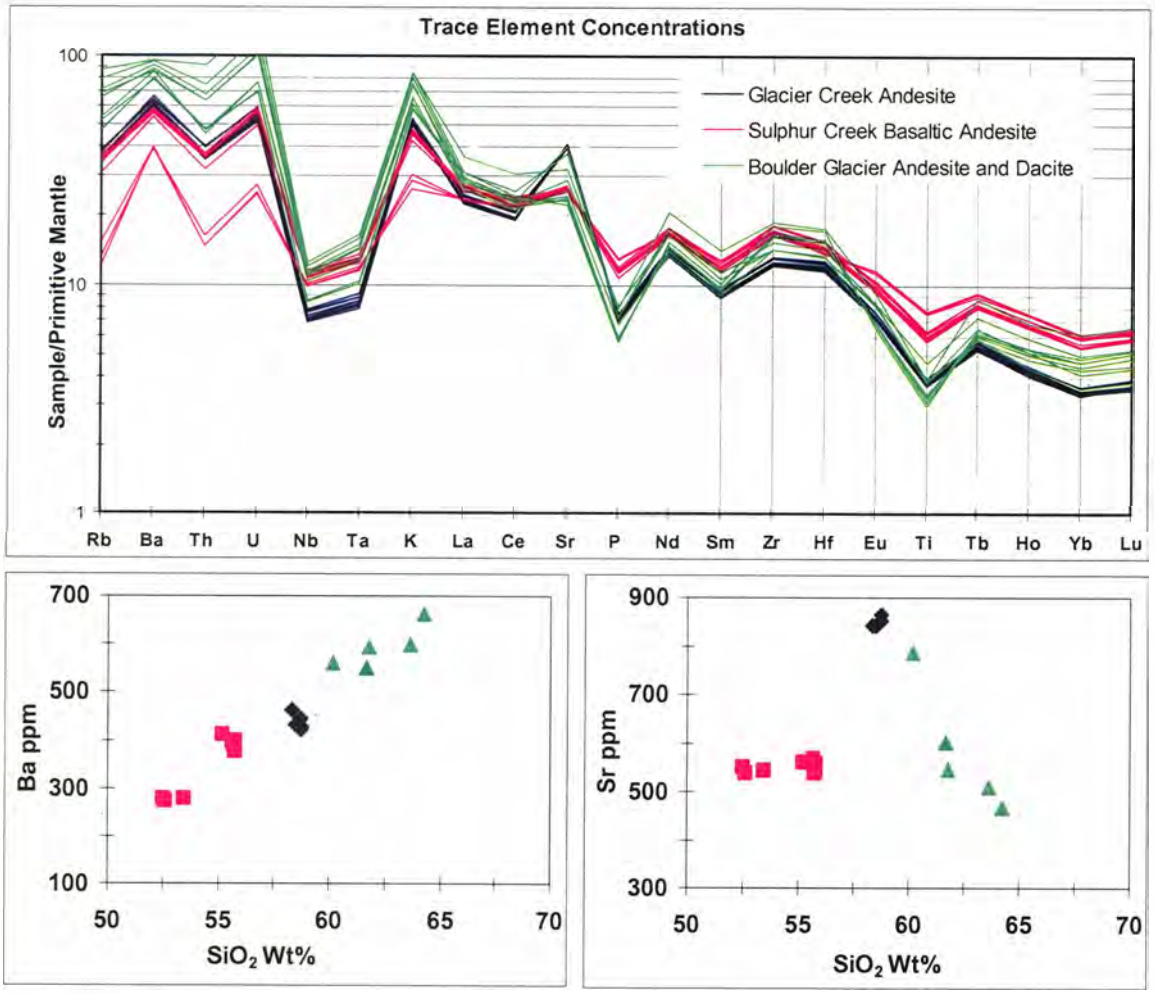

Figure 8.
Primitive mantle normalized trace element diagram. Values are normalized to primitive mantle concentrations of Sun & McDonough (1989). Select trace elements are plotted against SiO_2 to show how trace element patterns change with differentiation. Symbols are the same as in Figure 7.

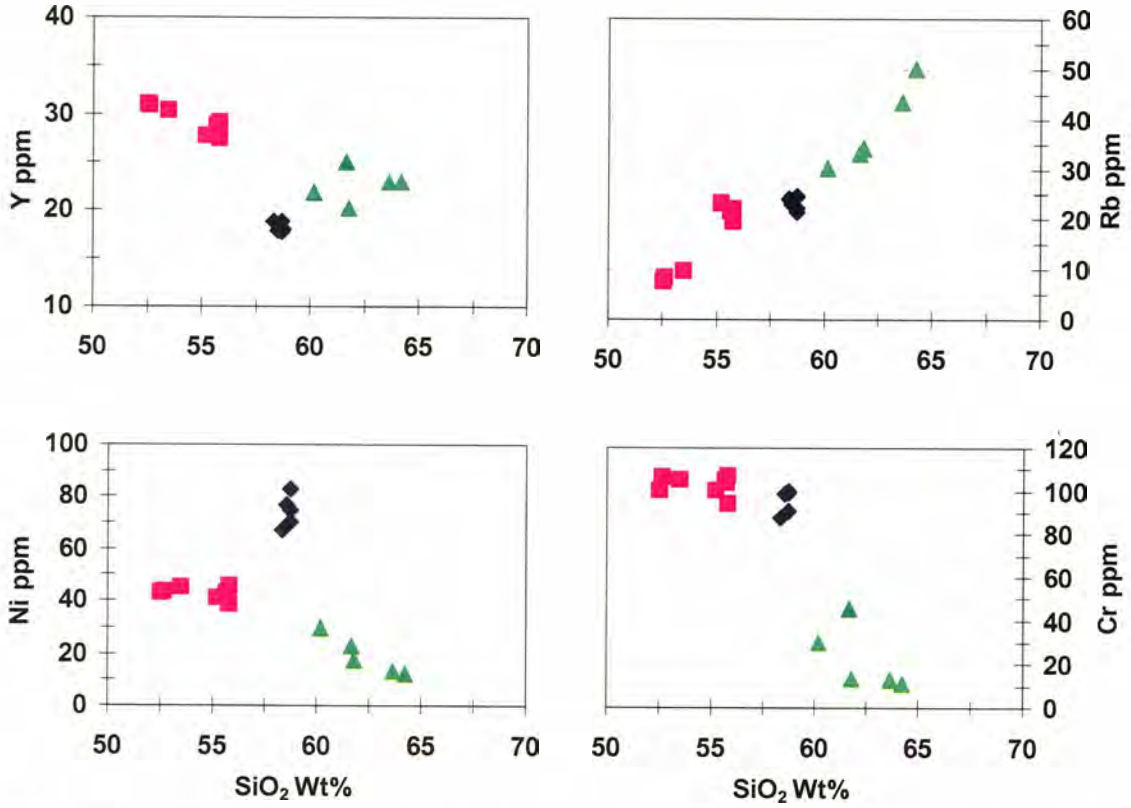

Figure 9.
Select trace elements plotted against SiO_2 on the x-axis. Symbols are the same as in Figure 7.

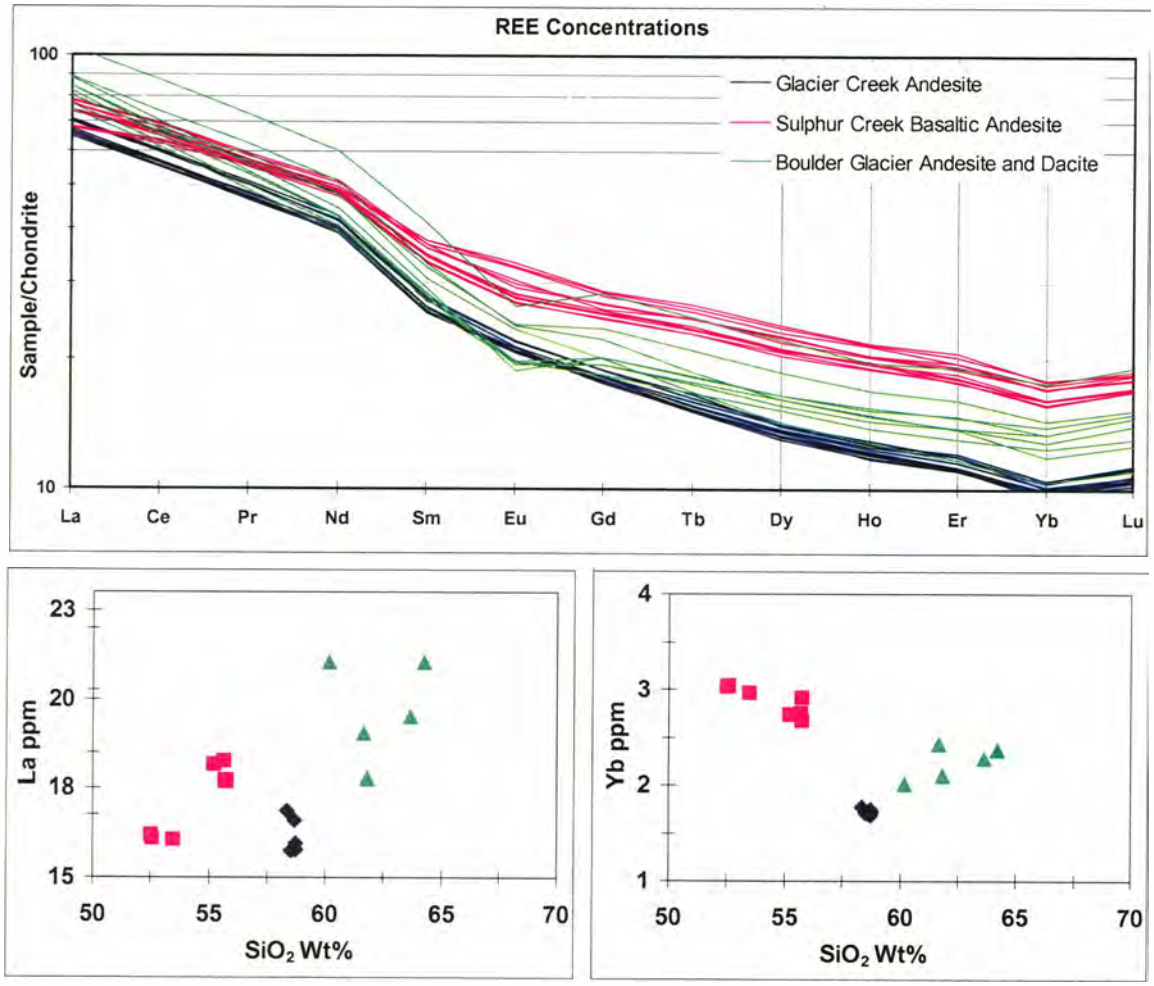

Figure 10.
Chondrite normalized Rare Earth Element diagram. Values are normalized to chondrite concentrations of Sun and McDonough (1989). Select REE's are plotted against SiO_2 to show how REE patterns change with differentiation.

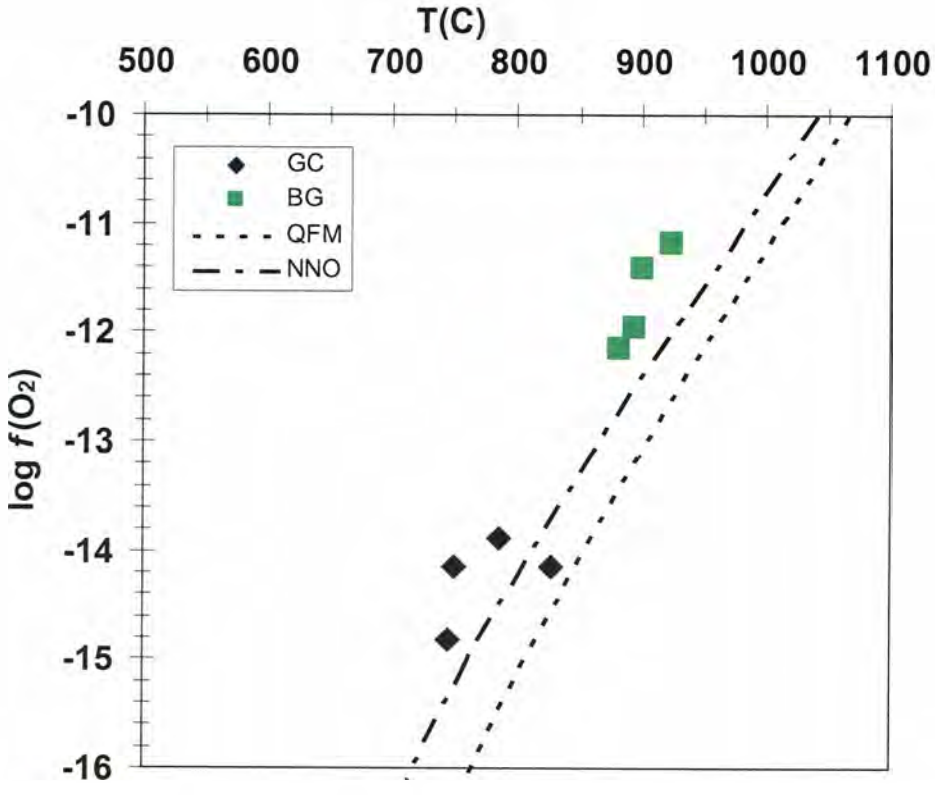

Figure 11.
Liquidus temperatures and fo_2 conditions estimated from Fe-Ti oxide pairs in the Glacier Creek (GC) and Boulder Glacier (BG) units. Diagram and location of buffer curves are redrawn from Eugster and Wones (1962). QFM- Quartz-Faylite-Magnetite buffer curve, NNO- Nickel-Nickel Oxide buffer curve.

12A.

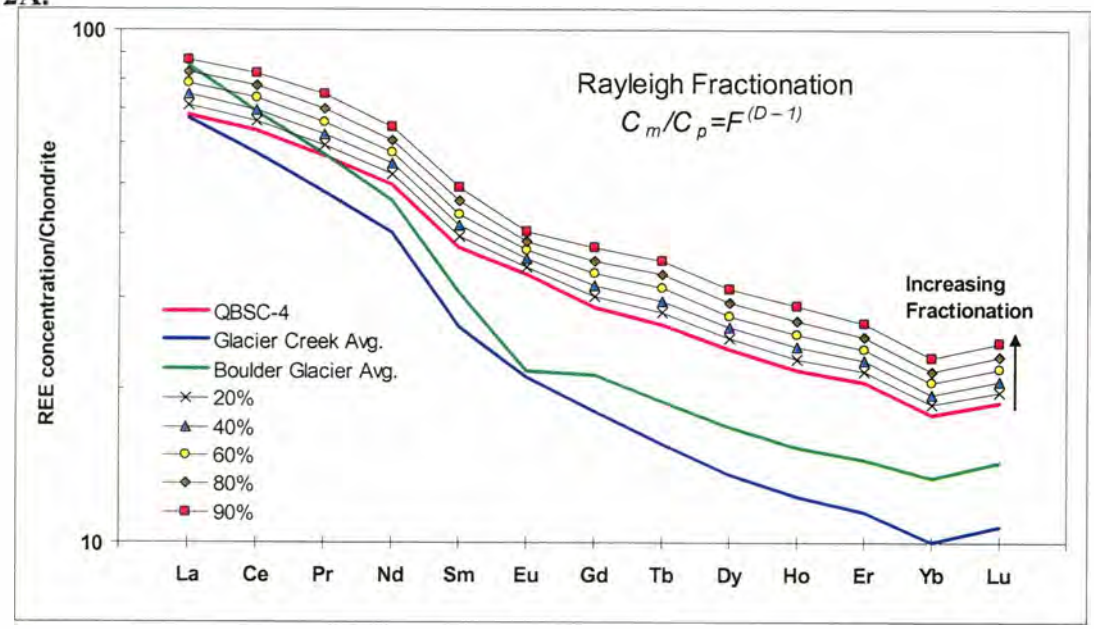

12B.

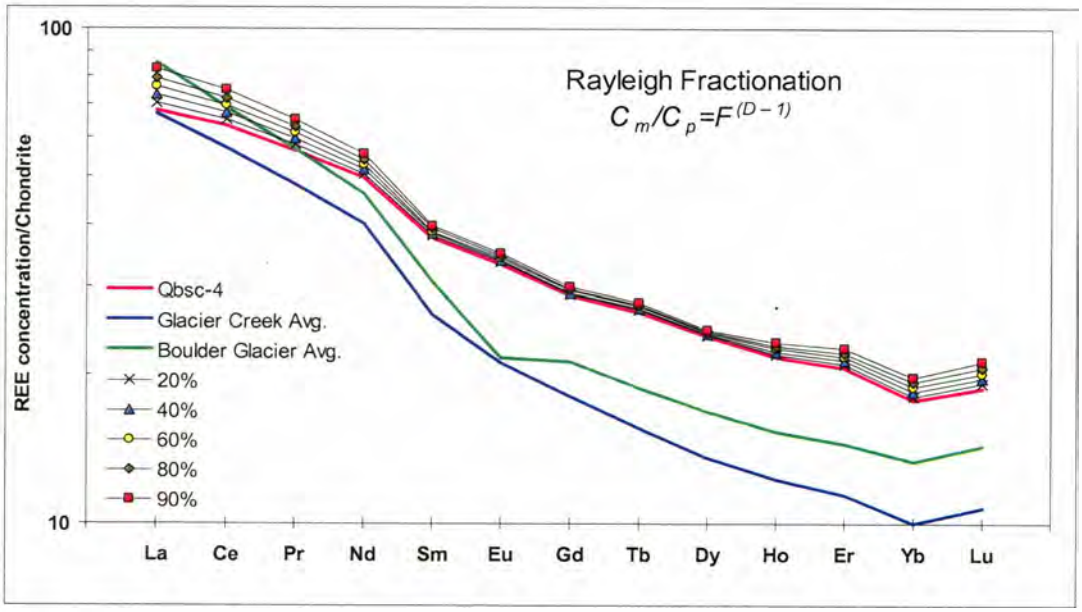

Figure 12.
Results of Rayleigh fractional crystallization of the most mafic Sulphur Creek basalt sample compared to average Glacier Creek and Boulder Glacier compositions. C_m is concentration in residual melt, C_p is concentration in parent magma, F is melt fraction, D is bulk distribution coefficient. Modeled results are denoted by percent fractionation. **A)** Fractionating assemblages are 69% plagioclase + 20% orthopyroxene + 10% olivine + 1% magnetite. **B)** Fractionating assemblages include hypothetical amounts of hornblende and apatite and are 50% plagioclase + 30% hornblende + 10% olivine + 9.5% orthopyroxene + 0.5% apatite. Sample Qbsc-4 is the most mafic sample and is used as the starting composition.

13A.

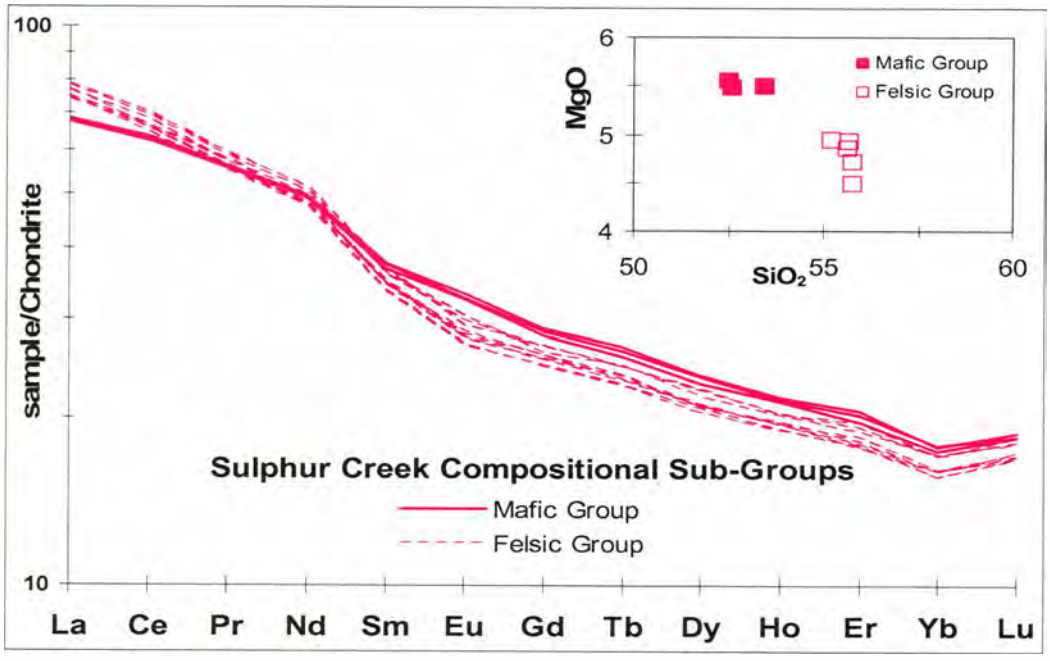

13B.

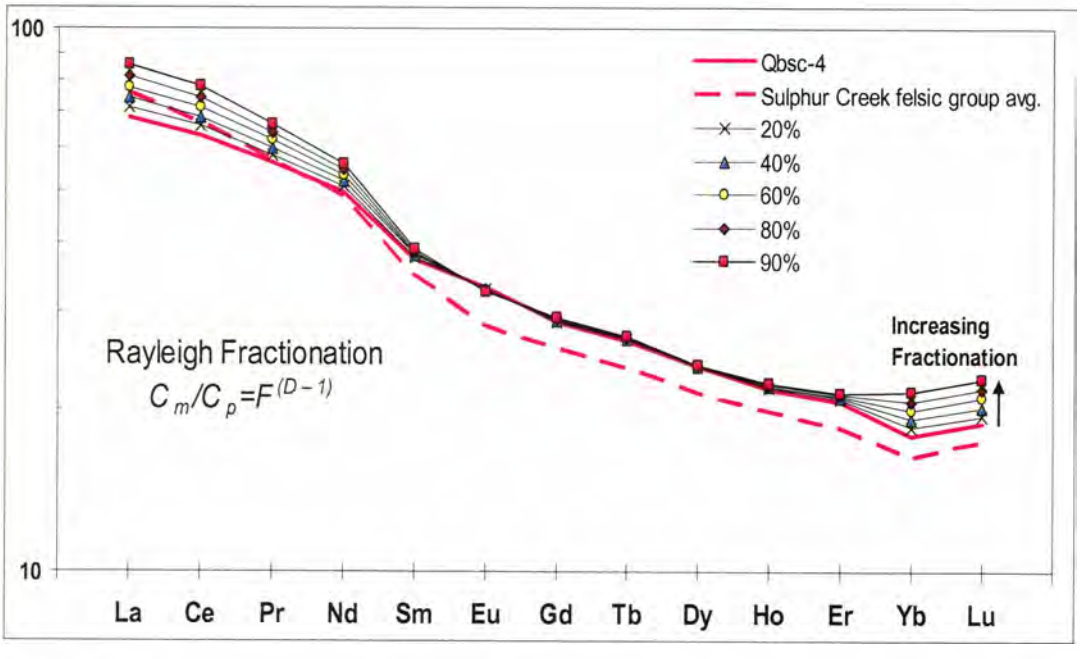

Figure 13.
A) Sulphur Creek compositional sub-groups. The Sulphur Creek unit is broken into a more felsic group and a more mafic group based on a compositional gap observed in major and trace element compositions. **B)** Results of a Rayleigh fractionation model with a starting compositions of Qbsc-4 and a hypothetical fractionating assemblage of 50% plagioclase + 20% hornblende + 14% olivine + 8% orthopyroxene + 8% clinopyroxene.

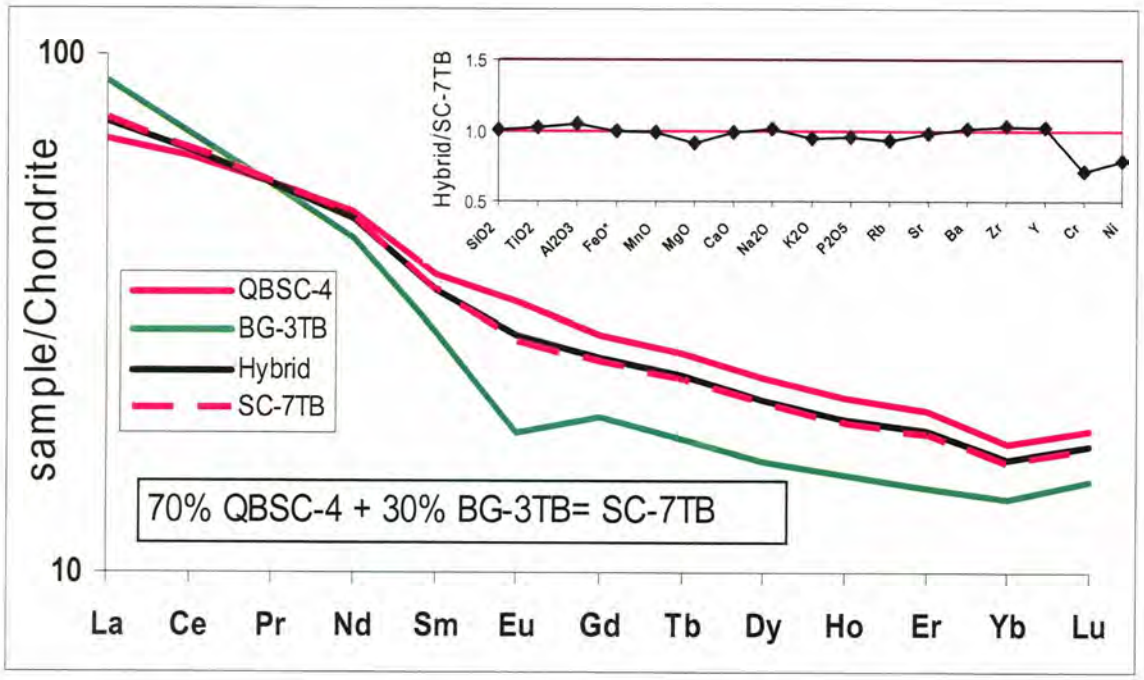

Figure 14.
Magma mixing model between the mafic Sulphur Creek compositions and Boulder Glacier dacites. A hybrid liquid composed of 70% Qbsc-4 and 30% BG-3TB is compared to a measured felsic Sulphur Creek sample, SC-7TB. REE results are shown on a chondrite normalized diagram. Major element and select trace element results are shown by comparing the calculated hybrid liquid to measured element concentrations for SC-7TB.

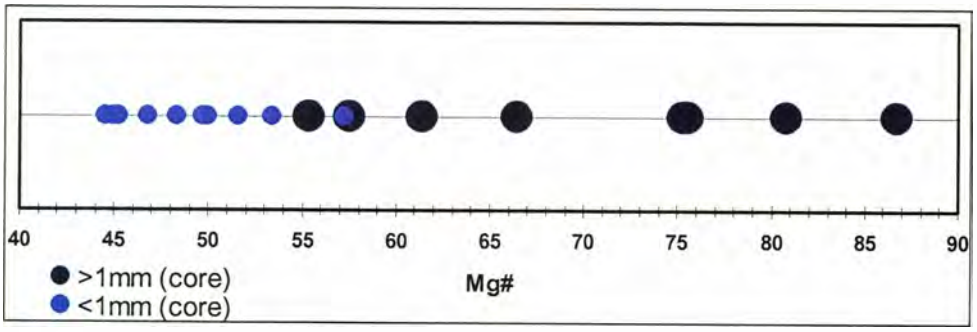

Figure 15.
Mg# and size relationship of Olivine phenocrysts from SEM analyses in the Glacier Creek unit. Each circle represents a core composition of a single olivine phenocryst. Composition data in figure 15 are from qualitative SEM analyses and should not be compared directly to microprobe data.

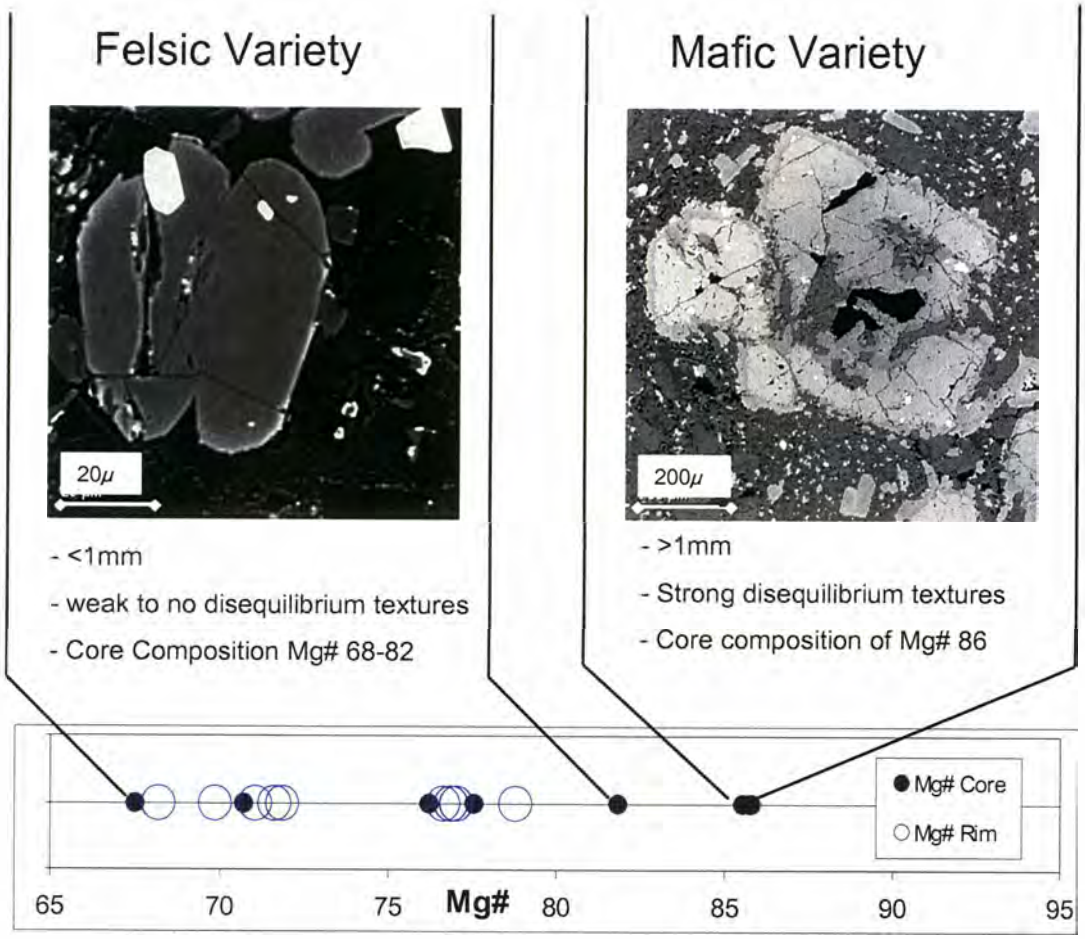

Figure 16. Figure highlights the characteristics of the bimodal olivine population in the Glacier Creek Andesite. Grey scale images are SEM backscatter electron images.

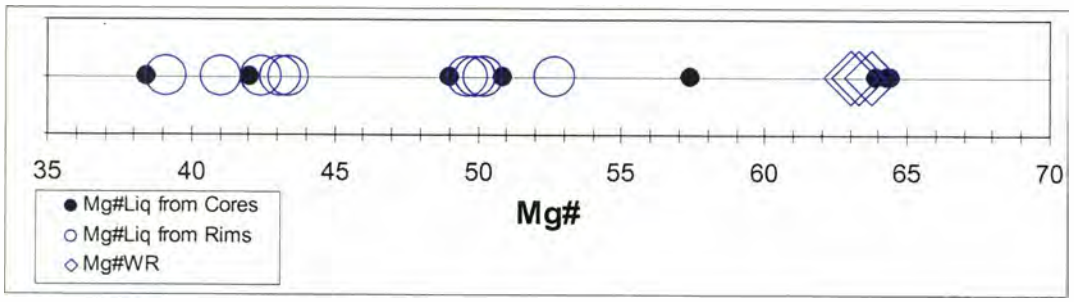

Figure 17.
Comparison of Glacier Creek whole-Rock Mg#'s (open blue diamonds) and liquid Mg#'s calculated from olivine phenocryst core (solid blue circle) and rim (open blue circle) compositions from microprobe data using the liquid/olivine equilibrium conditions described by Roeder and Emslie (1970).

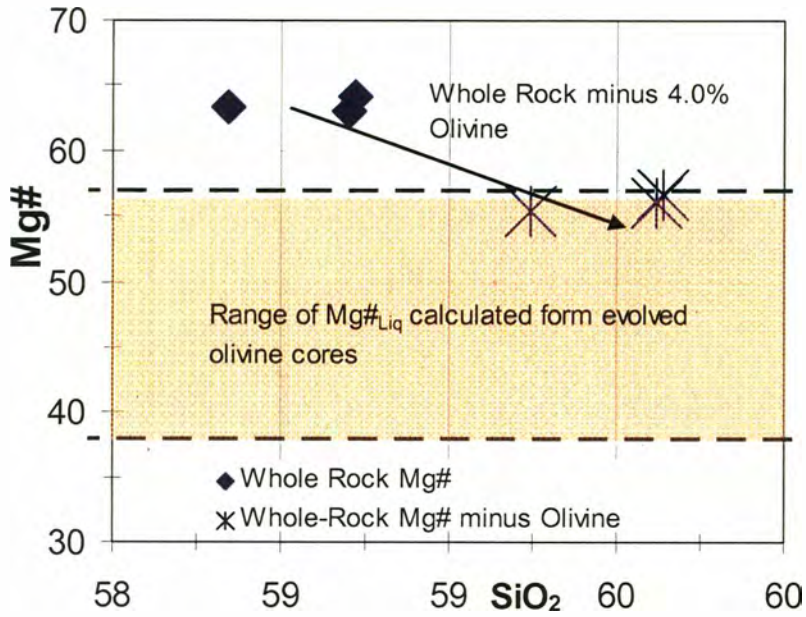

Figure 18.
Glacier Creek olivine subtraction model. Shaded area indicates Mg# of liquid in equilibrium with cores from the evolved olivine population calculated using the liquid/olivine equilibrium conditions described by Roeder and Emslie (1970). See Table 9 for $Mg\#_{Liq}$ values. Solid diamonds represent Glacier Creek whole-rock compositions. Subtraction of 4.0 wt. % xenocrystic olivine from Glacier Creek whole-rock compositions results in new Glacier Creek compositions (blue x's) that are in equilibrium with liquid compositions suggested by cores from evolved olivine phenocrysts.

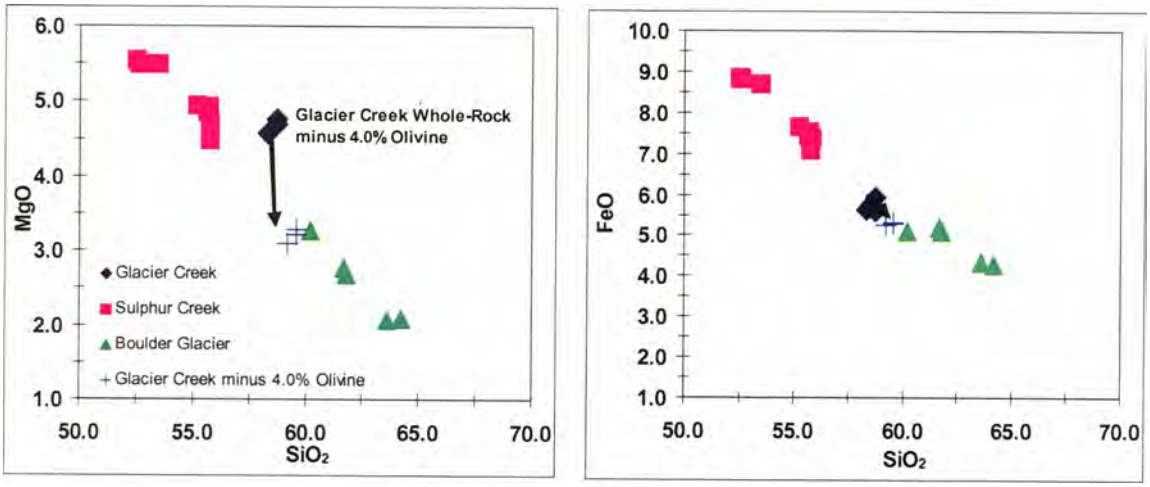

Figure 19.
Glacier Creek compositions prior to olivine accumulation (blue crosses) compared to Sulphur Creek and Boulder Glacier compositions. Blue crosses denote estimated Glacier Creek compositions prior to accumulation of 4.0% olivine. Blue diamonds represent observed Glacier Creek whole-rock compositions. Black arrows chart the change in composition as a result of olivine subtraction in the Glacier Creek samples.

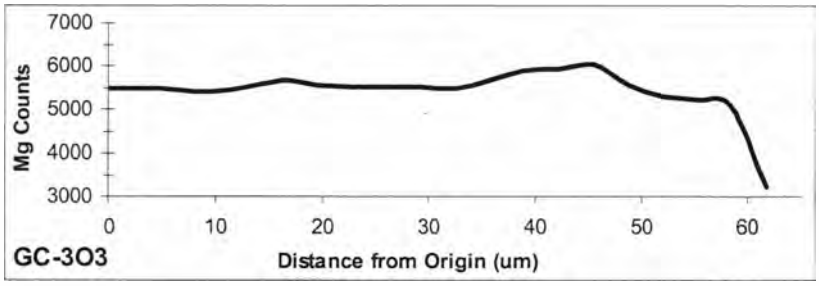

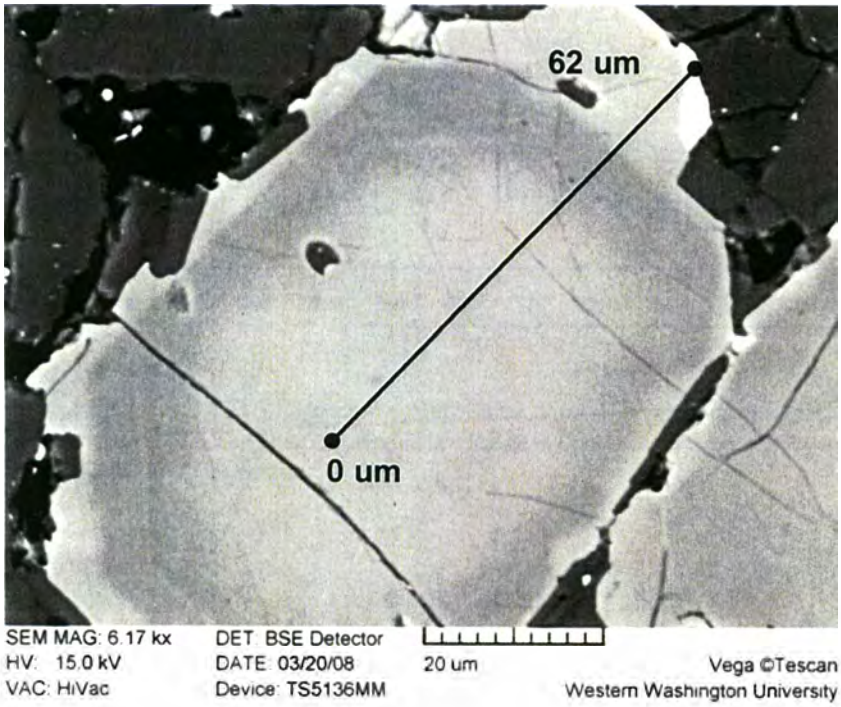

Figure 20.
Glacier Creek olivine phenocryst compositional profile. Olivine traverses were done using an EDAX equipped SEM. Compositions are considered qualitative and are only used to image compositional profiles. Traverse paths are shown on backscatter electron images while compositions are described by EDAX Mg counts along the line of traverse. The traverse profile for olivine GC-3O3 was created by taking an Mg count every 3.25 um for a dwell time of 30 seconds along the line of traverse. This particular olivine shows a reverse chemical zoning profile where Mg counts increase where the darker shades are located on the electron backscatter image.

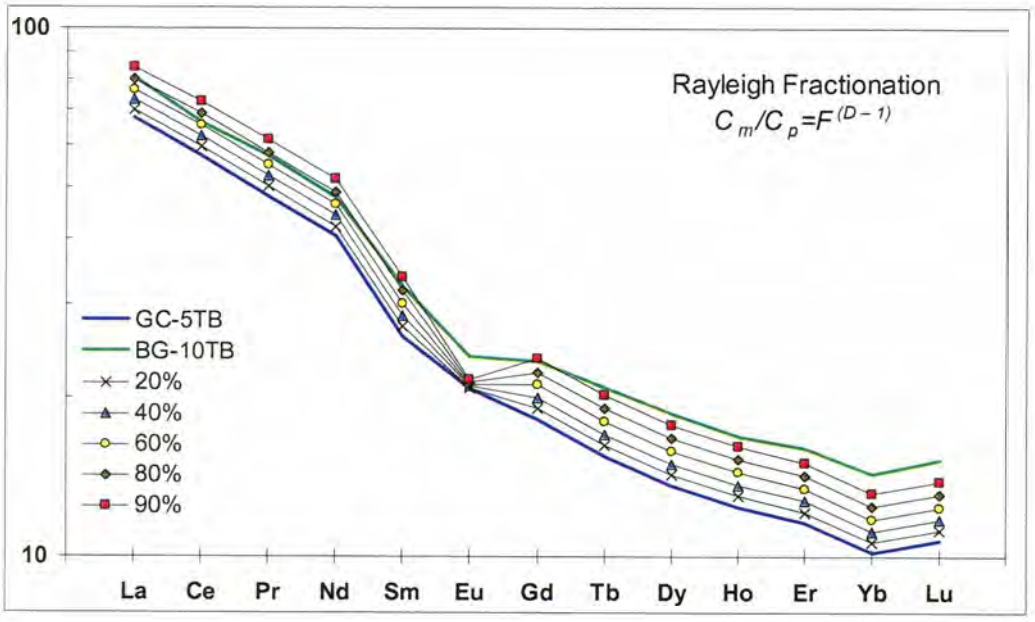

Figure 21.
Boulder Glacier composition (BG-10TB compared to calculated compositions from Rayleigh fractionation of a Glacier Creek andesite (GC-5TB). The fractionating assemblage is 70% plagioclase + 18% orthopyroxene + 10% olivine + 2% magnetite + 0.1% apatite.

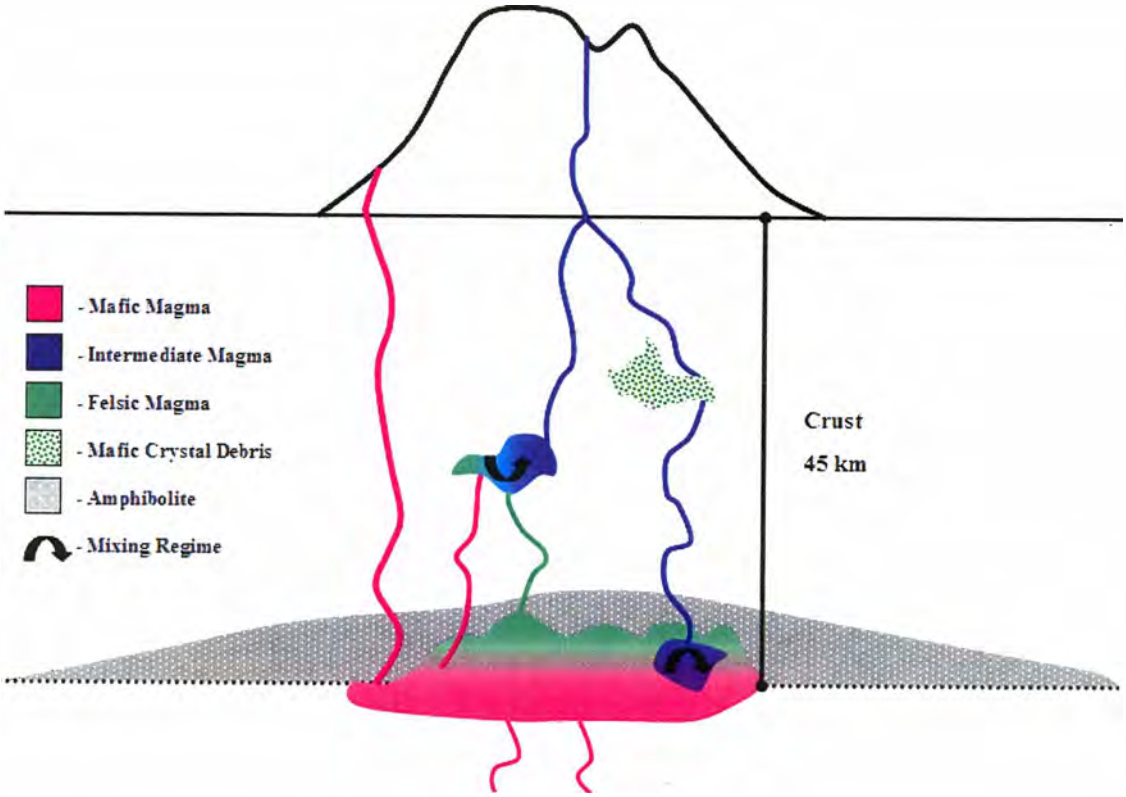

Figure 22.
Schematic model of intermediate magma generation at Mount Baker. Under plating of mantle-derived basalt (pink) induces partial melting of an amphibolite crustal protolith to generate felsic crustal melts (green). Mixing at various levels in the crust between the crustal melts and basalts produce intermediate compositions (blue). Interaction and addition of mafic crystal debris (green and white pattern) may further modify intermediate magma compositions.

APPENDICIES

Appendix 1 – XRF and ICP-MS Sample Preparation Protocol

Introduction

The following describes a protocol developed to prepare whole rock samples for XRF (X-Ray fluorescence) and ICP-MS (inductively coupled plasma mass spectrometer) analyses. The protocol is designed to meet the criteria of the Geo-Analytical lab at Washington State University. Preparing samples prior to submission for XRF and ICP-MS is an effective way to reduce whole-rock analysis cost.

The methods that follow are presented in step wise fashion and include steps from crushing whole rock samples through fusion of glass beads. Sample preparation for XRF and ICP-MS are similar, but there are significant differences that will be highlighted.

Procedure

Step 1 - Crush hand sample.

During this step a hand sample is crushed into pea sized or slightly larger pieces on a metal plate with a hammer in order to obtain a representative sample amount and size of rock material. First, the working area, hammer, and metal plate must be clean and free of dust and debris. In general, larger grain or more porphyritic samples require greater sample masses. For a fine grained porphyritic volcanic rock, a minimum of 50 g is adequate. Rock fragments should come from the freshest part of the sample (often at the center) and should be hand selected and individually inspected for excess dirt or weathering characteristics and should be wiped clean of dust. The number of hammer blows should be minimized as small amounts of metal from the hammer or metal plate may contaminate the sample.

Step 2 - Crush selected pieces in a mechanical Chipmunk rock crusher

During this step the hand selected rock pieces are further crushed into smaller chips. At this step it becomes important to consider the type of material that is being used in the rock crushing equipment. Mechanical crushers at WWU are equipped with two crushing plates and two cheek plates. These plates can be made out of a variety of material. Consult the specification book provided by the manufacture to identify what elements the different types of material may contaminate the sample with. In this protocol tungsten carbide crushing equipment is used for samples prepared for XRF and alumina ceramic crushing equipment is used for samples prepared for ICP-MS. The appropriate cheek and crushing plates must be installed into the Chipmunk Crusher. The mechanical crusher must be free of dust and debris. Drop one rock piece in at a time until the entire sample has been crushed.

Step 3 - Milling rock chips into a powder using the Shatterbox rock crusher

This step covers the process of using a milling chamber and a Shatterbox shaker to mill the sample in to a fine powder. During this step it is also very important to consider what type of material the milling chamber is made of. If samples are being prepared for XRF then tungsten carbide is suggested, if samples are being prepared for ICP-MS, then alumina ceramic is suggested. Once again, specification books can be consulted to identify potential contaminants. The milling chamber must be very dry, clean and free of dust. If there is caked residual rock powder then a small amount of alcohol should be applied and scrubbed with a tooth brush. Place only enough (~20g) chipped rock material in the bottom of the mill, including the mill's crushing puck, to cover the bottom of the chamber. The amount placed in the chamber is dependent on the amount of powder needed and size of rock chips. The main concern is not to overload the chamber. Overloading may result in a damaged milling

chamber or insufficient grinding. Place the lid on the chamber and secure it in the shaker. Run the shaker for 10 minutes. After the shaking period, check the consistency of the rock powder. It should be about the consistency of powdered sugar. If further grinding is needed, then repeat grinding with 2 minute intervals until the desired consistency is reached. Carefully remove the powder and place into a container with a lid. Be sure to thoroughly clean the grinding chamber with water, a tooth brush and alcohol if needed between samples. The chamber can be dried with a hair dryer.

Step 4 – Mixing rock powder and flux

This step covers the procedure for combining rock powder with flux (dilithium tetraborate) prior to fusion. There are several brands of flux available, however, to stay consistent with WSU procedures use Spectromelt A-10. The flux should be kept dry and the lid should be secure when not in use. If the flux develops small chunks, it may be slightly hydrated. Prior to using, make sure the rock powders and flux are completely dry by placing the individual powdered rock samples and an adequate amount of flux in an oven at 110° C for a minimum of 4 hours. Once samples and flux are taken out of the oven they should be used within 1 hour. The ratio of dry flux to dry rock powder is 2:1 for samples prepared for XRF and 1:1 for ICP-MS. Recommended masses for the prescribed ratios are 7 g flux and 3.5 g rock powder for XRF and 2 g of rock powder and flux for ICP-MS. Masses should be weighed within ± 0.002 g for XRF ± .001 g for ICP-MS. Once the flux and rock powders are weighed they should be carefully mixed with a mortar and pestle. Step 5 should be executed as soon as possible at this point.

Step 5 – Fusing Glass Beads

This step covers the process of fusing the mixed flux and rock powders into a glass bead using a furnace. Begin by heating a furnace to 1000° C. This can be done while executing step 4. Prepare an appropriate number of graphite crucibles by gently rubbing away any excess graphite dust inside the crucible while wearing a rubber glove. Beads fused for XRF need to be circular in shape and have a circumference in the range of 29.5-31.5 mm at the bottom and <32mm at the top. Crucibles that cast beads in these dimensions should be used in preparing samples for XRF. ICP-MS bead dimensions do not matter, as they are in powder form when preparation is complete. Once crucibles are clean and the furnace is to temperature, carefully place the mixed flux and powder for each sample into a crucible. Place crucibles into the furnace and fuse for ten minuets. Start counting the ten minutes only after the furnace has reached the 1000° C after the samples are introduced. After fusion is complete, carefully remove crucibles from the furnace and place them on a heat resistant surface. Allow to cool to room temperature and carefully remove the bead from the crucible.

Step 6 – Second Fusion

In order to assure a completely homogenous sample, the fused bead is crushed into a powder and fused a second time. Steps for milling the bead and refusing are identical to steps 4 and 5, however the glass bead should be broken prior to milling as follows. Place the glass bead in a clean metal mortar. Strike the glass bead with a metal pestle directly on top with one clean blow in order to shatter the bead. To help contain the glass shards a cloth may be placed over the mortar while shattering the bead. Collect all glass shards which will be used when repeating steps 4 and 5. If samples are being prepared for ICP-MS, preparation is

complete after the second milling, and are sent as powders. Only samples that are to be used for XRF need to be fused a second time and sent to the lab as beads. Once beads have been refused they may be carefully labeled on the rounded top surface with a dremel tool.

Appendix 2.

Table A1. Kd values used in Rayleigh fractionation REE models

	Olv	Cpx	Opx	Plag	Amph	Mag	Ilm	Apt	Grnt
	Basalt and Basaltic Andesite								
(Ref)	(1)	(1)	(1)	(1)	(1)	(6)			(1)
La	0.0067	0.056	*0.01*	0.190	0.5442	1.5			*0.02*
Ce	0.0060	0.092	0.02	0.111	0.8430	2.0			0.03
Pr	*0.0060*	*0.161*	*0.03*	*0.100*	*1.0911*	*2.5*			0.05
Nd	0.0059	0.23	0.03	0.090	1.3395	3.0			0.07
Sm	0.0070	0.445	0.05	0.072	1.8035	1.6			0.29
Eu	0.0074	0.474	0.05	0.443	1.5565	1.0			0.49
Gd	0.0100	0.556	0.09	0.071	2.0165	*1.3*			0.97
Tb	*0.0115*	0.570	*0.12*	*0.067*	*2.0200*	1.5			*2.07*
Dy	0.0130	0.582	0.15	0.063	2.0235	*1.3*			3.17
Ho	*0.0193*	*0.583*	*0.19*	*0.060*	*1.8818*	*1.3*			*4.87*
Er	0.0256	0.583	0.23	0.057	1.7400	*1.3*			6.56
Yb	0.0491	0.542	0.34	0.056	1.6420	1.4			11.5
Lu	0.0454	0.506	0.42	0.053	1.5625	1.5			11.9
	Andesite								
(Ref)		(1)	(1)	(1)	(1)	(8)	(3)	(3)	(2)	(7)
La		0.0468	0.031	0.3017	0.366	0.48	0.22	0.01	28.2	0.08
Ce		0.0838	0.0277	0.2214	0.574	0.95	0.26	0.01	37.4	*1.00*
Pr		*0.1333*	*0.0278*	*0.1851*	*0.793*	*1.66*	*0.28*	*0.01*	*49.3*	*1.00*
Nd		0.1828	0.0279	0.1487	1.012	2.36	0.30	0.01	61.2	*1.10*
Sm		0.3774	0.0278	0.1024	1.386	3.85	0.35	0.01	98.5	1.25
Eu		*0.48*	0.0276	1.214	1.212	*4.01*	0.26	0.01	17.1	1.52
Gd		0.5826	0.0388	0.0665	1.490	*4.18*	0.32	0.02	95.6	5.20
Tb		*0.6783*	*0.0575*	*0.0582*	*1.551*	*4.25*	*0.30*	*0.02*	*78.3*	7.10
Dy		0.7739	0.0762	0.0498	1.611	4.35	0.28	0.03	61.0	*15.45*
Ho		*0.7409*	*0.1144*	*0.0473*	*1.554*	*4.1*	*0.25*	*0.04*	*51.3*	23.80
Er		0.7078	0.1526	0.0448	1.496	3.85	0.22	0.05	41.6	*38.40*
Yb		0.6335	0.254	0.041	1.488	1.03	0.18	0.08	27.6	53.00
Lu		0.6654	0.323	0.0389	1.325	*0.5*	0.18	0.10	21.5	57.00
	Dacite								
(Ref)		(1)	(1)	(1)		(5)			
La		0.0154	0.0146	0.3926		0.03			
Ce		0.0440	0.0163	0.2511		0.03			
Pr		*0.1051*	*0.0163*	*0.2201*		*0.03*			
Nd		0.1661	0.0162	0.1890		0.03			
Sm		0.4574	0.0174	0.1366		0.03			
Eu		0.4108	0.0222	1.1130		0.03			
Gd		0.7028	0.0270	0.1202		*0.04*			
Tb		*0.7394*	*0.0341*	*0.1159*		0.05			
Dy		0.7759	0.0412	0.1116		*0.08*			
Ho		*0.7376*	*0.0569*	*0.1166*		*0.09*			
Er		0.6993	0.0725	0.1216		*0.10*			
Yb		0.6400	0.1149	0.1323		0.10			
Lu		0.6830	0.1540	0.1384		*0.10*			

Olv- olivine, Cpx- clinopyroxene, Opx- orthopyroxene, Plag- plagioclase, Amph- amphibole, Mag- magnetite, Ilm- ilmenite, Apt- apatite, Grnt- garnet. Italicized values are estimated by averaging kd values of the REE with the next higher and lower compatibility. References are indicated by bracketed numbers: (1) Fujimaki (1984), (2) Fujimaki (1986), (3) Martin (1987), (4) Arth (1987), (5) Smith and Leeman (1987), (6) Schock (1979), (7) Irving and Frey (1978), Sission (1994).

Appendix 3 – Utilization of the MELTS model to test for Crystal Fractionation

Introduction

This appendix discusses the use of the use of the MELTS model (Ghiorso, 1993) to test a crystal fractionation model in intermediate volcanic rocks ranging in age from the late Pleistocene to Holocene from Mount Baker. MELTS is a thermodynamic calculator that calculates the compositions of coexisting melts and solid phases for realistic geologic systems.

Methods

Hildreth et al. (2003) provide major oxide data for all late Pleistocene and Holocene units described at Mount Baker. A starting composition was selected from the most mafic sample from the Holocene basalt and basaltic andesite of Sulphur Creek. Sample bsc 442 is the most mafic sample from the late Pleistocene eruptive units and contains 51.4 wt. % SiO_2, and 5.58 wt. % MgO (Table A2). The model is used to produce intermediate compositions through crystal fractionation of bsc 442.

Melts has several variables to set up before the model is run. The intensive variables used in the crystal fractionation model are oxygen fugacity (fO_2), pressure, and temperature. Water content is not included in the composition for bsc 442, so it is also treated as an intensive variable. The intensive parameters are selected as described below.

In MELTS it is possible to set a starting temperature and a stopping temperature for each execution of the model. The starting temperature is always set to the liquidus temperature. MELTS has an option to find the liquidus and will depend on the other variables in the system. It is estimated that a temperature range of 150° C for the fractionation process will result in a liquid within andesitic compositions. Therefore the stopping temperature is

always set to the liquidus temperature minus 150° C. A larger range of temperature will result in a differentiated liquid that has fractionated past andesitic compositions. The temperature decrease is done with one iteration of the MELTS program.

H_2O is an important variable in arc systems because dehydration of subducting slabs releases H_2O which incorporated into arc magmas as aqueous fluids. A typical arc system has a relatively high H_2O component, but the Cascade arc system has relatively low amounts of H_2O incorporated in to arc magmas because it is thought the subducting young and still hot Juan de Fuca slab is mostly dehydrated before it reaches conditions at which typical arc magmas are generated. A range of 2%, 1%, and 0.5% H_2O is tested in the MELTS model.

Pressure constraints are set based on estimated depth of crystal fractionation in the Cascade arc. The Mount Baker andesites were most likely differentiated within the crust, so pressure constraints are a result of crustal thickness. Crustal thickness under Mount Baker is estimated to be 40-45 km (Mooney and Weaver, 1998), so corresponding pressure constraints are set at 15 kbar-5 kbar and modeled in 5 kbar increments. The model is not modeling multiple fractionation depths, but rather is comparing results from fractionation at different depths.

Oxygen fugacity (fO_2) is defined as the activity of O_2 within a system. Fugacity is considered an intensive variable because it affects the redox potential of a system at equilibrium. Fugacity is directly related to the oxidation of a system, and arc lavas are thought to be a more oxidized magma relative to other magma types. Two different fO_2 states are modeled in this study. The higher fugacity of the two is the Ni-NiO buffer, and the other is a slightly lower Quartz-Faylite-Magnetite buffer +2.

Once the constraints of the intensive variables were set, a systematic approach of testing each possible combination of variables was developed. As result there are 18 different combinations of the above variables that were tested. The combinations of variables are labeled as test runs (Table A2). To test the hypothesis, the resulting liquid composition of each test run is compared to actual andesite compositions from late Pleistocene and Holocene units described by Hildreth et al., (2003) (Figure A1). If the resulting liquid composition is in the range the actual Mount Baker andesite compositions then it is possible that crystal fractionation took place in the generation of the Mount Baker andesites.

Results

The results yielded liquid composition that ranged from slightly more felsic and slightly more mafic then Mount Baker andesites (Table A2). SiO_2 compositions are in the range of 56.55-63.37 wt. % SiO_2, and increase with decreasing pressure and H_2O. TiO_2 is in the range of 0.67-1.81 wt. % and increases with decreasing pressure and H_2O content. Al_2O_3 is in the range of 12.75-17.53 wt. %, and tends to decrease with decreasing in H_2O and pressure. FeO is in the range of 0.66-1.39 wt. % and tends to be higher with the QFM + 2 buffer. Fe_2O_3 is in the range of 1.75- 6.79 wt% and displays no trend. MnO is in the range of 0.22-0.47 wt. %, and increases with decreasing pressure and H_2O content. MgO is in the range of 1.52-2.47 wt. % and is not correlated with pressure and H_2O content. CaO is in the range of 5.02-5.55 wt. % and is not correlated with pressure and H_2O content. Na_2O is in the range of 5.69-6.27 wt. % and increases with decreasing pressure and H_2O content. K_2O is in the range of 1.31-2.14 wt. % and increases with decreasing H_2O content and pressure. P_2O_5 is in the range of 0.76-1.26 wt. % and increases with decreasing pressure and

H_2O content. H_2O content in the resulting liquids ranges from 1.43 wt. % to 3.68 wt. % and decreases with pressure.

Major oxide wt% in the results varies by about ± .5 wt. % with the exception of Al_2O_3, which varies about ± 2.5 wt. %, and SiO_2 which varies about ± 4 wt. %. A comparison of Mount Baker andesite compositions with the calculated liquid compositions shows that some of the major oxide compositions for the results are in range with andesite compositions (including SiO_2, TiO_2, A_2O_3 and FeO*) and others are not (including MgO, CaO, Na_2O, MnO and P_2O_5). The MELTS output yields major oxide concentrations that are higher then the concentrations in Mount Baker andesite for Na_2O, MnO and P_2O_5 and lower concentrations for MgO and CaO.

Discussion

If intermediate compositions modeled by MELTS falls within range of Mount Baker andesites for a particular oxide, then MELTS has successfully modeled that particular oxide. For example, the range for SiO_2 of the results is 56.55 wt. % to 63.37 wt. %, which is well within range of observed SiO_2 concentrations. Therefore some combination within the variable constraints will give the target SiO_2 concentrations. Figure A1 shows that calculated compositions of SiO_2, TiO_2, Al_2O_3, FeO, and K_2O are within range of Mount Baker andesite compositions. A comparison of the modeled liquids and an average andesite composition (Table A1) calculated from all intermediate units in the Pleistocene and Holocene shows the difference between the results and the average andesite (Fig. 2A). The average andesite composition does not lie within modeled compositions for MnO, MgO, CaO, Na_2O and P_2O_5.

Conclusion

MELTS was not successful in modeling andesitic composition from the Late Pleistocene and Holocene eruptive units at Mount Baker through crystal fractionation of sample bsc442. MELTS was able to model some major oxides, but gave results that are consistently too low in MgO wt. % and CaO wt. % and consistently too high in MnO wt%, Na_2O wt. %, and P_2O_5 wt. %. It is more likely the Mount Baker andesites are a result of an open system differentiation process that may include assimilation, fractional crystallization and/or magma mixing processes.

Table A2. MELTS test run parameters and results with starting composition

	Intensive Variables			*Composition of modeled results*													
Test Run	$f(O_2)$	P kbar	H_2O	SiO_2	TiO_2	Al_2O_3	Fe_2O_3	FeO	FeO*	MnO	MgO	CaO	Na_2O	K_2O	P_2O_5	H_2O	
1	NI-NO		15	2	56.55	0.89	17.53	0.83	4.97	5.80	0.22	2.02	5.43	5.69	1.37	0.81	3.68
2	NI-NO		15	1	59.23	0.90	14.42	0.75	6.57	7.32	0.34	1.52	5.02	6.27	1.76	0.78	2.44
3	NI-NO		15	1	59.61	1.18	13.42	0.76	6.79	7.55	0.45	1.60	5.18	6.39	2.14	0.92	1.55
4	NI-NO		10	2	57.08	0.88	16.60	0.70	5.63	6.33	0.24	1.88	5.53	5.82	1.33	0.78	3.53
5	NI-NO		10	1	60.25	1.01	14.11	0.66	5.83	6.49	0.28	1.61	5.18	6.14	1.72	0.84	2.38
6	NI-NO		10	1	60.26	1.19	13.09	0.78	6.45	7.23	0.41	1.66	5.35	6.24	2.07	0.98	1.50
7	NI-NO		5	2	60.87	0.88	13.92	0.65	5.40	6.05	0.27	1.55	5.06	6.25	1.73	0.84	2.59
8	NI-NO		5	1	60.39	0.97	13.93	0.68	5.72	6.40	0.27	1.67	5.30	6.14	1.71	0.88	2.35
9	NI-NO		5	1	60.88	1.18	12.72	0.80	6.28	7.08	0.34	1.70	5.55	6.06	2.00	1.05	1.43
10	Q-F-M		15	2	56.78	0.83	17.06	1.25	5.14	6.39	0.24	2.03	5.35	5.77	1.31	0.76	3.47
11	Q-F-M		15	1	59.55	0.99	14.81	1.29	4.99	6.28	0.33	1.77	5.04	6.21	1.76	0.83	2.44
12	Q-F-M		15	1	61.00	1.16	13.15	1.39	5.25	6.64	0.42	1.65	5.10	6.23	2.14	0.96	1.56
13	Q-F-M		10	2	58.18	0.67	16.30	1.18	4.55	5.73	0.25	1.75	5.07	6.03	1.42	0.82	3.78
14	Q-F-M		10	1	59.81	0.91	14.42	1.34	5.14	6.48	0.31	1.78	5.19	6.14	1.72	0.87	2.38
15	Q-F-M		10	1	61.09	1.11	12.99	1.40	5.23	6.63	0.40	1.72	5.21	6.22	2.10	1.01	1.52
16	Q-F-M		5	2	60.55	0.83	14.23	1.26	4.68	5.94	0.28	1.76	5.07	6.22	1.68	0.88	2.58
17	Q-F-M		5	1	60.70	1.16	15.53	1.17	1.75	2.92	0.47	2.47	5.51	5.71	1.91	1.09	2.53
18	Q-F-M		5	1	63.37	1.81	12.75	1.27	1.81	3.08	0.45	2.31	5.49	6.05	2.00	1.26	1.43
				Composition of bsc 442													
					51.40	1.67	18.07			9.16	0.17	5.58	8.17	4.16	0.78	0.44	
				Composition of average andesite													
					59.10	0.88	17.34			5.74	0.11	3.93	6.56	3.93	1.73	0.28	

Table A1. Modeling parameters used in the application of the MELTS model. Each test run denotes a specific array of intensive variables as inputs into the model. The results of each test run are described of each oxide in wt%. Also, the composition of the starting composition (bsc 442 from Hildreth et al. 2003) is listed along with a calculated average andesite composition from the late Pleistocene units described by Hildreth et al. (2005)

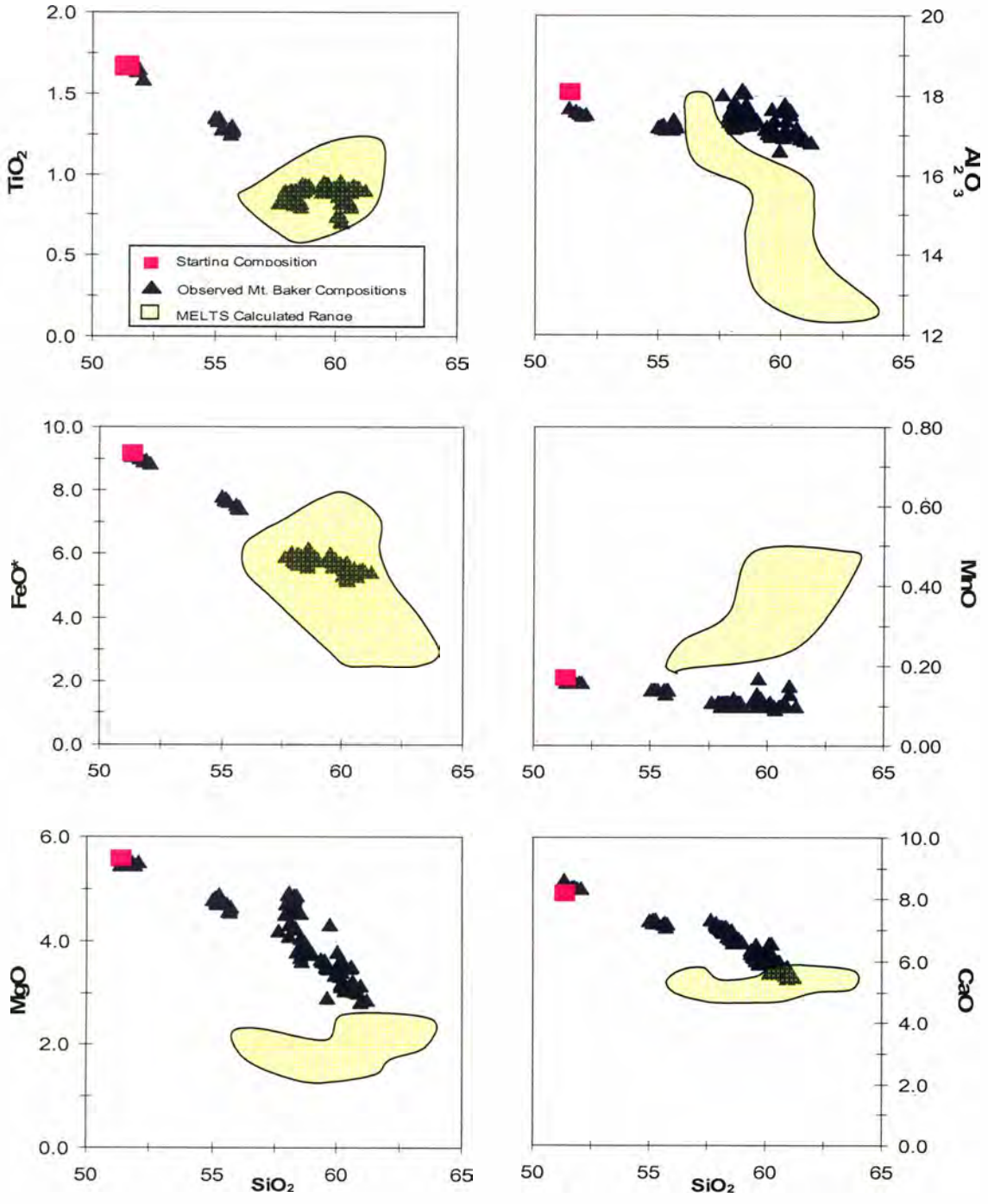

Figure A1. Graphic display of observed andesite compositions from the late Pleistocene described by Hildreth et al. 2003 (blue triangles) compared to modeled compositions from the MELTS model (pink squares). Values on all x-axis are SiO_2 wt% while all y-axis values are in wt%.

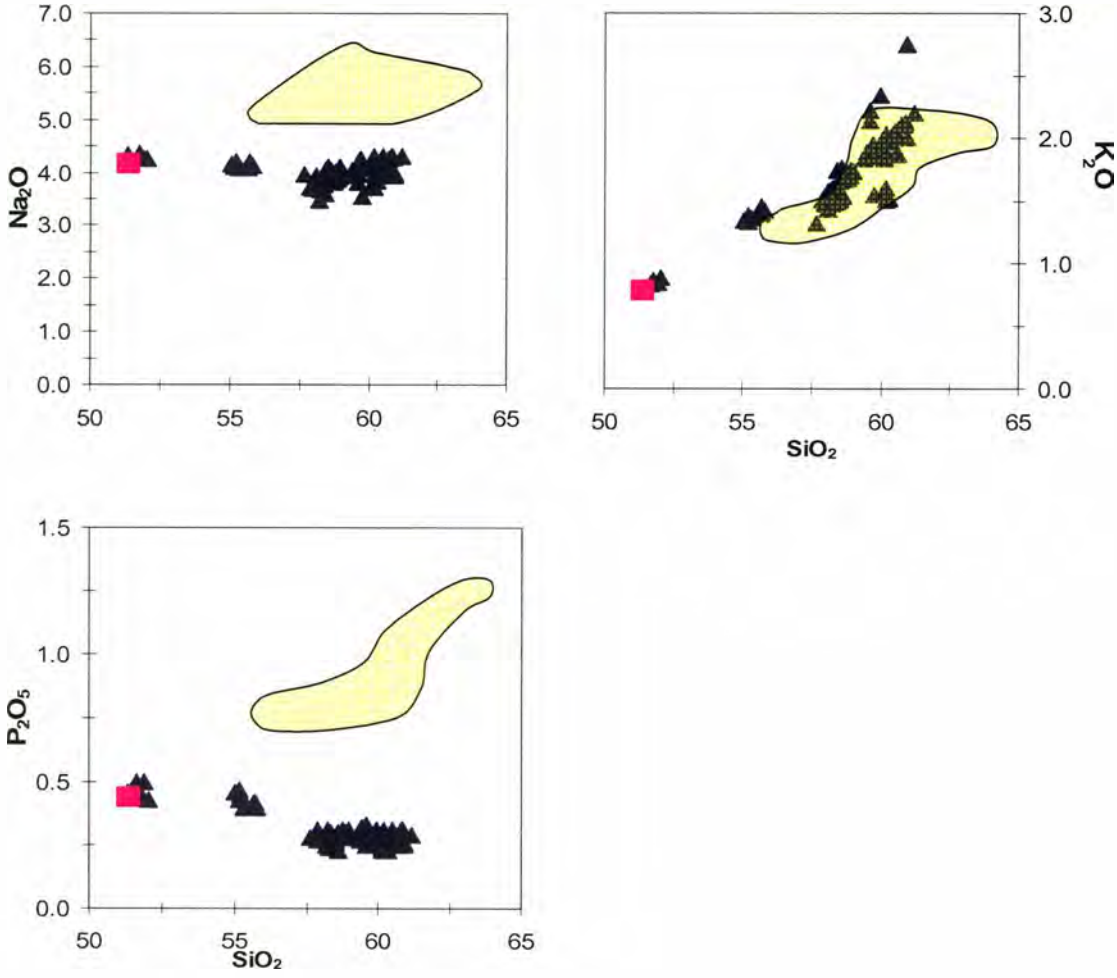

Figure A1 cont.

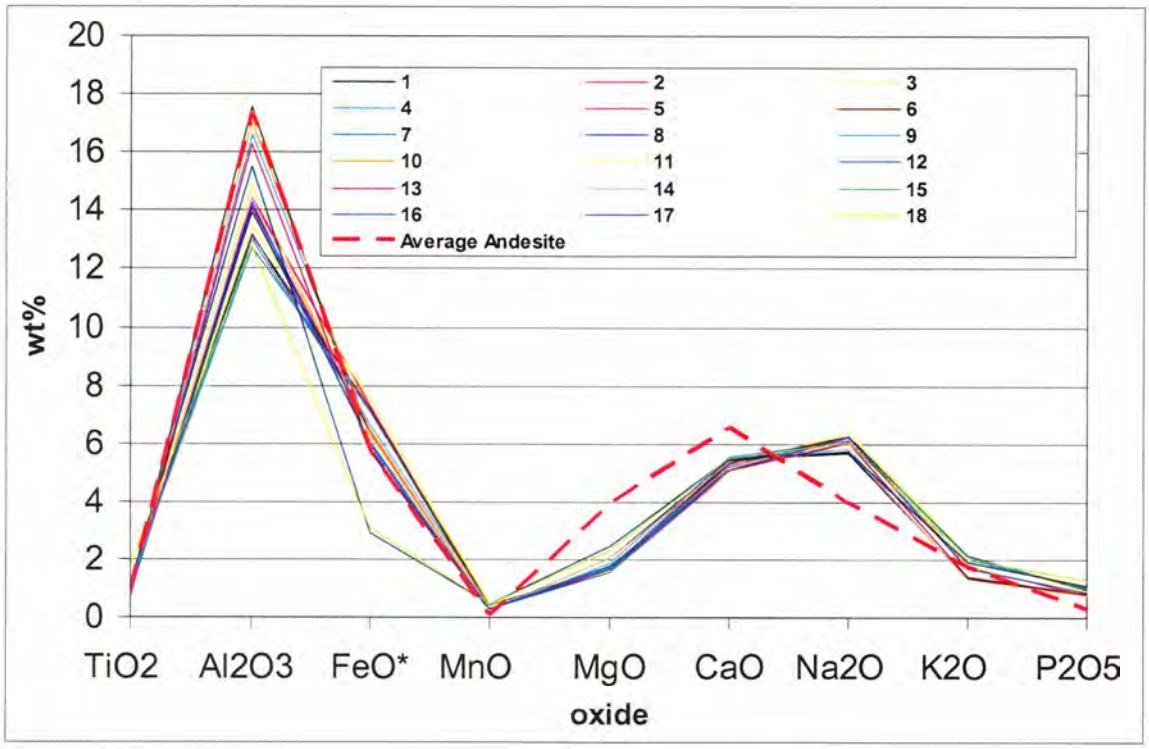

Figure A2. Average andesite compositions (red dashed line) compared to modeled results of each test run. Each different test run is denoted by a number and color in the legend.